AD-A091 764 SIGNATRON INC LEXINGTON MA F/G 9/5
ADAPTIVE ANTENNA CONTROL (AAC) PROGRAM.(U)
AUG 80 P MONSEN, S PARL DAAB07-76-C-8085
UNCLASSIFIED A212 CSA-76-8085-F NL

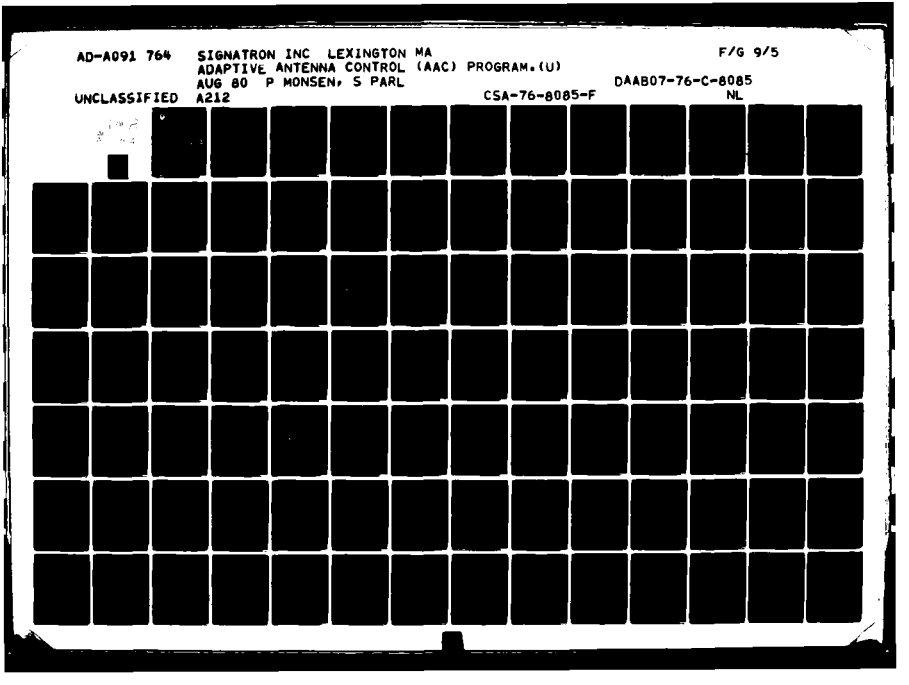

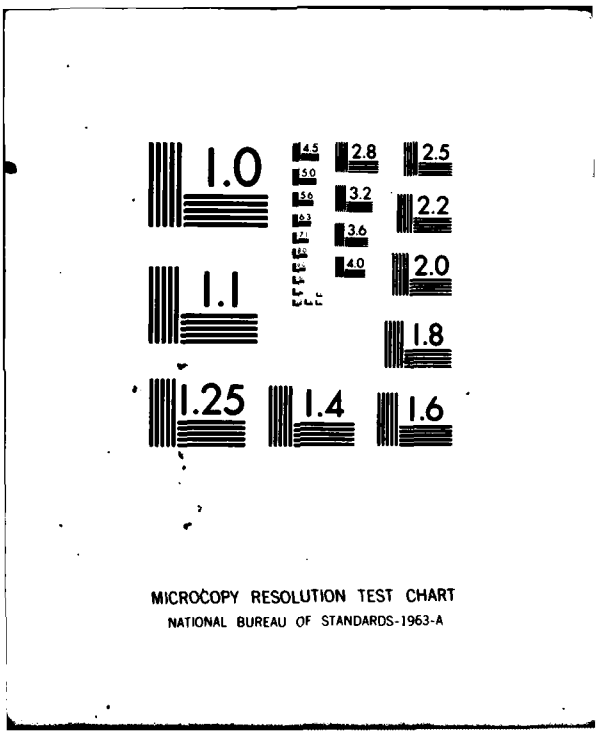
1.0
1.1
1.25
1.4
1.6
1.8
2.0
2.2
2.5
2.8
3.2
3.6
4.0
4.5
5.0
5.6
6.3
7.1
8.0
9.0
MICROCOPY RESOLUTION TEST CHART
NATIONAL BUREAU OF STANDARDS-1963-A

Report No. CSA-76-8085-F

LEVEL II

Contract No. DAAB07-76-C-8085

12

FINAL REPORT

ADAPTIVE ANTENNA CONTROL (AAC) PROGRAM

AUGUST 1980

DR. P. MONSEN
DR. S. PARL

SIGNATRON, Inc.
12 Hartwell Avenue
Lexington, Massachusetts 02173

DISTRIBUTION STATEMENT

Approved for public release; distribution unlimited.

U.S. ARMY
COMMUNICATIONS SYSTEMS AGENCY
Fort Monmouth, New Jersey

MONITORING OFFICE

U.S. ARMY
COMMUNICATIONS R&D COMMAND
Fort Monmouth, NJ

NOTICES

Disclaimers

The citation of trade names and names of manufacturers in this report is not to be construed as official Government indorsement or approval of commercial products or services referenced herein.

Disposition

Destroy this report when it is no longer needed. Do not return it to the originator.

UNCLASSIFIED

SECURITY CLASSIFICATION OF THIS PAGE (When Data Entered)

(19) REPORT DOCUMENTATION PAGE	READ INSTRUCTIONS BEFORE COMPLETING FORM
(18) 1. REPORT NUMBER: CSA-76-8085-F	2. GOVT ACCESSION NO.: AD-A097 764	3. RECIPIENT'S CATALOG NUMBER
(6) 4. TITLE (and Subtitle): Adaptive Antenna Control (AAC) Program	5. TYPE OF REPORT & PERIOD COVERED: (9) Final Report, Jun 78-Mar 80
(14)	6. PERFORMING ORG. REPORT NUMBER: A212
7. AUTHOR(s): (10) Peter Monsen, Steen Parl	8. CONTRACT OR GRANT NUMBER(s): (15) DAAB07-76-C-8085
9. PERFORMING ORGANIZATION NAME AND ADDRESS: SIGNATRON, Inc. 12 Hartwell Avenue Lexington, MA 02173	10. PROGRAM ELEMENT, PROJECT, TASK AREA & WORK UNIT NUMBERS: (16) 1X763707D245 1702 (17) 17
11. CONTROLLING OFFICE NAME AND ADDRESS: U.S. Army Communications Systems Agency Fort Monmouth, New Jersey	12. REPORT DATE: (11) Aug 1980; 13. NUMBER OF PAGES: 157
14. MONITORING AGENCY NAME & ADDRESS (if different from Controlling Office): U.S. Army Communications R&D Command Fort Monmouth, New Jersey Attn: DRDCO-COM-RM-3 (12) 159	15. SECURITY CLASS. (of this report): Unclassified; 15a. DECLASSIFICATION/DOWNGRADING SCHEDULE

16. DISTRIBUTION STATEMENT (of this Report)

Approved for public release; distribution unlimited.

17. DISTRIBUTION STATEMENT (of the abstract entered in Block 20, if different from Report)

18. SUPPLEMENTARY NOTES

Notes

19. KEY WORDS (Continue on reverse side if necessary and identify by block number)

Angle Diversity
Troposcatter
Path Loss Prediction
Decision Feedback Equalizer
Digital Troposcatter Communication
Coupling Loss
Antenna

20. ABSTRACT (Continue on reverse side if necessary and identify by block number)

A theoretical and empirical investigation of angle diversity for application on Defense Communications System (DCS) tropospheric scatter communication links has been completed. ~~This report summarizes the principal areas of this investigation.~~ The major results are:

(continued on reverse side)

DD FORM 1 JAN 73 1473 EDITION OF 1 NOV 65 IS OBSOLETE

UNCLASSIFIED

SECURITY CLASSIFICATION OF THIS PAGE (When Data Entered)

33,360

20. (continued)

(1) Development of a new propagation prediction model applicable at frequencies up to 5 GHz.

(2) Development of a modem prediction model for calculating the bit error rate and fade outage on a fading multipath channel for the MD-918/GRC modem.

(3) A trade-off analysis to determine the optimum angle diversity system.

(4) Design and development of a 4.4-5.0 GHz (C-Band) angle diversity feedhorn which gives a beam separation within about 1/2 dB of optimum.

(5) Theoretical and empirical evidence that angle diversity has a performance advantage over frequency diversity.

(6) Discovery of reduced correlation effects in angle diversity when wideband signals are employed.

(7) Development of a methodology and a statistical base for development of future angle diversity systems.

This effort impacts the development of future digital troposcatter circuits by establishing a new technology which will allow conversion from frequency to angle diversity with a resulting halving of frequency requirements and a positive system gain in almost all applications. The angle and frequency diversity systems have virtually the same level of complexity.

TABLE OF CONTENTS

TABLE OF CONTENTS CONT.

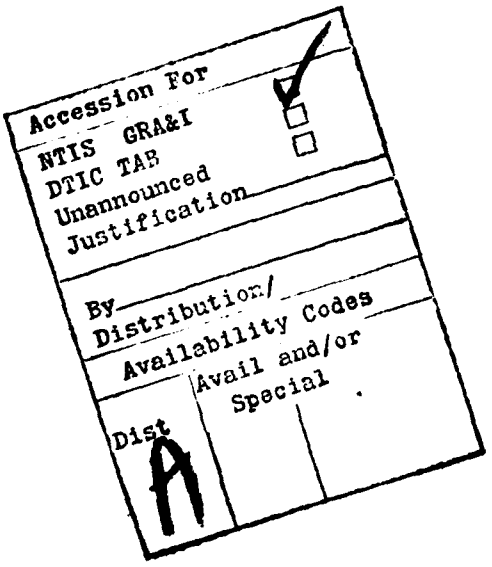

LIST OF FIGURES

LIST OF FIGURES CONT.

SECTION 1

INTRODUCTION

The Defense Communications Agency (DCA) and the military departments are upgrading the troposcatter links in the Defense Communications System (DCS). Present efforts are focused on DCS links in Europe. NATO is also contemplating an upgrade of the troposcatter links in its ACE-High system. Current planning for DCS troposcatter links calls for all digital traffic to meet the criteria set forth in the Defense Communications Engineering Center's Technical Report No. 12-76, "DCS Digital Transmission System Performance". The upgrade effort is complicated by a need to reduce frequency assignments and conserve spectrum bandwidth.

In response to DCA tasking for a solution to the above problem areas, the Department of Army has sponsored an investigation of angle diversity as a promising technique to combat short term fading, and alleviate aperture-to-medium coupling loss without expanding and possibly reducing current usage of the frequency spectrum. The effort consisted of three phases: the study phase, the equipment development phase and the link test. In brief, these phases consisted of the following:

- During the study phase, comprehensive models of the troposcatter propagation and digital modem characteristics were modeled. The propagation model emphasized the turbulent scatter mechanism as the limiting mode, particularly for S and C band (2.0-5.0 GHz) transmissions. This model was written in terms of spectrum slope, refractive index variance, and scale of turbulence. In the past, aperture-to-medium coupling loss has been included

in total path loss calculations as a separate parameter, i.e. the total path loss is the basic path loss with omnidirectional antennas, the antenna gains, and the coupling loss. The usefulness of this concept is questionable, since it uses properties of the atmospheric structure outside the actual antenna beams. The approach developed in this study calculated the total path loss directly by integrating over the common volume. The digital modem model was developed to predict bit error rate (BER) statistics for the MD-918 troposcatter modem. This modem employs a decision-feedback equalizer as the means of combining diversity channels and minimizing intersymbol interference effects. The MD-918 modem has been tested in DCS troposcatter configurations in both the United States and in Europe. The propagation and digital modem models were used to predict the performance of angle diversity in replacing space or frequency diversity and in augmenting either or both for systems providing up to eighth order diversity.

- Equipment Development Phase: The angle diversity design was selected as a vertical splay of two beams spaced by approximately 1 beamwidth. A C-Band angle diversity feed horn was developed with capability of duplex operation with up to 10 Kw transmitters and with dual polarization ports in both horn branches. A digital traffic capability was realized through the use of MD-918 digital tropo modems. A predetection combiner (PDC) was developed to implement up to 8th order diversity with the MD-918 for combining the signals of the elevated (i.e., the angle diversity) beams.

- Link Test Phase: The test program consisted of an extensive series of propagation and modem performance tests from October 1977 to May 1978 followed by an effort to collect long term propagation data. This second effort continued until October 1979. The test bed for these experiments was the RADC 168 mile C-band troposcatter system because Youngstown and Verona, N.Y. Specific parameters measured were hourly path loss distributions, long term distributions of hourly median path loss, multipath profiles and rms multipath spread, short term correlation between angle diversity paths, long term decorrelation of angle diversity hourly medians, angle diversity squint loss statistics, and BER statistics at 6.3 and 12.6 Mb/s.

The major results of this effort are best summarized with respect to the program phase in which it occurred.

a. Study Phase Results

1. A new troposcatter propagation prediction model applicable at frequencies up to 5 GHz was developed. The present NBS Tech Note 101 method for propagation prediction is a semi-empirical method limited to carrier frequencies of 1 GHz or less.

2. A method for predicting BER outage rate was developed for the MD-918 digital troposcatter modem. Previous performance calculations were based on an average probability of error concept which is a poor measure for digitized speech. DCS standards are now specified in terms of Bit Error outage rate.

3. A trade-off analysis was completed to determine the best angle diversity configuration. The optimized system consists of a main beam transmitter for each antenna and two vertically splayed beams for each antenna at the receiver. The antennas are aimed with boresight slightly above the horizon as with conventional dual space/dual frequency diversity (2S/2F) systems. A vertical splay of about 3/4 beamwidth is desirable although physical limitations in feedhorn design usually result in a somewhat larger splay. The dual space/dual angle (2S/2A) diversity system interfaces with the digital modem in the same manner as the conventional 2S/2F system, i.e., no modem changes are required.

4. A theoretical comparison of 2S/2F and 2S/2A diversity configurations showed the angle systems to be generally better than the frequency diversity systems. The importance of this result is reflected in the savings of two bandwidth allocations per link in a conversion from frequency to angle diversity.

b. Equipment Development Phase Results

1. A C-band (4.4 - 5.0 GHz) dual polarized feedhorn with a beam separation of 1.3 beamwidths was developed. This beam separation results in a system loss of about 1/2 dB relative to the optimum separation of 3/4 beamwidth. The insertion loss due to replacing the original horns with the angle diversity horns was on the order of 0.1 dB.

2. An extension of the MD-918 digital modem was developed to accommodate up to eight diversity inputs. The eighth order diversity system results when 2S/2F is augmented with angle diversity to produce 2S/2F/2A.

c. Link Test Results

1. Angle diversity was shown to have better performance than frequency diversity.
2. Eighth order diversity offers only a small improvement over fourth order systems.
3. The short term correlation between angle diversity beams has an insignificant effect on performance for wide bandwidth (~5 MHz) digital systems.
4. Elevated beam multipath spread exceeds main beam multipath spread by about a third or less. The distribution slopes of the multipath spread are about the same.
5. The elevated beam frequently has a stronger received signal than the main beam. Since the main beam has been aimed for maximum received power, this result requires an inhomogeneous atmospheric structure with respect to the two common volumes.

d. Conclusions

These results impact on the development of future digital troposcatter systems in a number of ways. Because analog FM/FDM troposcatter systems generally require less bandwidth than digital, by almost a factor of two, the conversion to digital of 2S/2F systems requires twice as many bandwidth allocations. If, however, the digital conversion is accompanied by a conversion of the frequency diversity to angle diversity, the same diversity performance is realized but with the same total bandwidth requirements as the analog system rather than twice these requirements. In geographic areas such as Europe, where frequency assignments are hard to obtain, digital conversion may not be possible without use of angle diversity. The performance advantage of angle over frequency diversity has

not been recognized in the past because of the emphasis on the squint loss and correlation of the elevated beam. Our results show that in wideband digital systems, correlation is not important and that the squint loss is compensated by both the second transmitter power amplifier which becomes available when a frequency to angle diversity conversion is made and an availability gain of angle diversity due to decorrelation in the two beams common volumes. Two power amplifiers are used in DCS communication applications to insure link reliability by providing redundancy.

The digital conversion of
will involve some links with carrier frequencies in the 4.4 to 5 GHz band. The new prediction model developed under this program will be essential for determining upgrade recommendations and calculating network performance. The use of previous methods which were not derived for this frequency range may have led to unsatisfactory link service.

The small improvement resulting from extension to eighth order diversity is due to the necessity to improve the outage rate at signal-to-noise values where the point of diminishing returns with respect to diversity has been reached. Thus systems which do not meet outage rate standards generally require brute force dB improvement such as larger power amplifiers or antennas.

The absence of a correlation degradation in wideband digital angle diversity systems is due to the decorrelation effects of multipath on the two beams. Thus a correlation coefficient of 0.6 measured with CW signals which would degrade a narrowband digital system by 1 dB has no significant effect on a wideband system. Thus in future design of angle diversity feedhorns every attempt should be made to reduce the beam separation and hence the squint loss. Reduction of the beam separation should not be at the expense of unacceptable coupling between horns, however.

The multipath spread results are encouraging in that on most systems the present MD-918 modem can accommodate the additional multipath spread associated with the elevated beam.

e. Report Contents

This report presents the significant results of this program in the following manner. Section 2 introduces key troposcatter concepts and develops the angle diversity design. The propagation model is presented in Section 3 along with a summary of the computer program for predicting path loss. Section 4 develops the performance model for the MD-918 digital troposcatter modem. In Section 5 the DCS performance standards are reviewed and an example computation of link performance is made and compared to these standards. During the course of this program, this link analysis was completed for all identified DCS and NATO links. The results of this analysis are available in a previous report [1.1]. The last section addresses the question of long term availability and the potential for gain in an angle diversity system. This section also presents key test results which are contained in greater detail in [1.2]. Additional details on specific phases of the program are given in the two interim reports [1.3, 1.4] which are available from the Defense Documentation Center.

SECTION 1

REFERENCES

1.1 P. Monsen, S. A. Parl, Assessment of Digital Tropo Transmission Using Angle Diversity, DAAB07-76-C-8085, Prepared by SIGNATRON, Lexington, MA., NATO RESTRICTED, October 1978.

1.2 J. Eschle, P. Monsen, AAC Test Report, CSA-80-8085-1, For U.S. Army, Ft. Monmouth, N.J., Prepared by SIGNATRON, Lexington, MA., March 1980.

1.3 P. Monsen, S. A. Parl, J. N. Pierce, Interim Technical Report, Adaptive Antenna Control, AD# A044416, For U.S. Army, Ft. Monmouth, N.J., Prepared by SIGNATRON, Lexington, MA., December 1976.

1.4 P. Monsen, S. A. Parl, Second Interim Technical Report, Adaptive Antenna Control, AD# AO55-820, For U.S. Army, Ft. Monmouth, N.J., Prepared by SIGNATRON, Lexington, MA., February 1978.

SECTION 2

ANGLE DIVERSITY IN DIGITAL TROPOSCATTER SYSTEMS

Studies of adaptive antenna control techniques under this program have shown that a small gain can be achieved on diffraction links with electro-mechanical antenna steering and that a significant savings in bandwidth allocations can be realized on scatter circuits by conversion of frequency diversity systems to angle diversity. Because of the importance of these angle diversity results, this report emphasizes the troposcatter problem.

Additional angle-diversity (AD) channels can be realized through the placement of extra feedhorns near the focal point of the radio antenna. In one of the early angle diversity experiments, Crawford et al.[2.1] confirmed that vertically displaced feeds provide essentially uncorrelated channels at both 460 and 4110 MHz. Their experiments with horizontally displaced feeds revealed considerable correlation at the lower frequency, but again essentially uncorrelated channels at the higher frequency. In another study of azimuthal angle diversity Chisholm et al.[2.2] determined correlation coefficients at two separations and the effective diversity gain. Vogelman et al.[2.3] also established the low correlation between AD signals.

Surenian[2.4] considered the use of angle diversity at super high frequencies (SHF). The use of SHF for troposcatter is limited by the increased path loss. Angle diversity promised a workable alternative to the use of additional or larger antennas to combat the additional path loss. His experiments at 8 GHz established that effective diversity can be achieved with only a single transmitter beam and multiple receiver

beams. The correlation between beams was adequately small (<0.6) and for a center cluster of beams only a 1 or 2 dB median difference in signal strength was observed. The use of angle diversity on a long troposcatter path was reported by Travis[2.5] who showed that there was substantial signal strength in the elevated beams and that the fading was essentially uncorrelated. The correlation coefficients for horizontally displaced feeds, however, were greater than 0.6, reducing the usefulness of azimuthal AD on such a system. An angle diversity test described by Monsen[2.6] provided data on the long-term decorrelation of the hourly medians and found close agreement between a dual frequency and triple angle diversity system. The relatively large squint angle (~1.6 beamwidths) in this experiment made dual angle poorer than dual frequency diversity for nominal antenna pointing angles.

Troitskiy[2.7] also remarked on the long-term hourly median decorrelation advantage of angle diversity and provided correlation results of a long-term test program. Angle diversity tests reported on by Gough, et al.[2.8] showed good agreement with early theoretical work by Koono, Hirai, et al[2.9].

Previous work on angle diversity, however, did not appropriately assess the impact of the following considerations:

1. Frequency diversity requires two power amplifiers, whereas a theoretical angle diversity requires only one. From a reliability redundancy viewpoint or an equal total transmit power argument, the systems should be compared on the basis of two power amplifiers in each system. Any operational angle diversity system would require a second power amplifier as a reliability spare. This fact increases the received power in the main beam by 3 dB in an angle diversity system. This 3 dB increase offsets up

to a 6 dB* squint loss in the combined diversity output.

2. The effect of correlation between diversity signals is reduced when signals are wideband with respect to the reciprocal of the multipath spread and adaptive signal processing techniques are used.

In addition to these factors, the potential for angle diversity increases when one considers that major disadvantages of an analog angle diversity system either disappear or become advantages when angle diversity is applied to a digital system with adaptive signal processing. These disadvantages in an analog system are the variation in delay between angle diversity beams and increased multipath spread in the elevated beam. In analog systems these effects led to intermodulation distortion which sharply limited message capacity. In digital systems, delay variation can be compensated for by an adaptive equalizer and additional multipath can, in many cases, lead to better performance as a result of added implicit diversity. This result assumes that an equalizer type signal processor with a delay span large enough to accommodate the delay variation and multipath spread is used. In almost all applications considered in this study, a three tap equalizer with one-half QPSK symbol spacing was found to be adequate.

In this section we develop the major design considerations for angle diversity. The preceding discussion has established the importance of adaptive signal processing in the angle diversity application. Thus, before proceeding with the design considerations, a review of adaptive systems on digital troposcatter is provided. This review addresses in particular the impact of these systems on analog to digital conversion of troposcatter links and the role of angle diversity.

---

*A squint loss of S dB results in a S/2 dB combining loss because the error rate is a function of the geometric mean of the signal-to-noise ratios.

a. Adaptive Signal Processing for Digital Troposcatter Systems

Troposcatter radio transmission was discovered after World War II when it was noted that microwave signals from beyond the horizon radars were much stronger than predicted from diffraction calculations over the earth's surface. A commonly held theory of this phenomenon is explained by Tatarski[2.10]. The theory is that random fluctuations in the dielectric constant in the troposphere divert some small fraction of the impinging energy back to the receiver. The name tropospheric scatter or troposcatter derives from this concept of random redirection of the incident wave by the troposphere. Significant scatter returns occur from a "common volume" defined by the antenna beam patterns. Scatter returns from different points within the common volume have different path delays, and, when these signal scatter points are separated by more than the decorrelation distance of the dielectric constant fluctuations, the scatter returns are not correlated. The impulse response characterizing this channel has a time-varying continuous multipath structure. A statistical measure of the width of the troposcatter channel impulse response is the multipath delay spread.

Troposcatter systems have been widely used in military applications for beyond line-of-sight communications up to about 600 miles. The frequency range for this application extends from about 400 to 5000 MHz. Reliable communications require redundant transmission paths provided through the use of multiple frequencies, antennas separated in space, or scatter at two different beam angles. The several redundant paths are referred to as diversity paths. The number of paths is termed the order of diversity. The multipath delay spread limits the channel capacity which can be achieved in present analog systems. Only transmission bandwidths less than the reciprocal of this multipath delay can be achieved. Signals of larger bandwidths become distorted due to the multipath dispersion.

In FM systems this dispersion causes intermodulation noise after detection.

With the introduction of satellite communication systems, which do not suffer from extensive multipath fading, the future of troposcatter systems appeared to be limited. Economic and security factors have altered this assessment, particularly for digital transmission. With digital signal formats, adaptive methods can be devised to measure the multipath structure and exploit it as an extra form of diversity to improve performance. Unlike the capacity of analog systems, the capacity of digital systems is not restricted by the reciprocal of the multipath width. Also from a network viewpoint in a digital system, fades in tandem links do not have a cumulative effect because the signal can be regenerated at each node.

Applicability of adaptive signal processing techniques is critically dependent on whether the rate of fading is slower than the rate of signaling. For transmission rates of interest, troposcatter radio links can be considered to be slow fading multipath channels.

(1) The Learning and Diversity Constraints

For digital communication over beyond-the-horizon radio links, an attempt is made to maintain transmission linearity, i.e., the receiver output is a linear superposition of the transmitter input plus channel noise. This is accomplished by operation of the power amplifier in a linear region or with saturating power amplifiers using constant envelope modulation techniques. For linear systems, multipath fading can be characterized by a transfer function of the channel: $H(f,\cdot t)$. This function is the two dimensional random process in frequency f and time t that is observed as carrier modulation at the output of the channel when sine wave excitation at the carrier frequency is applied to the channel input. For any continuous random process, we can determine the minimum separation required to guarantee decorrelation with respect to each argument.

For the time varying transfer function $H(f,\cdot t)$, let t_d and f_d be the decorrelation separations in the time and frequency variables, respectively. If t_d is a measure of the time decorrelation in seconds, then

$$\sigma_t = \frac{1}{2\pi t_d} \text{ Hz}$$

is a measure of the fading rate or bandwidth of the random channel. The quantity σ_t is often referred to as the Doppler spread because it is a measure of the width of the received spectrum when a single sine wave is transmitted through the channel. The dual relationship for the frequency decorrelation f_d in Hz suggests that a delay variable

$$\sigma_f = \frac{1}{2\pi f_d} \quad \text{seconds}$$

defines the extent of the multipath delay. The quantity σ_f is often referred to as the multipath delay spread as it is a measure of the width of the received process in the time domain when a single impulse function is transmitted through the channel.

Typical values of these spread factors for troposcatter communication are

TROPOSCATTER

$\sigma_t \sim 1$ Hz: Doppler Spread

$\sigma_f \sim 10^{-7}$ seconds: Delay Spread

where the symbol $\sim$ denotes "on the order of".

The spreads can be defined precisely as moments of spectra in a channel model which assumes Wide Sense Stationarity

(WSS) in the time variable and Uncorrelated Scattering (US) in a multipath delay variable. This WSSUS model and the assumption of Gaussian statistics for $H(f,\cdot t)$ provide a statistical description in terms of a single two-dimensional correlation function of the random process $H(f,\cdot t)$.

This characterization has been quite useful and accurate for a variety of radio link applications. However the stationarity and Gaussian assumptions are not necessary for the utilization of adaptive signal processing techniques on these channels. What is necessary is first that sufficient time exist to "learn" the channel characteristics before they change and second, that decorrelated portions of the frequency band be excited such that a diversity effect can be realized. These conditions are reflected in the following two relationships in terms of the data rate R, the bandwidth B, and two previously defined channel factors, VIZ;

$R(b/s) >> \sigma_t(Hz)$ Learning Constraint

$B(Hz) \gtrsim f_d(Hz)$ Diversity Constraint.

where the symbol $\gtrsim$ denotes " on the order of or greater than ".

The learning constraint insures that sufficient signal-to-noise ratio (SNR) exists for reliable communication at rate R over the channel. Clearly if $R \sim \sigma_t$, the channel would change before significant energy for measurement purposes could be collected. When $R >> \sigma_t$, the received data symbols can be viewed as the result of a channel sounding signal and appropriate processing can generate estimates of the channel character during that particular stationary epoch. The signal processing techniques in an adaptive receiver do not necessarily need to measure the channel directly

in the optimization of the receiver but the requirements on learning are approximately the same. If only information symbols are used in the sounding signal, the learning mode is referred to as Decision-Directed. When digital symbols known to both the transmitter and receiver are employed, the learning mode is called Reference-Directed. An important advantage of digital systems is that in many adaptive communications applications, adaptation of the receiver with no wasted power for sounding signals can be accomplished using the decision-directed mode. This is possible in digital systems because of the finite number of parameters or levels in the transmitted source symbols and the high likelihood that receiver decisions are correct.

Diversity in fading applications is used to provide redundant communications channels so that when some of the channels fade, communication will still be possible over the others that are not in a fade. Some of the forms of diversity employed are space using multiple antennas, angle of arrival using multiple feedhorns, polarization, frequency, and time. These diversity techniques are sometimes called explicit diversity because of their externally visible nature. An alternate form of diversity is termed implicit diversity because the channel itself provides redundancy. In order to capitalize on this implicit diversity for added protection, proper receiver techniques have to be employed to correctly assess and combine the redundant information. The potential for implicit frequency diversity arises because different parts of the frequency band fade independently. Thus, while one section of the band may be in a deep fade the remainder can be used for reliable communications. However, if the transmitted bandwidth B is small compared to the frequency decorrelation interval f_d, the entire band will fade and no implicit diversity can result. Thus, the second constraint $B \geq f_d$ must be met if an implicity diversity gain is to be realized. In diversity systems a little decorrelation between alternate signal paths can provide significant diversity gain.

It is easy to establish that for the transmission rates of interest, troposcatter systems satisfy both the learning and diversity constraint. Digital troposcatter systems are being planned with data rates on the order of 5 Mb/s with approximately the same bandwidth. The constraints are then

$$R = 5 \times 10^6 >> \sigma_t \sim 1: \text{ Learning Constraint}$$

$$B = 5 \times 10^6 \gtrsim f_d \sim 1.6 \times 10^6: \text{ Diversity Constraint}$$

This means that adaptive signal processing techniques can be applied to the digital troposcatter receiver with the result that channel variations can be tracked and additional diversity due to multipath will be realized. Note this result is opposite to present analog technology where channel tracking using the received information signal is not possible and multipath degrades rather than helps performance. This concept has been successfully exploited to realize an increase in digital rate capability of about an order of magnitude. A digital modem technique [2.11,2.12] using an adaptive decision-feedback equalizer has been successfully field tested at digital rates up to 12.6 Mb/s in a 15 MHz RF bandwidth allocation. We shall see subsequently that not only does this new technology make angle diversity more feasible to implement but angle diversity provides a large potential for bandwidth conservation in the new digital systems.

(2) Conversion to Digital Troposcatter Systems: Bandwidth Considerations

The majority of troposcatter link traffic consists of speech transmissions. In an analog system these signals are frequency division multiplexed in 4 KHz subchannels to produce a baseband spectrum of approximately 60 KHz + N x 4 KHz, where N is the number of voice channels. The FM system expands this bandwidth depending on the selected frequency deviation. If we

let Δf_{rms} be the rms frequency deviation per channel, the peak frequency deviation is $\sqrt{2N}\ \Delta f_{rms}$ and using Carson's rule, the FM RF bandwidth is approximately

$$B_{RF} = 2\ (4N+60+\sqrt{2N}\ \Delta f_{rms})\ \text{KHz}.$$

For a 120 channel system with a typical 150 KHz rms frequency deviation, the RF bandwidth is 5.7 MHz.

A 120 channel digital system with 64 Kb/s Pulse Code Modulation (PCM) requires a data rate of approximately 8 Mb/s when framing and overhead are added. This example illustrates the general result that conversion of troposcatter systems from aaalog to digital requires modem technology with better than 1 bit/second/Hz packing if the spectral requirements for the same number of message channels is to be unchanged. Present modem technology[2.11,2.12] achieves 1 bit/second/Hz packing in the troposcatter channel but degrades with larger densities. At 1.3 bit/second/Hz the degradation is about 1 dB. In many cases the best solution is to combine spectrum efficient modem technology with a diversity configuration that minimizes system spectral occupancy. Angle diversity in conjunction with space diversity achieves minimum system spectral occupancy.

(3) Angle Diversity for Bandwidth Conservation

Conventional troposcatter systems use two antennas per terminal and two bandwidth allocations per direction to achieve dual space/dual frequency (2S/2F) diversity. Angle diversity provides redundant paths by collecting different angle of arrival signals at the receiver. A dual angle diversity system, for example, would employ a two horn primary feed at the parabolic reflector focus instead of the conventional one horn primary feed. In the frequency diversity system, a power amplifier is required at each of the two RF carriers. To convert from dual

frequency to dual angle, the second power amplifier is tuned to the same frequency as the first and a new feed structure is provided. The resulting dual space/dual angle (2S/2A) system now requires only one bandwidth allocation in both directions. Conversion to angle diversity halves the frequency requirements of present 2S/2F quadruple diversity systems. Since both diversity configurations have 4 diversity outputs, the systems are identical from the input to the receivers down through the modem to the data output. Figures 2.1 and 2.2 illustrate the 2S/2F and 2S/2A configurations. The 2S/2A system does not require a diplexer as does the 2S/2F system, but an additional waveguide run is needed from the feedhorn to the receivers. The 2S/2F system requires transmitters tuned to two frequencies, a single horn feed, and diplexers to separate the frequencies. The 2S/2A system has both transmitters tuned to the same frequency and a dual horn feed. The receivers and modem are identical in both configurations. The second transmitter in the 2S/2A configuratin is required for redundancy in case of failure. Its on-the-air use provides 3 dB more scattered power per diversity which tends to offset the squint loss from the elevated beam in the dual angle diversity structure.

This savings in bandwidth through use of angle diversity is potentially present with analog troposcatter systems, but it is largely dissipated by the more difficult implementation disadvantages of analog angle diversity. In an analog system, the time delay variation between the main and elevated beam and the additional multipath spread of the elevated beam are serious problems. The adaptive processor concept previously described for the troposcatter application compensates for these effects in a digital system. The compensation takes the form of adaptive equalization using the received signal in a decision-directed technique.

DUAL SPACE/DUAL FREQUENCY (2S/2F)
QUADRUPLE DIVERSITY TROPOSCATTER TERMINAL

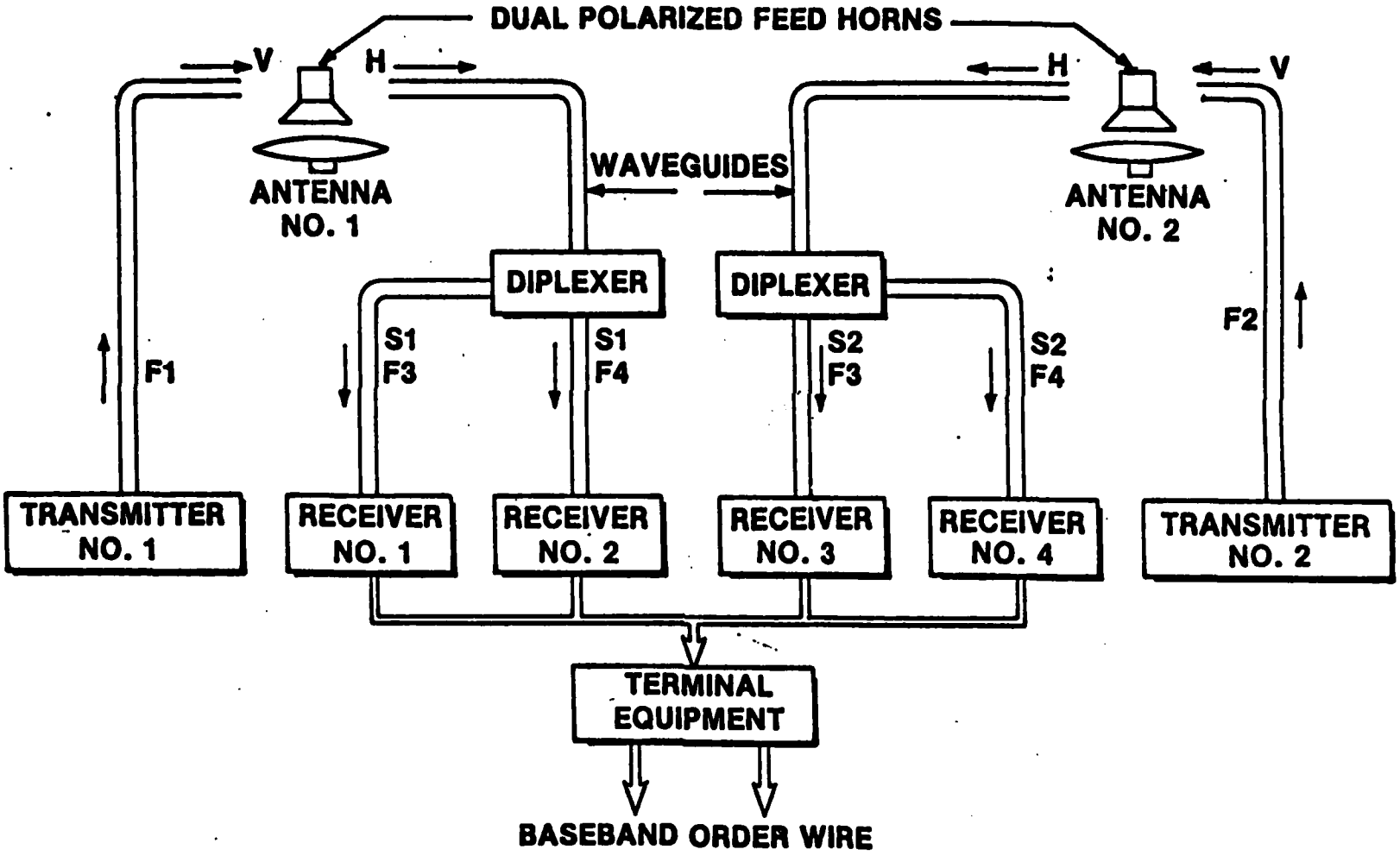

Figure 2.1 2S/2F CONFIGURATION

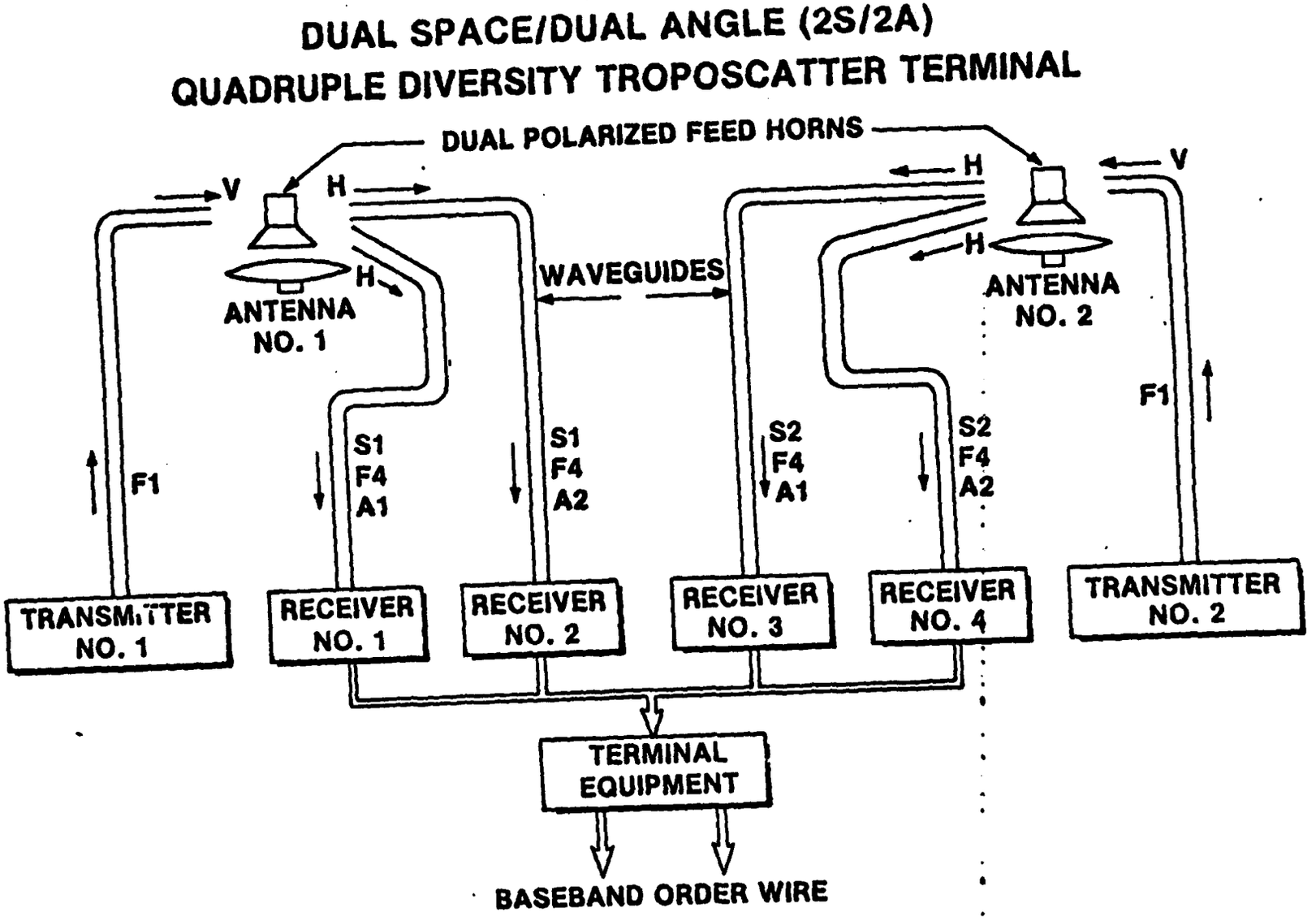

Figure 2.2 2S/2A CONFIGURATION

b. Angle Diversity Design

The short term (~ seconds) fading characteristics of troposcatter signal reception are mitigated by the provision of redundant, i.e., diversity, channels and an associated combining scheme to utilize the stronger received signals and eliminate the weaker ones. One method of realizing additional diversity channels is to use multiple feedhorns at the focal point of a parabolic reflector to realize multiple angle of arrival signals. This method is normally only employed at the receiver since the production of multiple transmit beams requires either additional power amplifiers or a reduction in power with power splitters. Thus, conventional angle diversity has one transmit beam and two or more angle of arrival receive beams.

One of the first questions a system designer may ask concerns the relative advantages of beams spread either vertically or horizontally. Since the diversity advantage stems from the lack of correlation between the two received diversity signals, the correlation fall-off as a function of squint angle in the vertical and horizontal directions is the determining factor in assessing the performance difference. The power loss fall-off as a function of squint angle is of the same order for the two directions and therefore is not significant in the selection process. The correlation fall-off as a function of squint angle can be related to the correlation distance in the plane of the receive antenna. The correlation distance r_c may be defined in terms of two point antennas, one located on the great circle path and one at a distance r_c, where the received processes on the two point antennas have a normalized correlation coefficient of 1/e. Clearly if the correlation distance is much greater than the troposcatter system parabolic reflector then the correlation between squinted beams will be very high whereas if the correlation distance is

small compared to the parabolic reflector the squinted beam correlation will be small. The correlation distance is defined in terms of a vector $\underline{u}$ in the plane of the parabolic reflector as

$$\varphi(\underline{u}) = \overline{E(\underline{r})\ E^{*}(\underline{r} + \underline{u})}$$

where $E(\underline{r})$ is the received electric field at a distance $\underline{r}$ from the center of the scattering volume. This spatial correlation function is related to the scattering volume "size" through a three dimensional Fourier integral

$$\varphi(\underline{u}) = C \iiint V(\underline{r}')\ e^{jk \frac{\underline{u}\cdot\underline{r}'}{r}}\ d^3r' \ .$$

The integration is over the scattering volume defined by $V(\underline{r}')$ which is determined by the antenna gain patterns and the refractive index spectrum fall-off as a function of scattering angle. The constant k is equal to $2\pi f_o/c$ where f_o the carrier frequency and c is the speed of light. Now Fourier variables in one domain are inversely related to Fourier variables in the other domain, e.g., a short time pulse corresponds to a wide frequency band. Thus the correlation distance in a particular direction at the receiver is inversely related to the common volume size in that same direction. In Fig. 2.3 we examine the common volume dimensions in the vertical (side view) and horizontal (top view) directions. For angle diversity systems, the transmit beamwidth Ω is typically smaller than the minimum scattering angle θ_o in order to minimize the loss associated with the squinted beam. The common volume "size" in the horizontal direction is then limited by the transmit beamwidth and is on the order of $\gamma_H r \doteq \Omega r$. In the vertical direction, the common volume "size" is not limited by the beamwidth as much as the re-

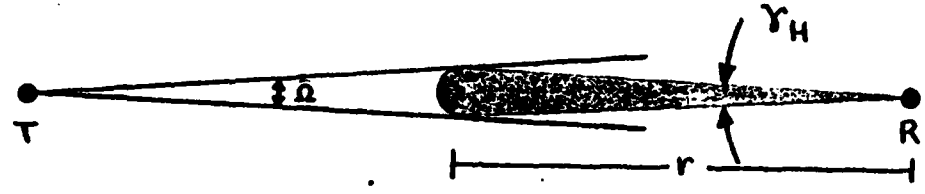

TOP VIEW

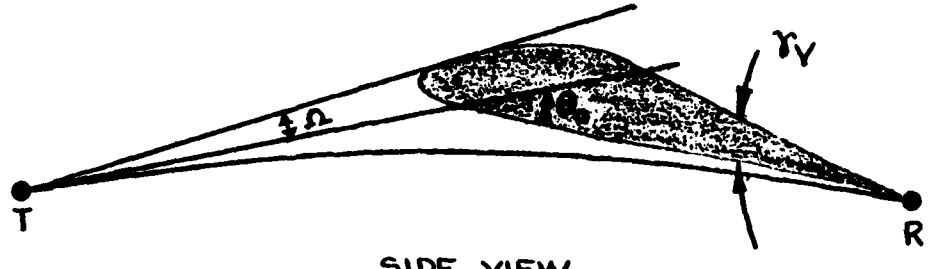

SIDE VIEW

Fig. 2.3 Troposcatter Path Structure

fractive index spectrum fall-off which has a dependence of $\theta^{-11/3}$ where θ is the scattering angle. Since $\theta > \theta_o > \Omega$ the vertical common volume size $\gamma_V r$ is larger than the horizontal common volume size $\gamma_H r$. The area of useful scattering energy returned to the receiver is figuratively shown in Fig. 2.3 as a shaded area. Since $\gamma_V > \gamma_H$ it follows that the vertical correlation distance will be <u>less</u> than the horizontal correlation distance for narrow beamwidth antennas. Thus the vertical angle diversity system will result in a lower correlation between squinted beams than a horizontal angle diversity system.

It turns out that as the transmit beamwidth is increased such that $\Omega >> \theta_o$, the situation reverses and γ_V becomes smaller than γ_H with the result of a smaller horizontal correlation distance than vertical. This result is consistent with "fat" transmitter beam measurements and analysis [2.4] of correlation distances in the vertical and horizontal planes. However, in any practical application, the transmit beams must be narrow in order to provide the required antenna gain for successful operation.

Because the vertical correlation distance is smaller than the horizontal correlation distance for practical systems, the angle diversity design should utilize a vertical squinted beam as the first additional angle of arrival signal. The use of more angle of arrival signals than two is not advantageous both because of system complexity and the diminishing return from additional diversity. Thus we fix the system design as a dual feedhorn AD system and turn our attention to the choice of vertical squint angle and antenna boresight/horizon angle.

The angle between the centerlines of the antenna patterns of the two feedhorns in a dual AD system is defined as the squint angle. When the squint angle is appreciably more than a beamwidth,

the correlation between the received angle diversity signals is small but the relative signal loss of the elevated beam may be excessive due to the increased scattering angle. Decreasing the squint angle reduces this loss but increases the correlation between diversity signals. The effect of this correlation is to reduce the diversity gain. It becomes necessary to distinguish between narrowband and wideband correlation effects on diversity combining loss. When the diversity signals are smeared by a multipath spread that has width on the order of the reciprocal of the signal bandwidth, the correlation between diversity signals also becomes smeared. Thus the diversity combining loss due to diversity beam correlation is less for wideband (~ on the order of a reciprocal multipath spread) than for narrowband (much less than a reciprocal multipath spread) transmissions. In the propagation/modem model developed under this program the effects of correlation on wideband signaling is correctly taken into account through the introduction of a cross channel multipath profile. For narrowband signaling the signal correlation loss can be expressed at large signal-to-noise ratios as

$$L = -5 \text{ LOG}(1-\rho^2) \qquad \text{(Narrowband Correlation Loss)}$$

where ρ is the normalized correlation coefficient between two complex Gaussian processes.

A simplified model developing the wideband correlation loss has not been derived. Instead we use an exact analysis requiring numerical integration over the common volume. The propagation prediction model and the modem performance model described subsequently in Sections 3 and 4, respectively are used to generate modem performance curves as a function of vertical squint angle. The performance measure used is outage rate defined as the probability that the short term 0.2 to 5 second bit error rate (BER) exceeds a value of 10^{-4}. The BER criterion of 10^{-4} has been selected by the Defense Communications Agency because at this level PCM voice begins to degrade. The use of outage rate has been established as a more meaningful performance measure with respect to digitized voice than

the use of average error rate. The results of the outage rate calculations for an example C-band and L-band (255-985 MHz) link are shown in Figures 2.4 and 2.5. These curves reflect the effects of both squint loss and diversity correlation as a function of squint angle measured in beamwidths (BW). The two examples have approximately the same main beam multipath spread. ($2\sigma_{MB}/T=0.45$). Figure 2.4 represents the RADC Youngstown-Verona test link while Figure 2.5 is the DCS SAHIN Tepesi-Yamanlar link.

The wideband correlation loss can be isolated by noting that the diversity loss in the absence of correlation is approximately one-half the squint loss.

Performance measures with unequal branch SNR in dB are well approximated by the geometric mean of the SNR or the arithmetic mean in dB. Thus by comparing the diversity loss of specific squint angle cases with a case with zero correlation coefficient, the wideband correlation loss can be computed from the curves of Figures 2.4 and 2.5. These computations are summarized in Tables 2.1 and 2.2. Note that the optimum squint angle is 1 beamwidth for narrowband signaling but at 6.3 Mb/s on these links the best performance occurs at 3/4 beamwidth due to smaller correlation effects in wideband transmission. Plots of the correlation coefficients and the wideband and narrowband correlation losses are given in Figures 2.6 and 2.7 for the two examples. The reduced effect of correlation between angle diversity branches with wideband signaling is due to the adaptive equalizer acting to combine individual multipath components on diversity pairs. These individual multipath components have less correlation than the correlation from the cumulative multipath structure.

In these examples and all others computed, the optimum squint angle was determined to be approximately 1 beamwidth for narrowband signaling and 3/4 beamwidth for wideband signaling. Thus, it is clear that the best squint angle for megabit data rates in angle diversity systems is less than one beamwidth. Feedhorn design constraints, however, make it difficult to achieve squint angles this small. Fortunately, the dB loss is small for squint

Fig. 2.4 Outage Rate for C-band Link

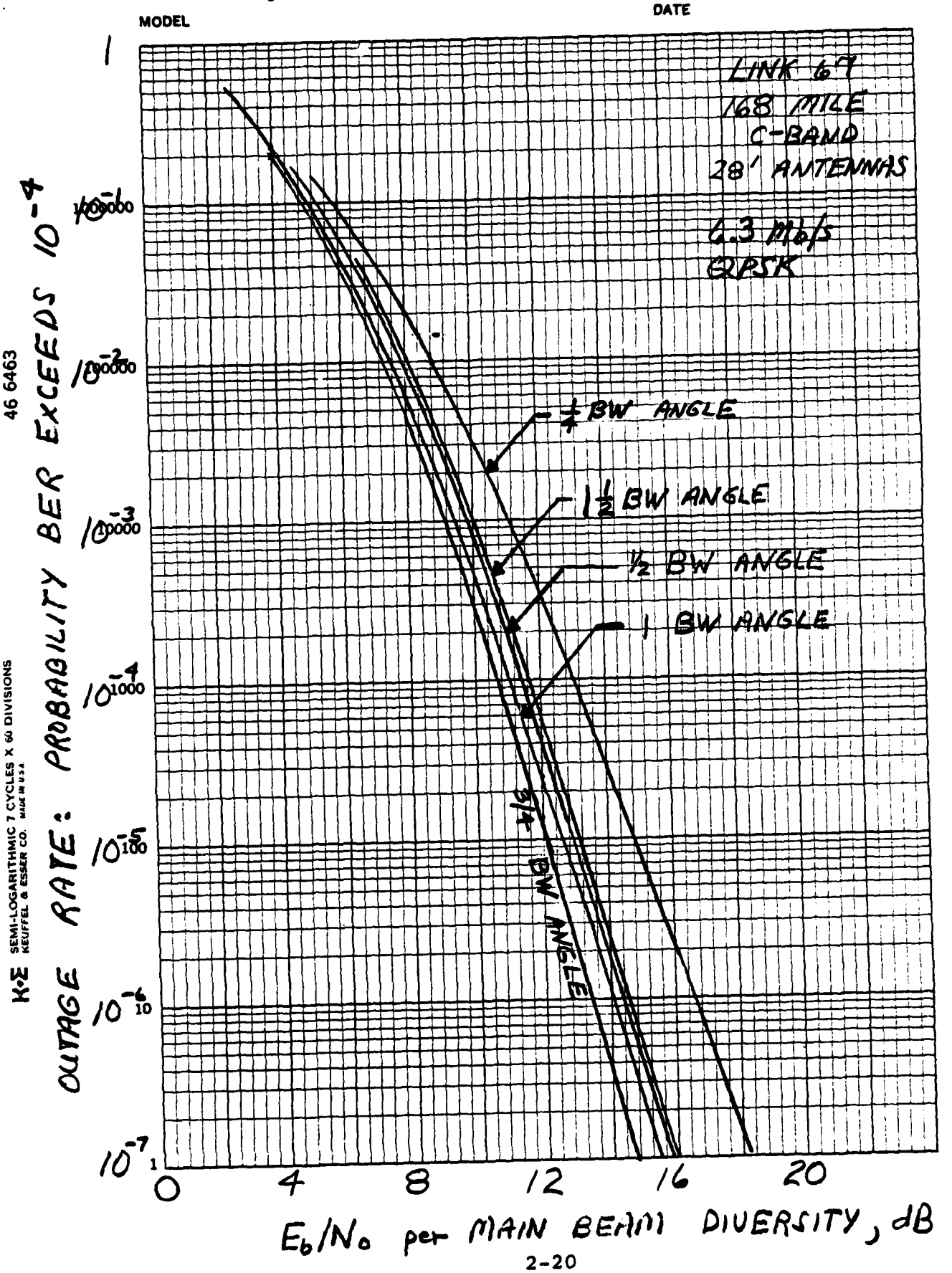

Fig. 2.5 Outage Rate for L-band Link

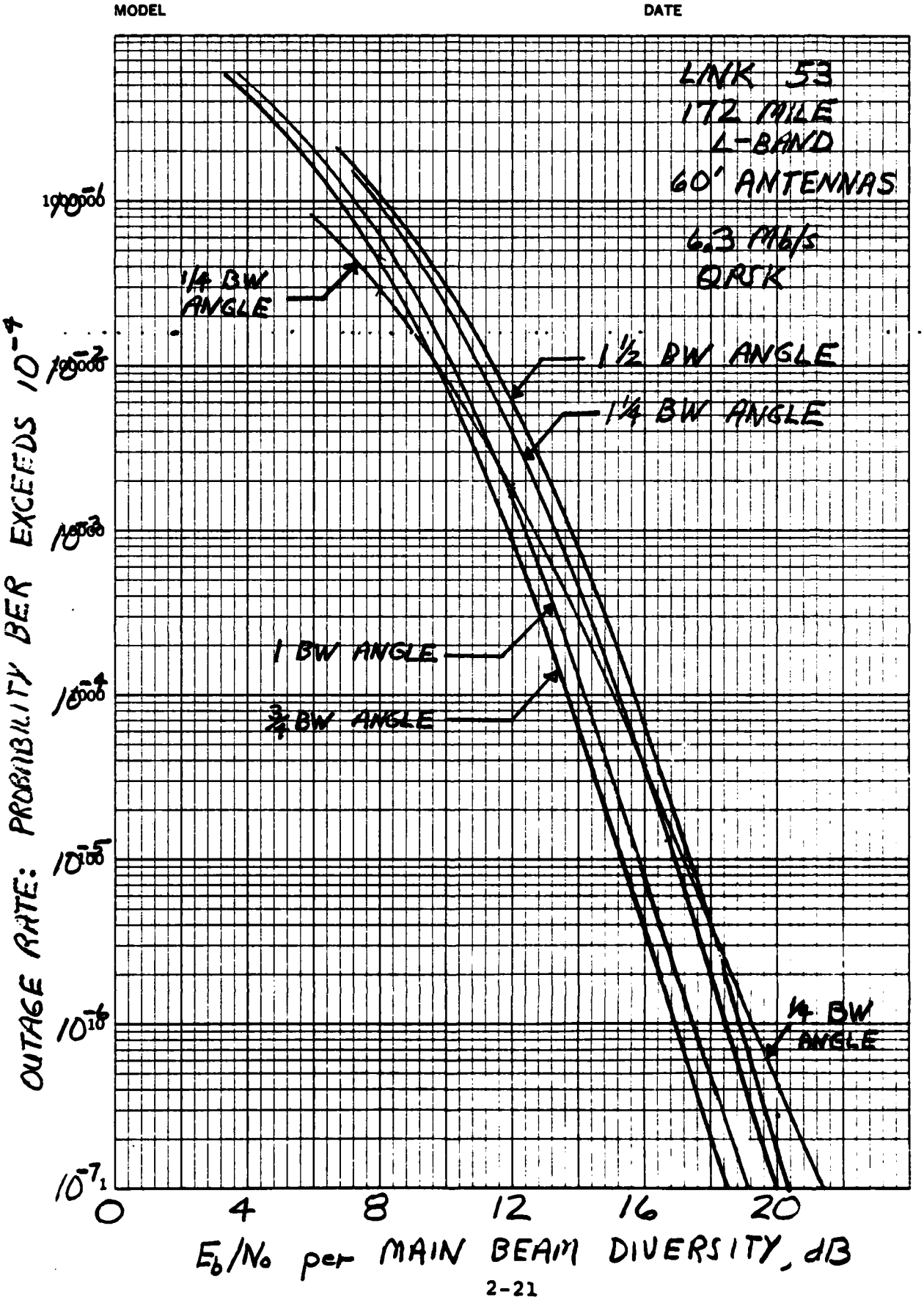

Table 2.1

Wideband Correlation Loss, RADC Youngstown-Verona Lind (C-band)

BEAM SEPARATION (beamwidth)	HALF SQUINT LOSS (dB)	CORRELATION COEFFICIENT	NARROWBAND CORRELATION LOSS (dB)	TOTAL NARROWBAND LOSS (dB)	TOTAL WIDEBAND LOSS* (dB)	WIDEBAND CORRELATION LOSS (dB)
$1\frac{1}{2}$	1.6	-0.11	0	1.6	1.6	0
$1\frac{1}{4}$	1.3	0.05	0	1.3	1.3	0
1	1.0	0.30	0.2	1.2	1.0	0
$\frac{3}{4}$	0.6	0.60	1.0	1.6	0.9	0.3
$\frac{1}{2}$	0.3	0.83	2.5	2.8	1.4	1.1
$\frac{1}{4}$	0.1	0.96	5.5	5.6	2.7	2.6

*Loss at 10^{-3} outage rate for BER Threshold level of 10^{-4}

Table 2.2

WIDEBAND CORRELATION LOSS, DCS SAHIN TEPESI-YAMANLAR (L-BAND)

BEAM SEPARATION (beamwidth)	HALF SQUINT LOSS (dB)	CORRELATION COEFFICIENT	NARROWBAND CORRELATION LOSS (dB)	TOTAL NARROWBAND LOSS (dB)	TOTAL WIDEBAND LOSS* (dB)	WIDEBAND CORRELATION LOSS (dB)
$1\frac{1}{2}$	5.6	-0.41	0.4	6.0	5.6	0
$1\frac{1}{4}$	4.9	0	0	4.9	4.9	0
1	3.8	0.41	0.4	4.2	4.0	0.2
$\frac{3}{4}$	2.4	0.76	1.9	4.3	3.5	1.1
$\frac{1}{2}$	1.1	0.92	4.1	5.2	4.3	3.2
$\frac{1}{4}$	0.3	0.985	7.6	7.9	4.3	4.0

*Loss at 10^{-3} outage rate for BER Threshold level of 10^{-4}

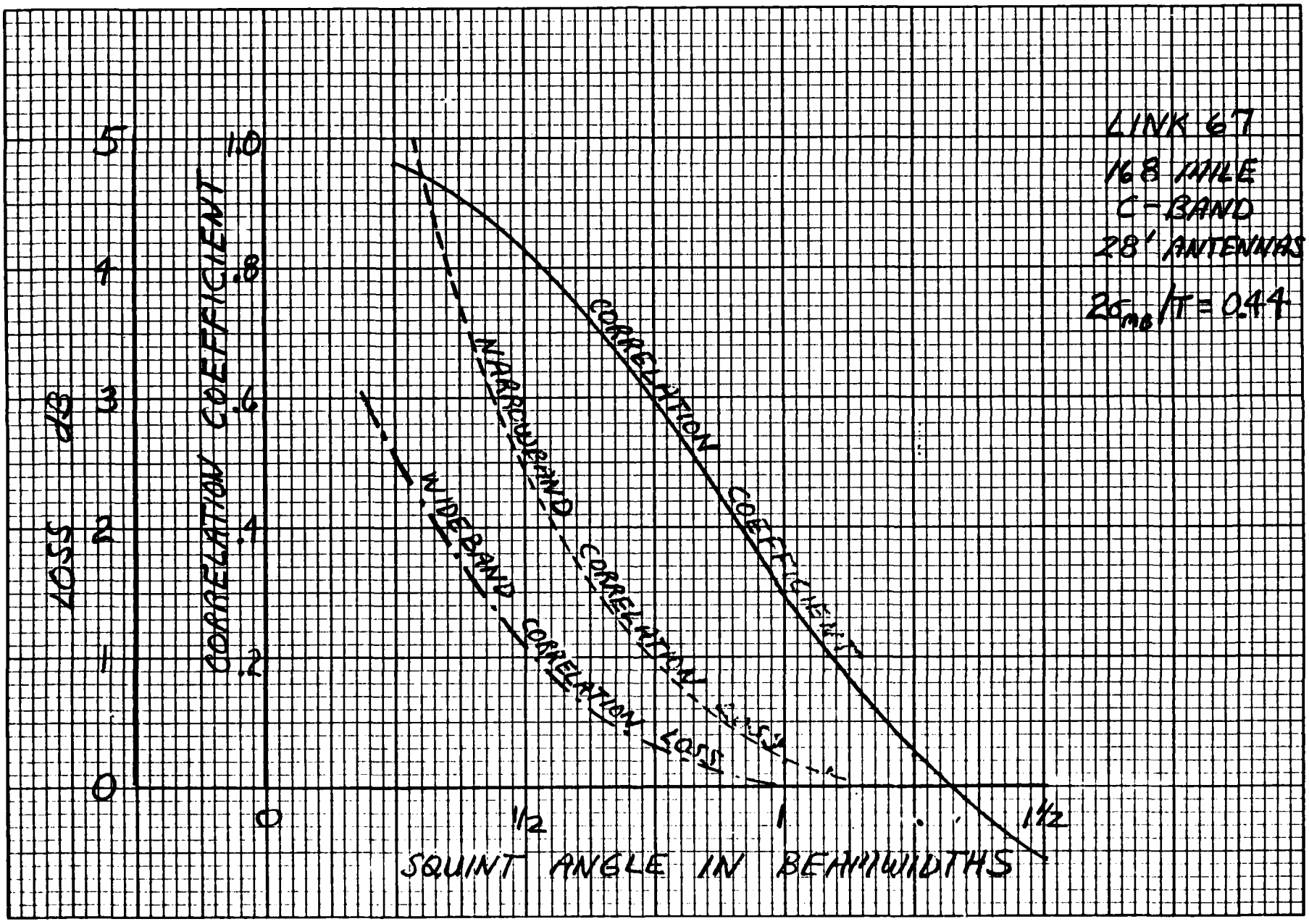

Fig. 2.6 Correlation Loss, C-band Link

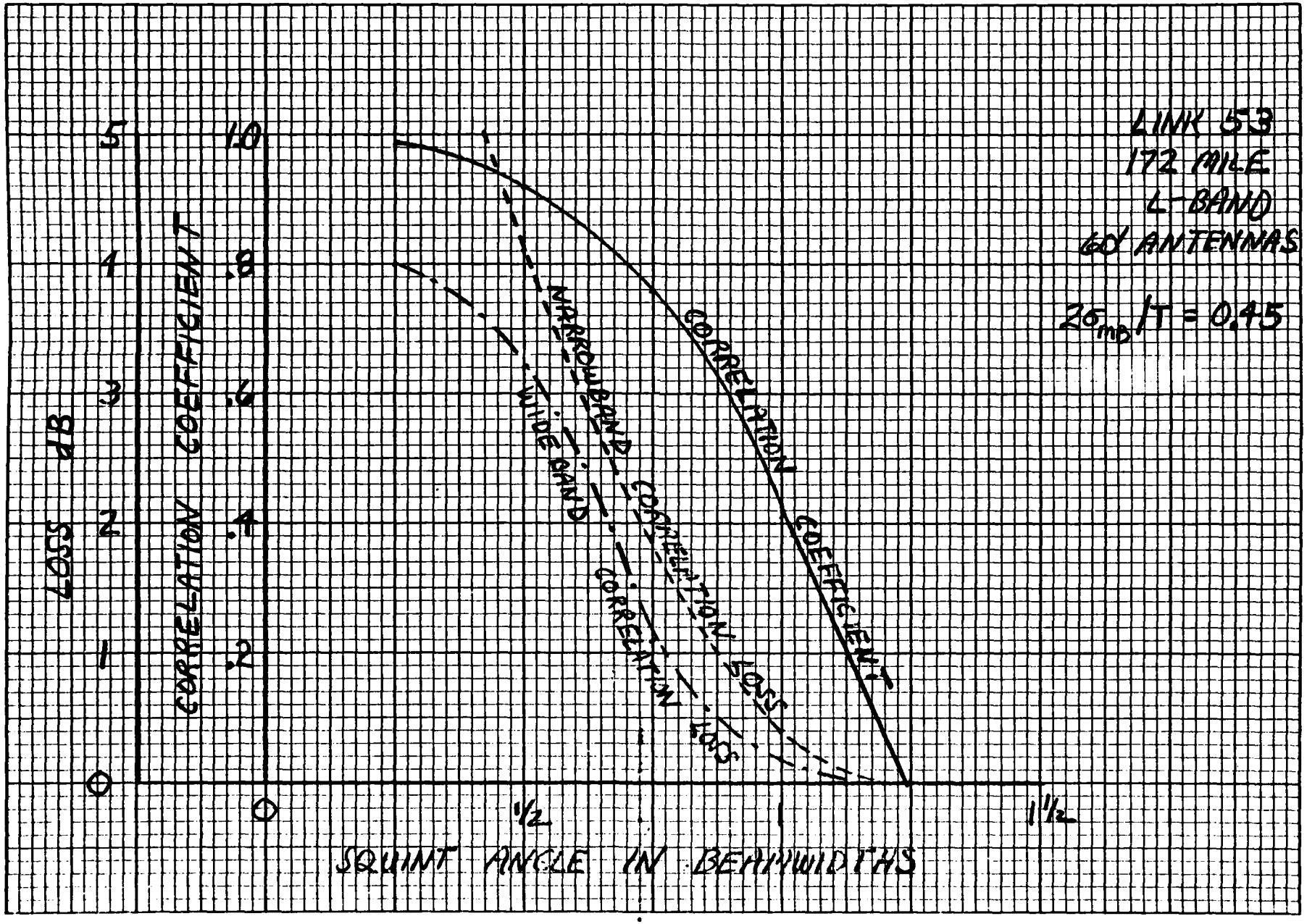

Fig. 2.7 Correlation Loss, L-band Link

angles larger than 3/4 beamwidth. Because of the feedhorn design problem, this result has important practical implications. The feedhorn design for the RADC test link resulted in the measured squint angles given in Table 2.3. Vertical polarization is used for signal reception in the RADC tests. The additional loss for this link resulting from a squint angle larger than 3/4 beamwidth can be determined from Fig. 2.4 to vary between 0.3 and 0.8 dB.

Table 2.3

Test Link Squint Angles

	Right Antenna		Left Antenna	
	H Pol.	V Pol.	H Pol.	V Pol.
Squint Angle	0.65°	0.73°	0.55°	0.68°
Half-Power Beamwidth	0.55°	0.53°	0.50°	0.50°

The next question to be addressed is the choice of antenna pointing angle, i.e., the angle between the main beam antenna pattern centerline (boresight) and the horizon. As this angle is decreased, the relative loss of the elevated beam is reduced but more of the main beam pattern is blocked by the radio horizon. Thus an optimum pointing angle exists. Since operational angle diversity system are utilized in both directions, the boresight/horizon angles at transmitter and receiver are constrained to be equal in the optimization search. Using a squint angle of one beamwidth*, the main beam loss for a conventional system was determined as a function of antenna pointing angle and in addition the diversity combining loss due to squint loss and narrowband correlation was computed. The minimum of the sum of these

*The design goal for the feedhorn

losses establishes the optimum pointing angles. The results for 3 example systems are shown in Figs. 2.8 - 2.10. In these and other examples the optimum boresight/horizon angle for the transmit and receiver antennas was found to fall between 1/4 and 1/2 beamwidth elevation above the local horizon. This result was only slightly influenced by the frequency of operation since lower frequency systems usually use larger antennas.

Note that the major effect in the optimization is the rapid increase in main beam loss when earth blockage begins to occur. For this reason correlation and squint loss have a small effect on the choice of optimum pointing angle. This large dependence on main beam blockage also establishes that the optimum pointing angles for conventional and angle diversity systems are approximately the same. Although other researchers have suggested in the past that an attempt to equalize the main and elevated beams is desirable, these results show that the main beam blockage from such a strategy would lead to an overall degradation. Under homogeneous atmospheric conditions, when the main beam signal is maximized, the elevated beam signal will be somewhat smaller. The frequent occurrence of nonhomogeneous atmospheric conditions causes the elevated beam signal to be stronger than the main beam signal. This phenomenon makes it necessary to aim the antenna system with a series of tests extending over at least several days in order to preclude pointing the antenna into the ground as a result of nonhomogeneous atmospheric conditions. It is likely that most DCS troposcatter antenna systems are aimed too low and 2 or 3 dB could be gained by careful aiming techniques.

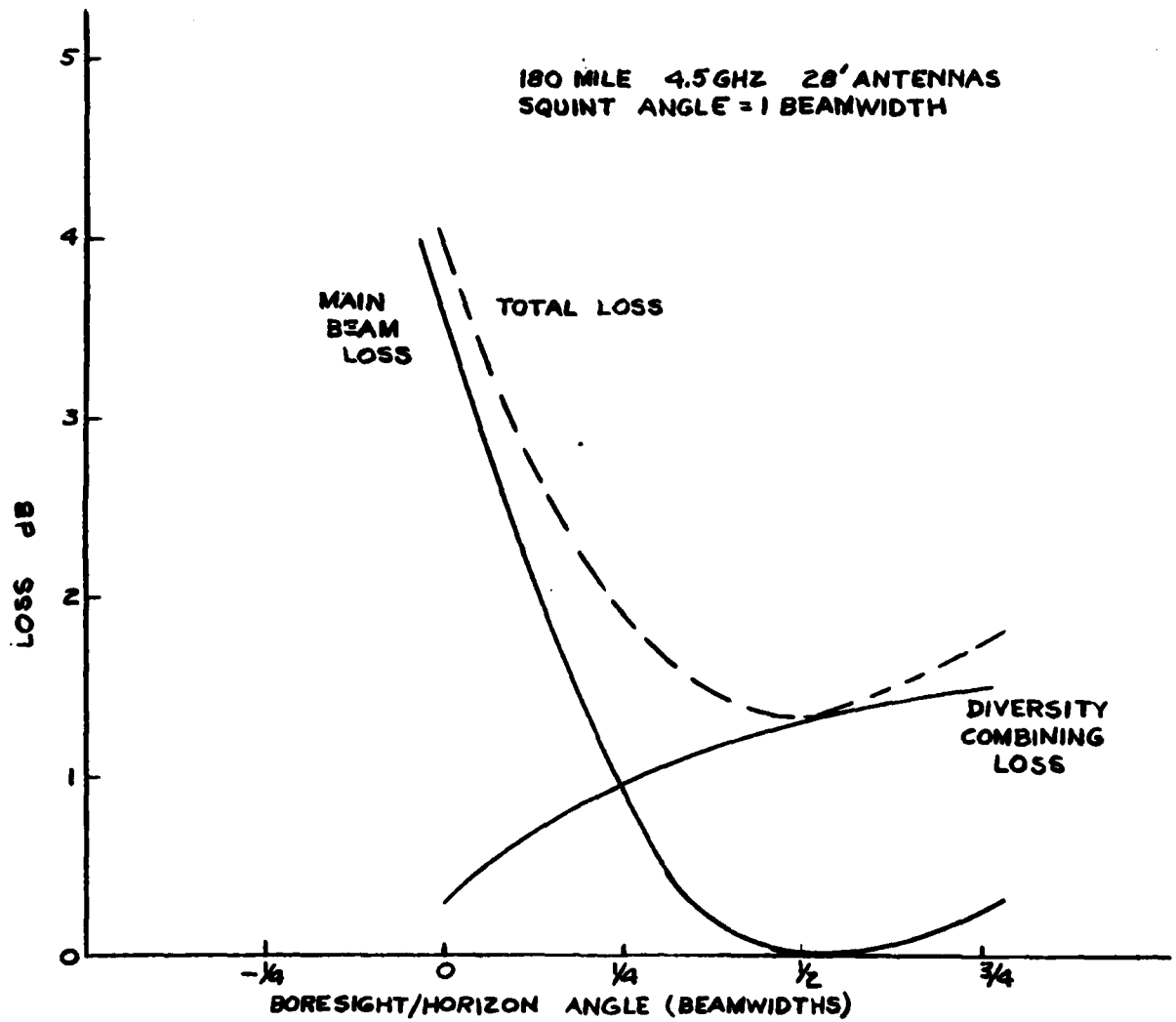

Fig. 2.8 Antenna Pointing Angle Optimization, RADC Test Link

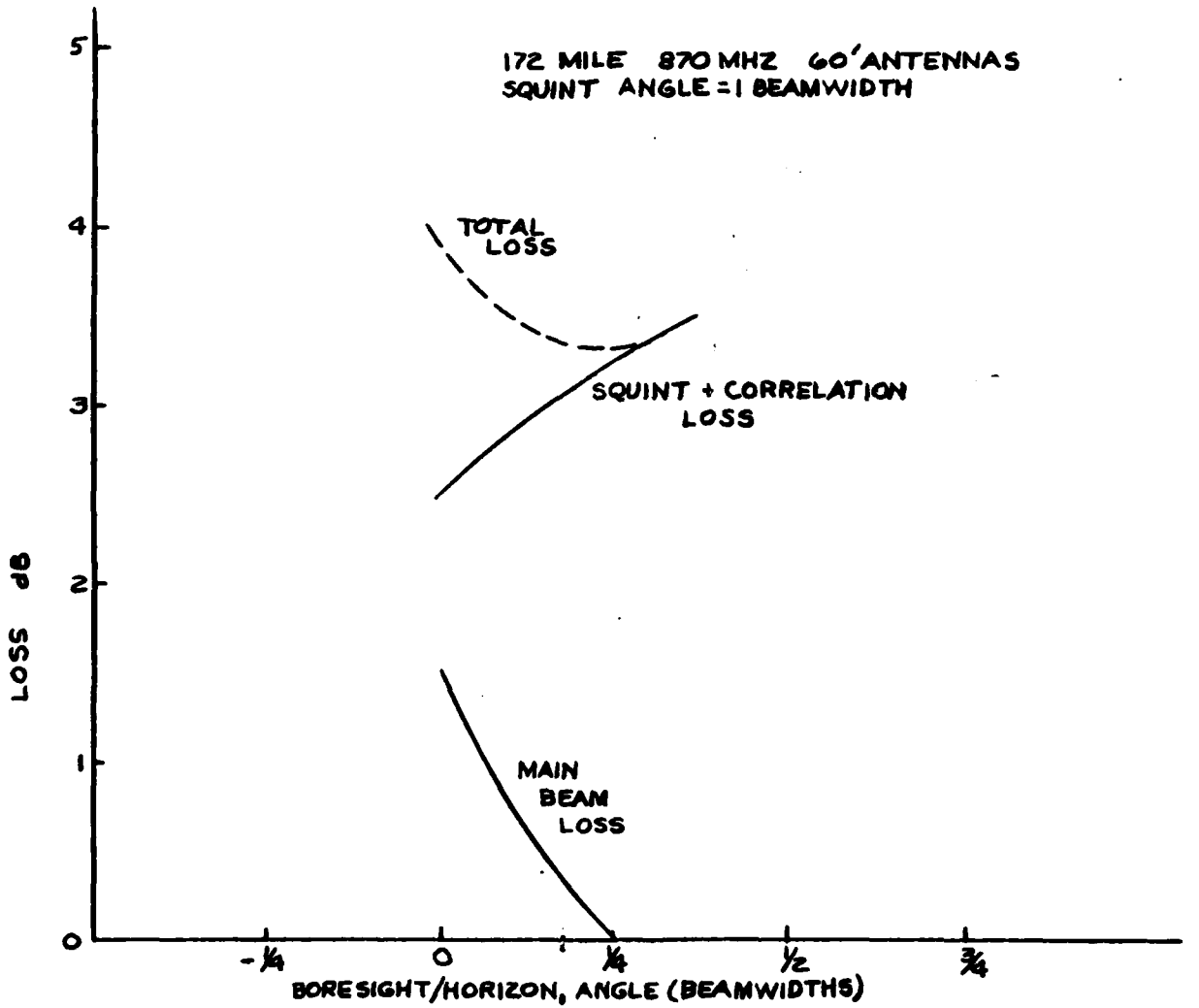

Fig. 2.9 Antenna Pointing Angle Optimization, S. Tepesi-Yamanlar

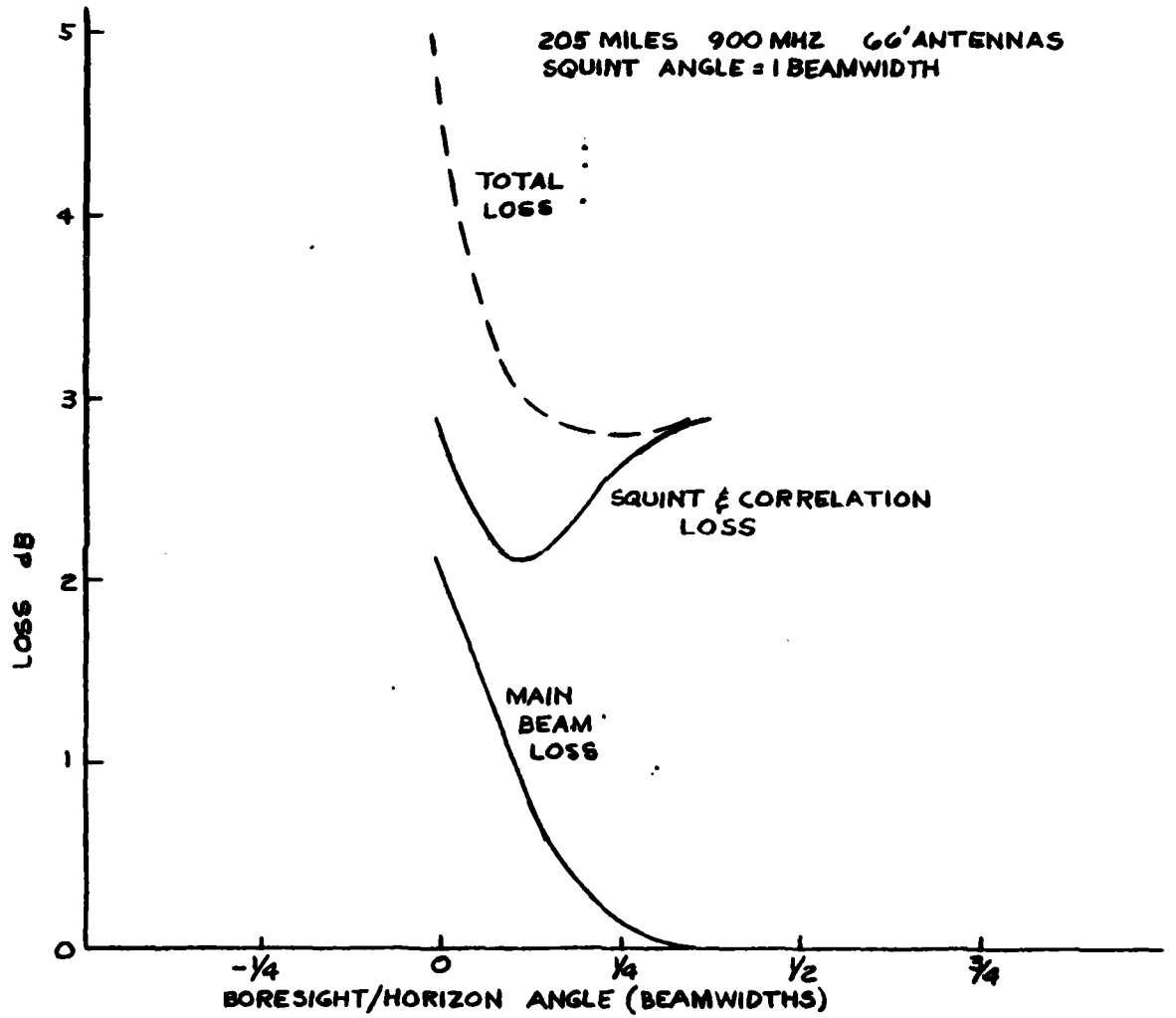

Fig. 2.10 Antenna Pointing Angle Optimization, Oslo-Kristiansand

A final consideration in choice of antenna pointing angle is the effect of increased multipath in both beams due to larger pointing angles. Because digital modems can utilize the multipath to increase the effective diversity order if the multipath spread is not too large, it is advantageous to choose a somewhat larger pointing angle if the nominal multipath spread is small compared to the data symbol interval. However, for L-band systems the multipath spread, particularly in the elevated beam, may exceed the multipath capabilities of the digital modem. In this situation degraded performance due to intersymbol interference results.

The results from the numerical integration of the common volume using a turbulent scattering hypothesis are shown in Figs. 2.11 - 2.13 for the example systems. The 2σ multipath spread of the product beam refers to the cross channel multipath profile. The C-band test link has small multipath spread* for data rates of interest and because of the small dB loss associated with larger pointing angles, the optimum pointing angle for a digital AD system is probably very close to the optimum pointing angle for a conventional 2S/2F analog troposcatter system, i.e., approximately 1/2 beamwidth. For the L-band systems there is considerably more multipath and a steeper slope with pointing angle. Optimum performance of a digital AD system at these frequencies may result from pointing angles somewhat less than 1/4 beamwidth.

In summary an optimized angle diversity system utilizes a squint angle of approximately 3/4 beamwidth with a boresight/horizon angle approximately equal to 1/2 beamwidth for C-band digital systems and somewhat less than 1/4 beamwidth for L-band systems. Under homogeneous atmospheric conditions this configuration results in less received signal power in the elevated beam. The use of pointing angles at much less than 1/4 beamwidth is suboptimum because too much power is blocked in the main beam by the radio horizon.

---

*Measured results from C-band systems tend to be larger due to the inclusion of the RF terminal equipment filter characteristics and measurement noise.

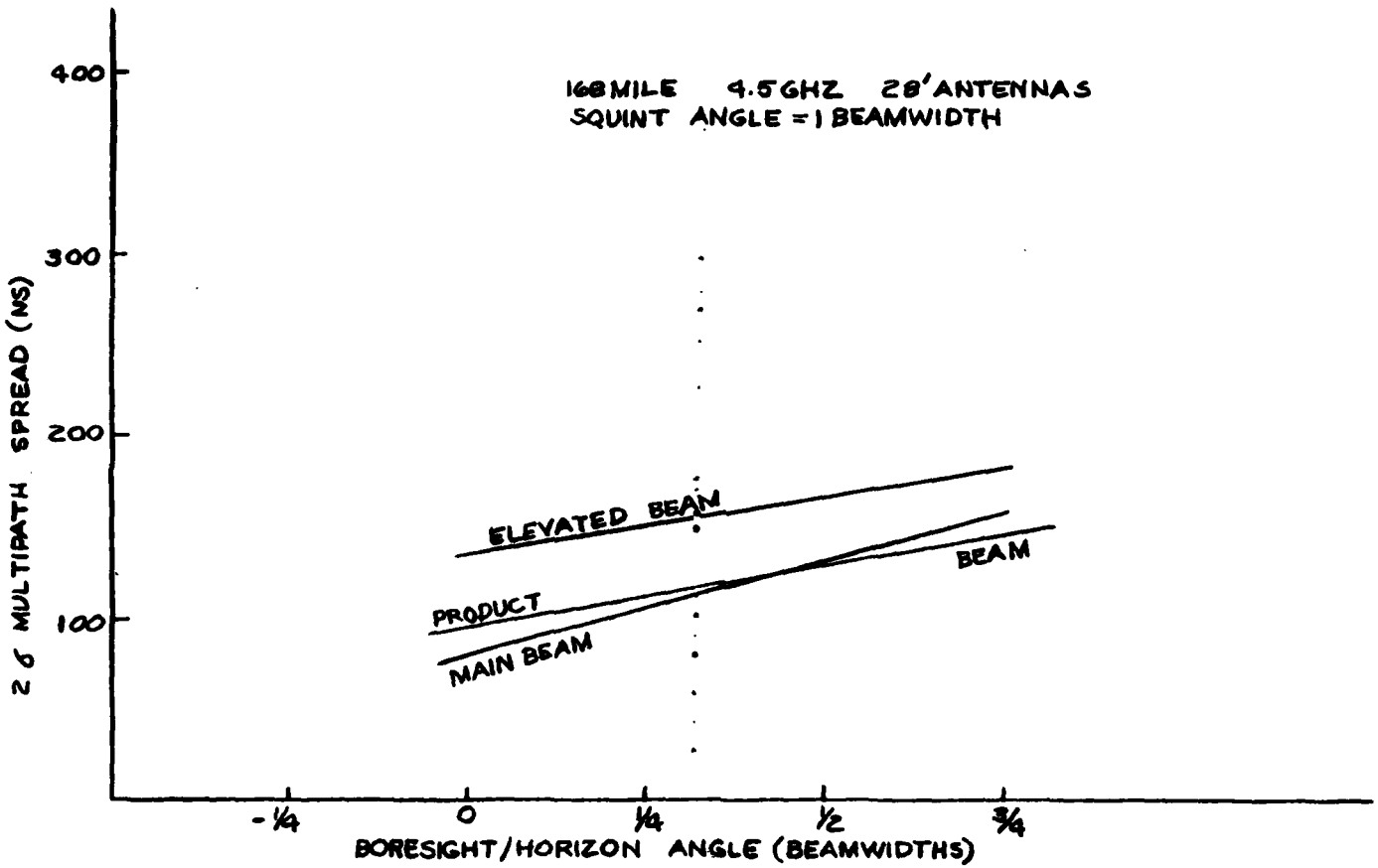

Fig. 2.11 Multipath Characteristics, RADC Test Link

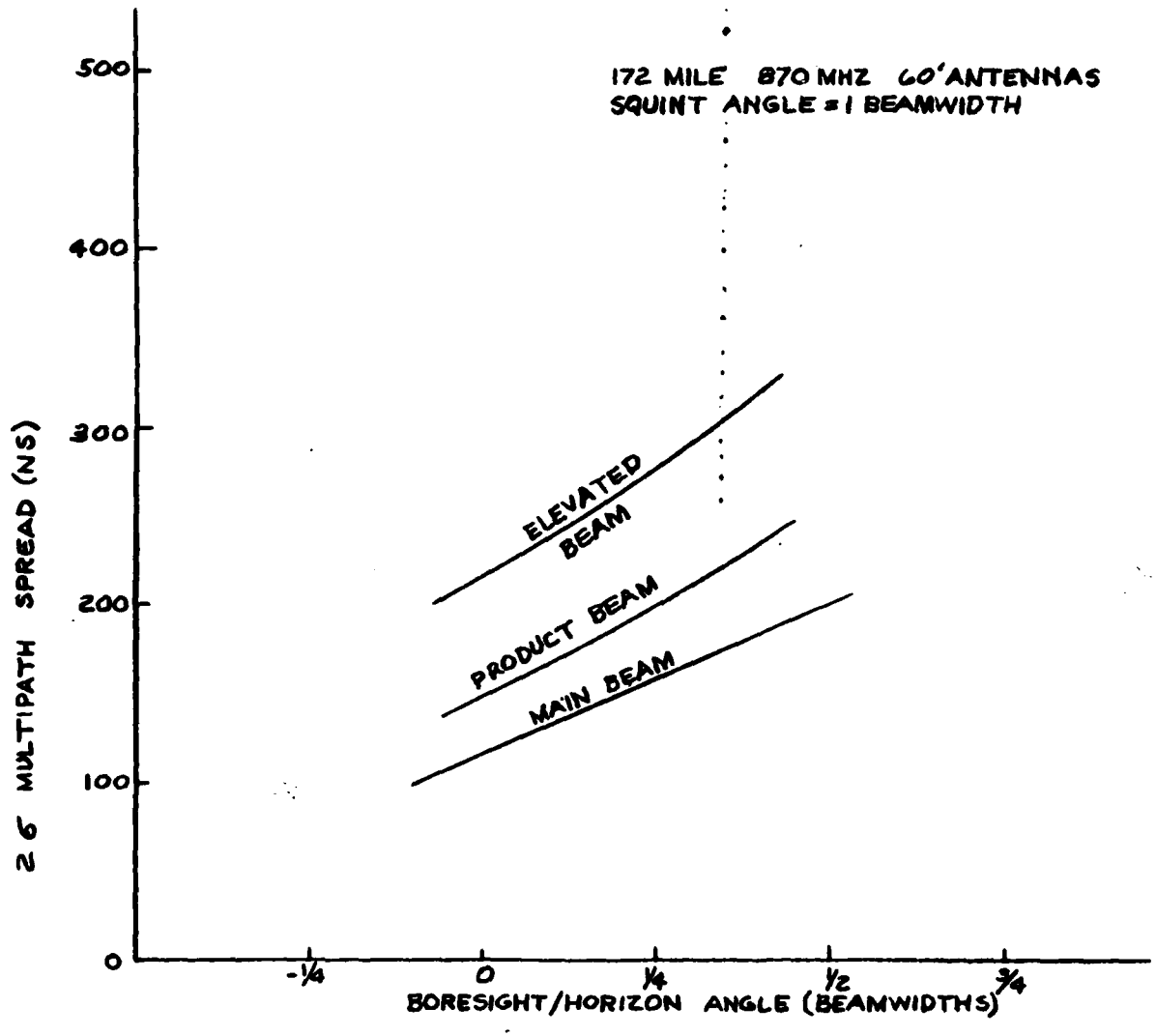

Fig. 2.12 Multipath Characteristics, S. Tepesi-Yamanlar

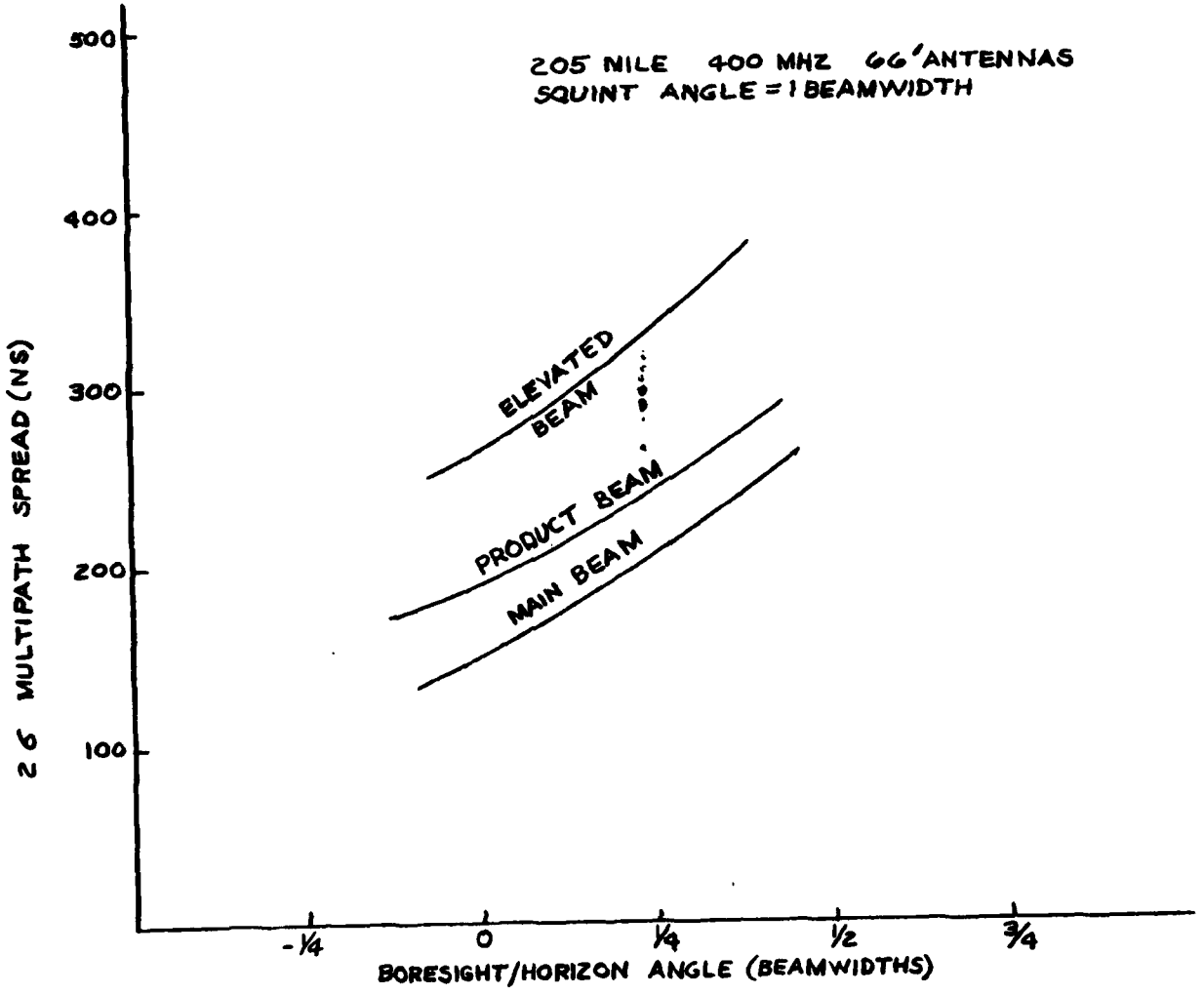

Fig. 2.13 Multipath Characteristics, Oslo-Kristiansand

REFERENCES

2.1 A. B. Crawford, D. D. Hogg, and W. H. Kummer, "Studies in Tropospheric Propagation Beyond the Horizon," Bell Syst. Tech. J., Vol. 38, pp. 1067-1178, Sept. 1959.

2.2 J. H. Chisholm, L. P. Rainville, J. R. Roche, and H. G. Root, "Angular Diversity Reception at 2290MC Over a 188-Mile Path," IRE Trans. Commun. Syst., Vol. CS-7, pp. 195-201, Sept. 1959.

2.3 J. H. Vogelman, J. L. Ryerson, and M. H. Bickelhaupt, "Tropospheric Scatter System Using Angle Diversity," Proc. IRE, Vol. 47, pp. 688-696, May 1959.

2.4 D. Surenian, "Experimental Results of Angle Diversity System Tests," IEEE Trans. Commun. Technol., Vol. COM-13, pp. 208-219, June 1965.

2.5 G. W. Travis, "Angle Diversity Tests," in Proc. Nat. Electron. Conf., Vol. 24, pp. 518-523, 1968.

2.6 P. Monsen, "Performance of an Experimental Angle-Diversity Troposcatter System," IEEE Trans. of Communications, Vol. COM-20, No. 2, April 1972.

2.7 V. N. Troitskiy, "Efficiency of Angle-Diversity Reception in Long-Distance Tropospheric Propagation," Telecommun. & Radio Eng., 1972, 27, pp. 17-23.

2.8 M. W. Gough, G. C. Rider, "Angle Diversity in Troposcatter Communications," Proc. IEE, Vol. 122, No. 7, July 1975, pp. 713-719.

2.9 T. Koono, T. Hirai, et al., "Antenna-Beam Deflection Loss and Signal Amplitude Correlation in Angle-Diversity Reception in UHF Beyond-Horizon Communication," J. Radio Res. Lab., 1962, 9, pp. 21-49.

2.10 V. I. Tatarskii, "The Effects of the Turbulent Atmosphere on Wave Propagation," Isreal Program for Scientific Translation, Jerusalem, Isreal, 1971.

2.11 P. Monsen, High Speed Digital Communication Receiver, U.S. Patent No. 3,879,664, April 22, 1975.

2.12 D.R. Kern and P. Monsen, Megabit Digital Troposcatter Subsystem, Final Report, ECOM-74-0040-F, April 1977.

SECTION 3

TROPOSCATTER PATH PREDICTION TECHNIQUE

a. Introduction

In this section we present new formulas for the path-loss and receiver correlation distances for several values of the spectrum slope m. For m = 11/3, our pathloss formula depends on certain standard atmospheric parameters, while for m = 5 it corresponds directly to the NBS model. This work forms the basis for the SIGNATRON propagation prediction model. This model and its assumptions are presented here.

The necessary background in the properties of tropospheric transmission is provided in subsection 3.2. Subsection establishes the basic pathloss formula with widebeam antennas and discusses the concept of aperture-to-medium coupling loss. The results for narrow beam antennas are treated in subsection 3.4, while the path loss with intermediate beam-sizes is derived in subsection 3.5. The section concludes with a summary of the troposcatter prediction model. We begin with a general discussion of previous work.

Theory and practical techniques for troposcatter communication started developing around 1950 [Booker and Gordon, 1950]. Two main theories have been proposed, the layer reflection theory [Friis, et al,1957] and the turbulent scattering theory based on the turbulence results developed by Obukhov and Kolmogorov in 1941 [see Tatarskii,1971]. Initially, various layer reflection theories received the most attention, partly because the predicted behaviour was close to the observed linear dependence of the scattering cross-section with wavelength. The layer reflection theory also predicts a dependence on the scattering angle close to the empirically determined dependence of the form θ^{-5}. In later years, experiments at higher frequencies and with narrower antenna beams [Eklund and Wickerts, 1968; Hardy and Katz ,1969]

have indicated the applicability of the turbulence theory, with a scattering angle dependence of the form $\theta^{-11/3}$ and a wavelength dependence for the scattering cross-section of the form $\lambda^{-1/3}$. In practice layer reflection and scattering will exist simultaneously with layer reflection being more frequent when widebeam antennas and low frequencies are used. Experimental results [Eklund and Wickerts,1968] indicate that the wavelength dependence can vary between λ^{-1} and λ^{3}. The scattering angle dependence has been measured to lie in the range of θ^{-2} to θ^{-6} [Gjessing, 1969]. The exponent in the scattering angle is frequently called the refractive index spectrum slope since it also indicates the fall-off of the wave number spectrum of the refractive index, provided the wavelength is in the so-called inertial subrange, i.e., between the inner and outer scale of turbulence.

A number of theoretical and computational models have been developed [Booker and Gordon,1950;Tatarskii,1971; Rice et al,1965; Hartman and Wilkerson,1959; Yeh, 1962]. Further references and a discussion of these models can be found in Larsen,[1968] or Panter, [1972]. The most generally accepted model is that of NBS [Rice, et.al,1965; Hartman and Wilkerson, 1959] which, based on a large number of empirical results, assumes the refractive index spectrum slope is five. Several arguments can be forwarded in support of using a spectrum slope of 11/3 instead. First, the trend is toward troposcatter links at higher frequencies where layer-reflection is less important. Second, on links with both turbulent scatter and layer reflection the turbulent scatter is the more critical effect since during the worst days, communication will be by scatter only and layer reflection, when present, tend to increase the received power.

b. Tropospheric Scatter Transmission

Radiowave propagation in the troposphere is determined by the refractive index. The refractive index can be described by its short-term mean and variance, both of which are highly dependent on geographic location, season, and time of day. The mean refractive index is usually linearly decreasing as a function of height, and can be handled by defining an effective earth radius. This well known technique will also be used here, but it is emphasized that for situations where the refractive index profile is not linear the effective earth radius used must be such that the correct scattering angle is found.

The refractive index flunctuations are characterized by the covariance function. If $n(\underline{r})$ is the refractive index at a point with coordinates $\underline{r}$ then define

$$n_1(\underline{r}) = n(\underline{r}) - E[n(\underline{r})],$$

and its covariance function

$$\varphi_n(\underline{r}_1, \underline{r}_2) = E\left[n_1(\underline{r}_1)\ n_1(\underline{r}_2)\right].$$

In a homogeneous medium this covariance is only a function of $\underline{r}_1 - \underline{r}_2$, and in such a case the wavenumber spectrum is defined by

$$\Phi_n(\underline{k}) = \frac{1}{(2\pi)^2} \iiint \varphi_n(\underline{r})\ e^{i\underline{k}\cdot\underline{r}}\ d^3\underline{r}.$$

Often the structure function is defined instead of the covariance function [Tatarskii,1971], however the present discussion will be simplified by assuming that the volume of the troposphere concerned can be considered homogeneous and isotropic. For the isotropic atmosphere the wavenumber spectrum is only a function of the magnitude k of

the wavenumber vector $\underline{k}$. The wavenumber spectrum is important since it has been shown [Tatarskii, 1971] that the scattering cross-section (a_s) of a small volume (dV) is

$$a_s = 8\pi^2 k^4 \Phi_n (2k \sin \frac{\theta}{2}) \, dV,$$

where θ is the scattering angle. Polarization losses are usually treated separately and have been neglected in this equation. The wavenumber spectrum is usually modeled by the von Kármán spectrum [Tatarskii,1971]

$$\Phi_n(k) = \frac{\Gamma\left(\frac{m}{2}\right)}{\pi^{3/2}\Gamma\left(\frac{m-3}{2}\right)} \sigma_n^2 \, r_o^3 \left(1 + k^2 r_o^2\right)^{-m/2}, \quad m > 3 \tag{3.1}$$

If $\Phi_n(k)$ is plotted on a doubly logarithmic scale against the wavenumber k, the slope falls off as m, so that m is called the spectrum slope. m has to be greater than 3 for $\Phi_n(k)$ to be integrable over the three dimensional wavenumber space. Values of m smaller than 3 are possible only in a limited wavelength region. The variance of the refractive index is then limited only by the small scale structure of the turbulence. It will be assumed here that the small scale turbulence can be ignored, so that m is larger than three. σ_n^2 is the variance of the refractive index and r_o is the correlation distance of the turbulence. The wavelength $\lambda = 2\pi/k$ is assumed to be in the inertial subrange:

$$l_o << \lambda << L_o,$$

where l_o and L_o are the inner and outer scales of turbulence, respectively. r_o in (1) can usually be identified with L_o.

The power received from a small scatterer at a point $\underline{r}$ and with the cross-section a_s is

$$dP_R(\underline{r}) = P_T \cdot \frac{G_T(\underline{r})}{4\pi R_T^2(\underline{r})} \cdot \frac{a_s(\underline{r})}{4\pi R_R^2(\underline{r})} \cdot \frac{\lambda^2 G_R(\underline{r})}{4\pi}$$

where

P_T (P_R) = Transmitted power (received power)

$G_T(\underline{r})$ $G_R(\underline{r})$) = Gain of transmitter (receiver) antenna toward the scattering point $\underline{r}$.

$R_T(\underline{r})$ ($R_R(\underline{r})$) = Distance from transmitter (receiver) to the scattering point $\underline{r}$.

Using the expression for the scattering cross-section and the von Kármán spectrum (1) assuming

$$kr_o >> 1$$

it is found that the received power is

$$P_R = P_T \cdot C \iiint_V \frac{G_T(\underline{r}) G_R(\underline{r})}{R_T^2(\underline{r}) R_R^2(\underline{r})} \left(2 \sin\frac{\theta(\underline{r})}{2}\right)^{-m} d^3\underline{r} \qquad (3.2)$$

where

$$C = \sigma_n^2 \, r_o^{3-m} \, k^{2-m} \, \Gamma\left(\frac{m}{2}\right) \Big/ \left(2\sqrt{\pi}\, \Gamma\left(\frac{m-3}{2}\right)\right), \qquad (3.3)$$

and the range of integration, V, is the total common volume. It is assumed that σ_n^2 and r_o do not vary appreciably throughtout the common volume.

While the Kolmogorov-Obukhov theory of turbulence predicts m=11/3, the above expression can be used formally for other values

of m. In particular, setting m=5 yields the expression used by the NBS model [Rice,et al.,1965]. In order to predict the received power P_R it is necessary to specify m, r_o and σ_n^2. As we assume r_o equal to L_o, we can use the value of L_o found by Fried [1967]. He found the following approximate expression for the outer scale of turbulence,

$$L_o \sim 2\sqrt{h \cdot 1 \text{ meter}}$$

where h is the height of the air mass. It must be emphasized that considerable variation from this value of L_o can be expected under different atmospheric conditions. Measurements and predictions of σ_n^2 have been presented by numerous authors [Hardy and Katz,1969 ; Fried,1967 ; Gossard,1977]. At radio frequencies,the variance σ_n^2 is strongly dependent on the humidity. For the dry atmosphere, measurements at radio- and at optical-frequencies yield nearly identical values of σ_n^2. Since dry atmosphere represents the worst case for radio wave scatter measurements, it will often be possible to apply optical results to the study of troposcatter at radio frequencies. This is useful since many more measurements have been made of the optical refractive index than of the radio refractive index. Fried [1967] suggested the following model of the optical refractive index variance:

$$\sigma^2_{n,opt} = 6.7 \cdot 10^{-14}\, e^{-h/3200\ m}.$$

New results indicate a stronger height dependence [Gossard,1977 ; Brookner , 1971],particularly for continental air masses.

σ_n^2 is the main source of variability in received signal levels, so a complete description of σ_n^2 variation versus weather, time-of-day, season, location, etc., is therefore desirable. Unfortunately, only sporadic measurements have been made. Gossard, [1977] has calculated both optical and radio refractive index

variations of several classes of air masses. Using this method, profiles of σ_n^2 (or the structure constant C_n^2) can be calculated as a function of geographic location, season, and time-of-day. Radiosonde data can also be used to predict the variance σ_n^2 for a troposcatter link using a formula by Tatarskii, [1971], [Sirkis, 1971]. Typical values of σ_n^2 at heights of 2 km or below are in the range 10^{-14} to 10^{-13}.

c. The Basic Pathloss

The approximate pathloss with omnidirectional antenna is now derived. The condition required for the validity of the approximation is that the minimum scattering angle θ_s be small. The geometry of the path is shown in Fig. 3.1, where also the necessary notation is defined. The integral over the common volume is evaluated by first integrating parallel to the z-axis (perpendicular to the great circle plane containing transmitter and receiver).

$$P_R/P_T = C \iiint_V \frac{1}{R_R^2(\underline{r}) R_T^2(\underline{r})} \left(2 \sin \frac{\theta(\underline{r})}{2}\right)^{-m} d^3\underline{r} \qquad (3.4)$$

$$= C \int_{\alpha_{TG}}^{\pi/2} \int_{\alpha_{RG}}^{\pi/2} \int_{-\infty}^{\infty} \frac{1}{(R_{oR}^2+z^2)(R_{oT}^2+z^2)} \left[2 \sin \frac{\theta(\alpha_T, \alpha_R, z)}{2}\right]^{-m} \frac{R_{oT} R_{oR}}{\sin \theta_o(\alpha_T, \alpha_R)} dz \, d\alpha_R d\alpha_T \qquad (3.5)$$

All subscript o parameters are in the great circle plane in Fig. 3.1. When the scattering angle is small the following approximation is valid:

$$2 \sin \frac{\theta(\alpha_R, \alpha_T, z)}{2} \simeq \left[\left(2 \sin \frac{\theta_o(\alpha_R, \alpha_T)}{2}\right)^2 + \left(\frac{z}{R_o}\right)^2\right]^{\frac{1}{2}}$$

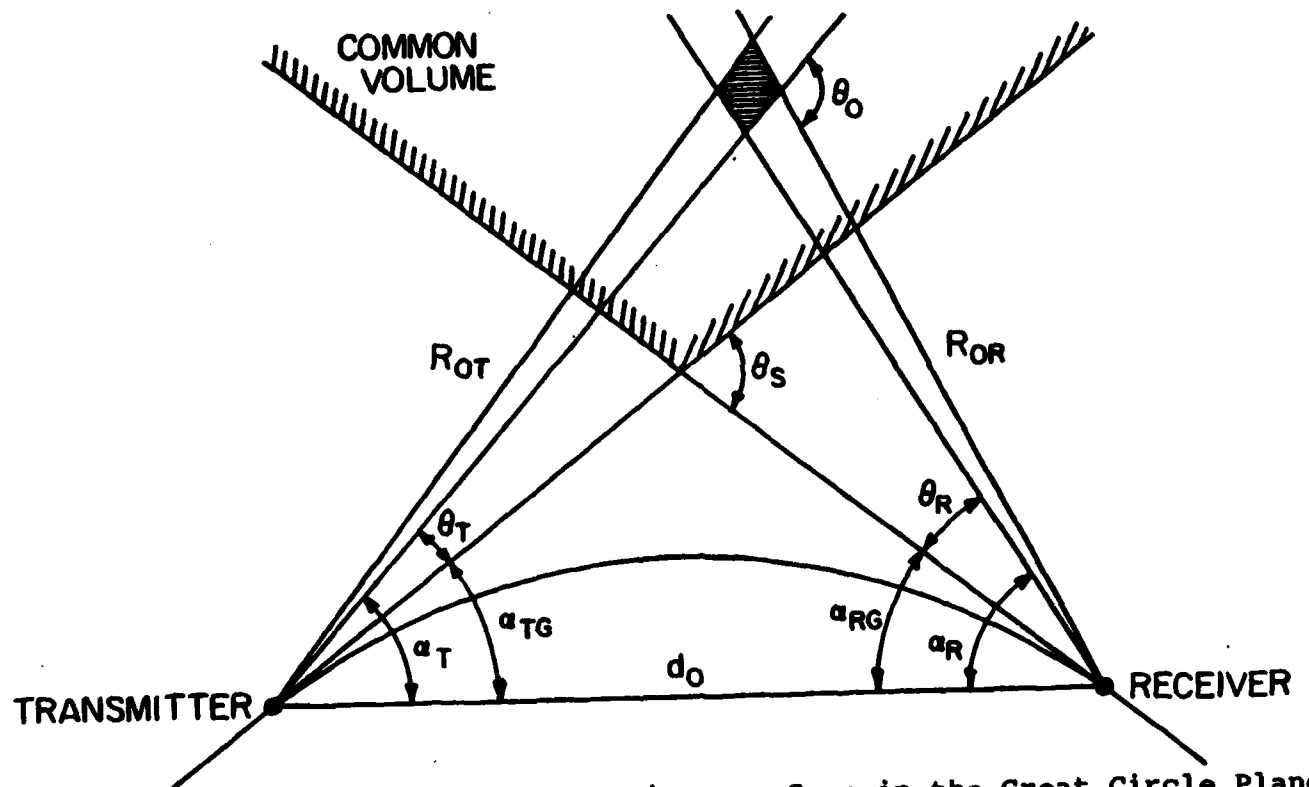

Fig. 3.1 The Common Volume Integration, as Seen in the Great Circle Plane

where

$$R_o = \frac{R_{oR} R_{oT}}{R_{oR} + R_{oT}} .$$

The integral is now reduced to

$$P_R/P_T \simeq C\, B\left(\frac{1}{2}, \frac{m-1}{2}\right) \int_{\alpha_{TG}}^{\pi/2} d\alpha_T \int_{\alpha_{RG}}^{\pi/2} d\alpha_R \left[\left(R_{oR}+R_{oT}\right)\sin\theta_o\left(2\sin\frac{\theta_o}{2}\right)^{m-1}\right]^{-1} , \tag{3.6}$$

where $B(x,y)$ is the Beta function,

$$B(x,y) = \frac{\Gamma(x)\Gamma(y)}{\Gamma(x+y)} .$$

Since the scattering angle is small, so that $\sin\theta(\underline{r}) \approx \theta(\underline{r})$, and $m > 3$, we find after some simple calculations that

$$P_R/P_T \simeq \frac{C\, B\left(\frac{1}{2}, \frac{m-1}{2}\right)}{d(m-1)(m-2)}\, \theta_s^{2-m} \tag{3.7}$$

$$= \sigma_n^2\, r_o^{3-m}\, k^{2-m}\, \frac{(m-3)}{4(m-1)(m-2)}\, (\theta_s^{2-m})/d \tag{3.8}$$

The parameters in this equation are

σ_n^2 = variance of refractive index fluctuations

r_o = correlation distance of refractive index

k = $2\pi/\lambda$ = wave number

m = spectrum slope ($m > 3$)

θ_s = $\alpha_{RG}+\alpha_{TG}$ = minimum scattering angle (angular distance in radians)

d = distance between the terminals.

The result (8) is valid for a small scattering angle, a condition, which will almost always be satisfied in practice. Height variations in σ_n^2 have been assumed weak enough so that C can be taken outside the integral sign in (3.6) and becomes a coefficient in equation (3.7). Comparison of (3.8) with an exact integration of (3.4) the special case where m is an even integer and the horizon elevation angles are zero [Waterman,1958] shows that the approximations we have made are exceedingly accurate as long as the distance d is much smaller than the effective earth radius. Since this condition is generally true, our result can be used for all practical troposcatter distances.

The initial assumption of omnidirectional antennas can be relaxed to generalize (3.8) to antenna beams wide enough to encompass the main scattering volume, except that antenna gain is then no longer unity and has to be taken into account.

The importance of the spectrum slope is evident from the result. As $k = 2\pi f/c$, it is clear, for instance, that setting $m = 5$ yields the cubic frequency dependence assumed in most models of tropospheric scatter. Since the frequency dependence with $m = 11/3$ is much weaker ($f^{-5/3}$), it is not surprising the turbulent scatter provides the dominant transmission at higher frequencies. Figure 3.2 illustrates some typical curves calculated for $m = 5$ using the short distance NBS formula [Rice, et al.,1965] and our (3.8) for $m = 11/3$ using σ_n^2 $5 \cdot 10^{-14}$ and $r_o = L_o = 70$ m. It can be seen that at high frequencies or long distance turbulent scatter tends to be more important than layer reflection or feuillet scattering. This leads to the important conclusion that, in general, it is not possible to use a single model (fixed m) to compare the performances at different frequencies or distances.

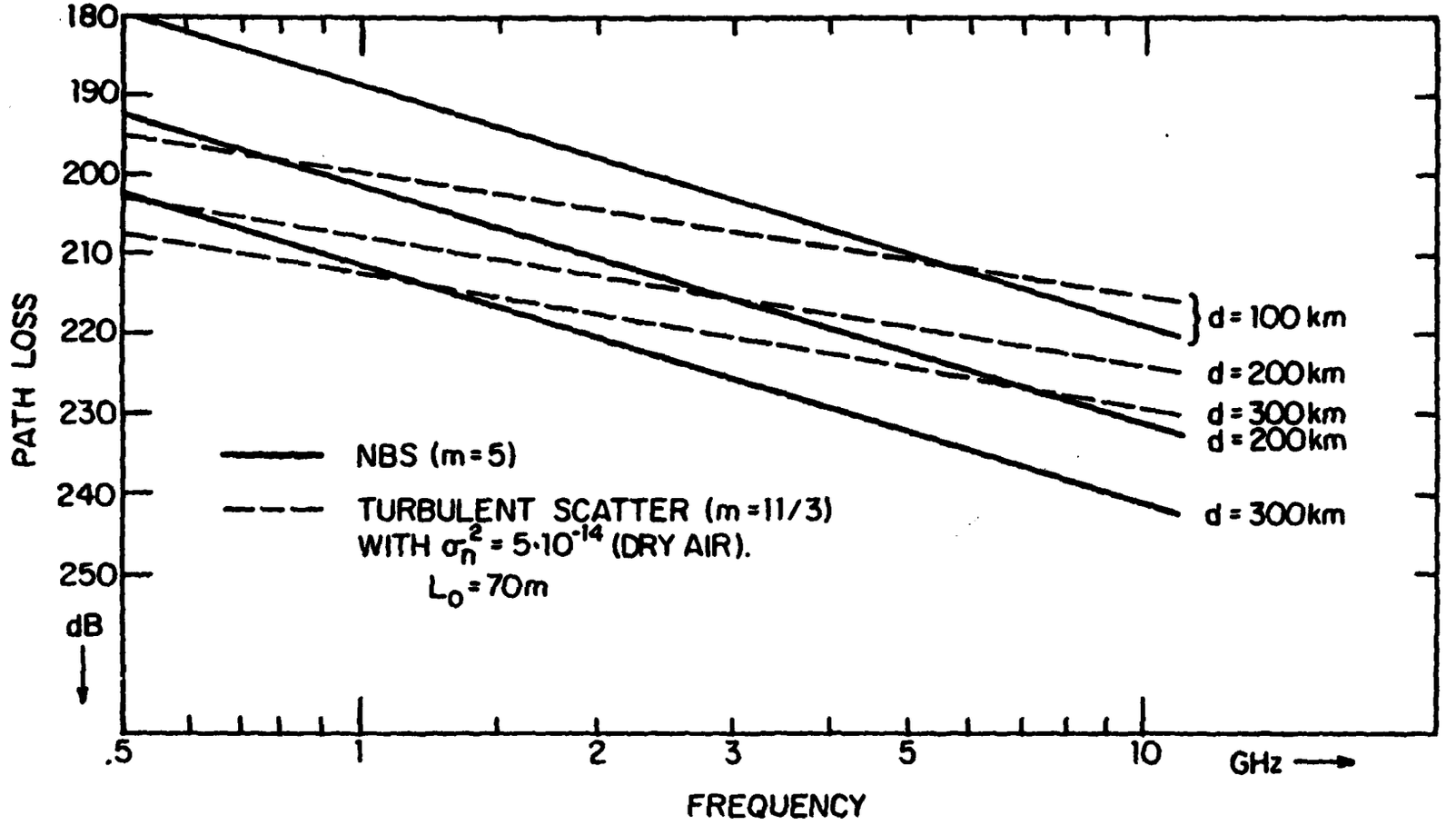

Fig. 3.2 Path Loss Versus Frequency from the NBS Model and from Eq.(8) for the Turbulent Scatter Theory with Typical Parameters

Another conclusion is that, if only one model were to be used, it is better to base a troposcatter link design on the turbulent scatter model. This model is accurate at high frequencies and is useful at lower frequencies to estimate the performance at the times when atmospheric layering is absent. This represents the kind of "worst case" situation that can be expected on a dry winter day, for instance.

If a beam is narrow then the pathloss calculated above is no longer valid since not all potential scatters are illuminated by the beam. It is customary to account for this by introducing the aperture-to-medium coupling loss. This coupling loss is defined by

Coupling loss in dB = total path loss in dB
+ antenna gains in dB
- basic pathloss in dB with omni-directional antennas.

It is important to realize that the coupling loss and the basic pathloss are complementary and must relate to the total path loss for one specific model. It is a common mistake to "calculate" the total path loss from the coupling loss and basic path loss mixing values from different tropospheric models. It is also necessary to take care when measuring the coupling loss directly by comparing transmission with a small and a large antenna on a given link since the result of such measurements depends on highly variable atmospheric conditions outside the smaller common volume of interest. While these measurements can provide useful statistical information, it is not possible to identify the measured results directly with the coupling loss of a pathloss prediction model when the assumption of homogeneity may not be valid.

In the following, approximate formulas will be presented for the coupling loss for different values of m.

d. Formulas for Extremely Narrow Antenna Beams

When one or both of the antenna beam widths tend to zero, then it is again possible to obtain simple formulas. Suppose first that the transmitting beam is wide while the receiving beam is narrow. The assumption of a narrow beam is seldom satisfied to the degree required here, but the results are still useful. They provide a simple bound on performance, and can be compared with similar results by other authors [Gjessing,1969; Waterman,1958; Gjessing and McCormack,1974]. The derivations of the results below follow the same lines as exemplified by the derivation in Section III.

We first evaluate expressions for the horizontal and vertical correlation distances in the plane of the receiver aperture. These quantities, while of interest in themselves, can be related to the coupling loss. Instead of viewing the coupling loss as caused by neglecting to illuminate certain scatterers, it is now viewed as a result of the incoherency of the received field over the aperture A_R. Let the received field $E_o(\underline{r})$, where $\underline{r}$ is a point in the aperture, have the correlation function $\rho(\underline{r} - \underline{r}')$,

$$\rho(\underline{r}, \underline{r}') = E\left\{E_o(\underline{r})\ E_o(\underline{r}')\right\} .$$

The received power is then proportional to

$$P_R = \iint_{A_R} d^2\underline{r} \iint_{A_R} d^2\underline{r}'\ \rho(\underline{r}-\underline{r}') .$$

The loss due to decorrelation of the field over the aperture is then

$$L_c = -10 \log \frac{1}{A_R^2 \rho(0)} \iiiint d^2\underline{r}\, d^2\underline{r}'\, \rho(\underline{r}-\underline{r}').$$

This can be shown to be equivalent to the coupling loss defined earlier, but for the receiving aperture only. A crude approximation to L_c can be found in terms of the horizontal and vertical correlation distances L_H and L_V defined below,

$$L_c \simeq -10 \log (L_H L_V / A_R).$$

The horizontal and vertical correlation distances are now found. Let

$$\rho_H(\ell) \text{ and } \rho_V(\ell)$$

be the horizontal and vertical correlation functions at the receiver. The horizontal correlation distances L_H is then defined by

$$L_H = \int_{-\infty}^{\infty} \rho_H(\ell)\, d\ell / \rho_H(0).$$

We find by an integration analogous to the one leading to (3.8),

$$L_H = \frac{\lambda}{\theta_s} \frac{m-2}{B\left(\frac{1}{2}, \frac{m-1}{2}\right)} \sum_{n=0}^{\infty} \frac{1}{n+m-1} \left(\frac{\alpha_{TG}}{\theta_s}\right)^n \qquad (3.9)$$

Note that for a troposcatter link with equal take-off angles at the transmitter and receiver we have

$$\alpha_{TG}/\theta_s = 1/2.$$

The evaluation of the vertical correlation distance should take into account the pointing angle of the antenna. If the receiver beam is steered for maximum power a simple result is obtained:

$$L_V = \frac{\lambda}{\theta_s} (m-2). \tag{3.10}$$

The coupling loss on a link with a widebeam transmitter and a narrow beam receiver can be expressed in the form

$$L_c = 10 \log \left[\frac{G_R}{4\pi} \frac{B\left(\frac{1}{2}, \frac{m-1}{2}\right)}{m-2} \theta_s \alpha_{RG} \right] \tag{3.11}$$

where G_R is the (large) gain of the receiving aperture (natural units). These asymptotic results (in the sense of an essentially infinitely large receiving aperture) may be compared with equivalent results by other authors. Gjessing and McCormick, [1974] report similar expressions under the additional assumption of zero degree take-off angles so that

$$\theta_s = 2 \alpha_{TG} = 2 \alpha_{RG} = \frac{d}{R_e}$$

(R_e is the effective earth radius). Their results are in reasonable agreement with ours (3.9), (3.10), and (3.11) (less than 3 dB difference in L_c).

If the transmitting antenna beam is also narrow, then the parallel results to the equations (3.9), (3.10) and (3.11), become

$$L_H \simeq \infty,$$

$$L_V = \frac{\lambda}{\theta_s} (m-1)$$

and

$$L_c = 10 \log \left[\frac{G_R G_{T,V}}{8\pi^2} \theta_s^2 \alpha_{RG} \frac{B\left(\frac{1}{2}, \frac{m-1}{2}\right)}{(m-1)(m-2)} \right]. \qquad (3.12)$$

In the expression (3.12) for the coupling loss L_c it has been assumed that $\beta_{R,H}/\beta_{T,H} < \alpha_{RG}/\alpha_{TG}$, where $\beta_{R,H}$ and $\beta_{T,H}$ are the horizontal beamwidths of receiver and transmitter, respectively. If this is not the case the role of receiver and transmitter is simply reversed before (12) is used. G_R is again the gain of the receiving aperture, but $G_{T,V}$ is the gain of the transmitter in the vertical plane only.

e. Approximate Formulas for Intermediate Beamwidths

So far we have only found accurate formulas for two extreme cases, very wide beams, and very narrow beams. For the majority of troposcatter links encountered in practice neither of these situations occur. It is therefore important to tackle the more difficult problem of finding the pathloss for beams of a more realistic size. Exact results can only be found by a numerical integration, but useful approximations will be found on the basis of ideal rectangular beam shapes.

Let $\beta_{T,V}$, $\beta_{T,H}$, $\beta_{R,V}$, $\beta_{R,H}$ denote the vertical and horizontal beamwidths of the transmitter and receiver antennas. For ideal rectangular beams the limits of integrals in (5) are changed so that

$$P_R/P_T = C \int_{\alpha_{TG}}^{\alpha_{TG}+\beta_{TV}} d\alpha_T \int_{\alpha_{RG}}^{\alpha_{RG}+\beta_{RV}} d\alpha_R \int_{-z_o(\alpha_R,\alpha_R)}^{z_o(\alpha_T,\alpha_R)} dz \; I(\alpha_T, \alpha_R, z)$$

(3.13)

where

$$I(\alpha_T, \alpha_R, z)$$

is the integrand in (5) and

$$z_o(\alpha_T, \alpha_R) = \frac{1}{2} \min \left[R_{oT}\, \beta_{T,H},\ R_{oR}\, \beta_{R,H} \right]$$

$$= \frac{1}{2} \frac{d_o}{\sin \theta_o(\alpha_R, \alpha_T)} \min \left(\beta_{T,H} \sin\alpha_R, \beta_{T,R} \sin\alpha_T \right). \tag{3.14}$$

This integral is now approximated in some special cases.

A. Wide Horizontal Beamwidths

In this case it can be assumed that $z_o \sim \infty$, and it is then found that

$$P_R/P_T \simeq \frac{C\, B\left(\frac{1}{2}, \frac{m-1}{2}\right)}{d(m-1)(m-2)} \theta_s^{2-m} F_{m-2}\left(\frac{\beta_{T,V}}{\theta_s}, \frac{\beta_{R,V}}{\theta_s}\right) \tag{3.15}$$

where we have defined the function

$$F_N(x,y) = 1 - (1+x)^{-N} - (1+y)^{-N} + (1+x+y)^{-N}.$$

(3.15) clearly reduces to (3.7) for very wide vertical beamwidths. The coupling loss is

$$-10 \log F_{m-2}\left(\frac{\beta_{T,V}}{\theta_s}, \frac{\beta_{R,V}}{\theta_s}\right).$$

B. Narrow Horizontal Beamwidths, $\beta_{T,H} = \beta_{R,H} = \beta_H$

Rather than attempting an exact integration we use the simple bounds

$$\frac{\sin\alpha_R \cdot \sin\alpha_T}{\sin\alpha_R + \sin\alpha_T} \leq \frac{2z_o}{d_o} \frac{\sin\theta_o(\alpha_T,\alpha_R)}{\beta_H} \leq 2 \frac{\sin\alpha_R \cdot \sin\alpha_T}{\sin\alpha_R + \sin\alpha_T}$$

Invoking the small angle approximation and the assumption that β_H is small the upper bound yields

$$P_R/P_T \leq C \cdot \frac{2\beta_H}{d} \frac{\theta_s^{1-m}}{m(m-1)} F_{m-1}\left(\frac{\beta_{T,V}}{\theta_s}, \frac{\beta_{R,V}}{\theta_s}\right) .$$

The function $F_{m-1}(x,y)$ is the same as defined above. The error in this bound is less than 3 dB, and this error can be substantially reduced by using an approximation between the lower and upper bounds. The correct approximation is the one which is equivalent to (3.12) for very narrow beams. This approximation is

$$\frac{P_R}{P_T} \simeq \frac{\theta_s}{2\cdot\max(\alpha_{TG},\alpha_{RG})} \cdot C \frac{2\beta_H}{d} \frac{\theta_s^{1-m}}{m(m-1)} F_{m-1}\left(\frac{\beta_{T,V}}{\theta_s}, \frac{\beta_{R,V}}{\theta_s}\right) .$$

Since

$$\theta_s = \alpha_{TG} + \alpha_{RG}$$

the coupling loss is found to be approximately

$$L_c \simeq 10 \log \left[\frac{mB\left(\frac{1}{2}, \frac{m-1}{2}\right)}{(m-2)} \frac{\theta_s + |\alpha_{TG} - \alpha_{RG}|}{2\beta_H} \Big/ F_{m-1}\left(\frac{\beta_{T,V}}{\theta_s} \frac{\beta_{R,V}}{\theta_s}\right) \right] \quad (3.16)$$

This reduces to (12) for very narrow beams. $\alpha_{TG}-\alpha_{RG}$ may in practice be approximated by

$$\alpha_{TG}-\alpha_{RG} = \frac{2(h_T-h_R)}{d} + (\theta_{TG}-\theta_{RG}),$$

where h_T and H_R are the altitudes of the antennas, and θ_{TG}, θ_{RG} are the horizon grazing angles relative to horizontal.

C. Narrow Horizontal Beamwidths, $\beta_{T,H} >> \beta_{R,H}$

In this case the horizontal dimension is essentially determined by the receiver beamwidth, and the following approximation is used:

$$2 z_o \simeq R_{oR} \beta_{R,H}.$$

This case is more complicated, and we just state the result of the integration:

$$P_R/P_T = \frac{C\beta_{R,H}}{d(m-1)} \theta_s^{1-m} \sum_{k=0}^{\infty} \frac{1}{m+k-1} \left(\frac{\alpha_{TG}}{\theta_s}\right)^k \left[1 - \left(1 + \frac{\beta_{R,V}}{\theta_s}\right)^{1-m-k} - \left(1 + \frac{\beta_{T,V}}{\alpha_T}\right)^k \left(\left(1 + \frac{\beta_{T,V}}{\theta_s}\right)^{1-m-k} - \left(1 + \frac{\beta_{T,V} + \beta_{R,V}}{\theta_s}\right)^{1-m-k} \right) \right] \tag{3.17}$$

The corresponding coupling loss also reduces to (3.12) for narrow beams.

D. Combined Formulas

The formulas may be combined to yield useful approximations over the entire range of parameter. Consider first the case where $\beta_{T,H} >> \beta_{R,H}$. Figure 3.3 shows the approximations in A. and C.above. Also shown is a combined curve calculated by simply adding the coupling losses (in natural units). This is a rather arbitrary approximation which, however, is asymptotically good. For the case illustrated in Fig. 3.3 it is seen that the approximation is excellent when compared with a numerical integration over the common volume.

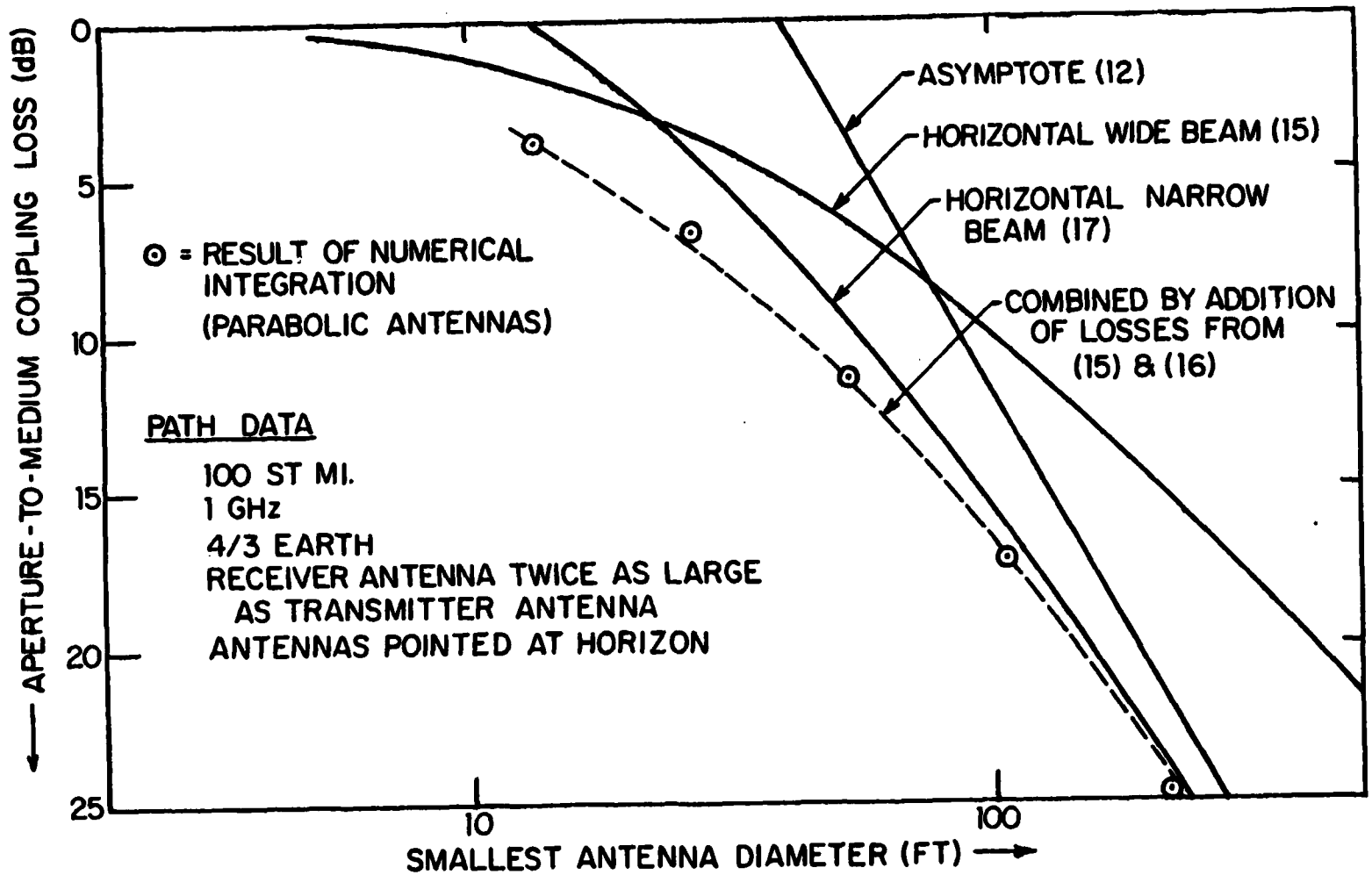

Fig. 3.3 Comparison of Derived Coupling Loss with Numerical Integration - Asymmetric Path

This integration used the non-rectangular beamshape associated with a parabolic antenna. Figure 3.4 shows a similar comparison for the case of antennas of equal size. It is seen again that a simple addition of the coupling losses yield an excellent approximation to the more exact numerical integration. In Figs. 3.3 and 3.4 the beamwidths used in the formulas and the size of the parabolic antennas are related such that the correct asymptote is achieved. This relation of beamwidth β to antenna diameter D is simply

$$\beta = \frac{4}{\pi} \frac{\lambda}{D} ,$$

where λ is the wavelength.

In the turbulent scatter model of tropospheric scatter communication developed here, the total pathloss on such a link is divided into two terms, the basic pathloss valid for wide beams, and the aperture-to-medium coupling loss accounting for the additional loss of narrow beams. It is important that basic pathloss and coupling loss relate to a single model of the scatter mechanism in order to yield a meaningful total pathloss.

We have shown how the atmospheric parameters can be related to the turbulent scatter model. Combined with the closed-formed expressions for the pathloss derived in this paper, this results in a useful method for predicting the performance of a link. However, more work is required to relate the important parameters σ_n^2 and r_0 to measurable or predictable atmospheric parameters. The method of Gossard [1977] may be used to find the refractive index variance for many different climates. Radiosonde data may also be used to determine this variance, which can then be used in our model to predict communication performance. We point out, however, that formation of atmospheric layers can partly invalidate the turbulent scat-

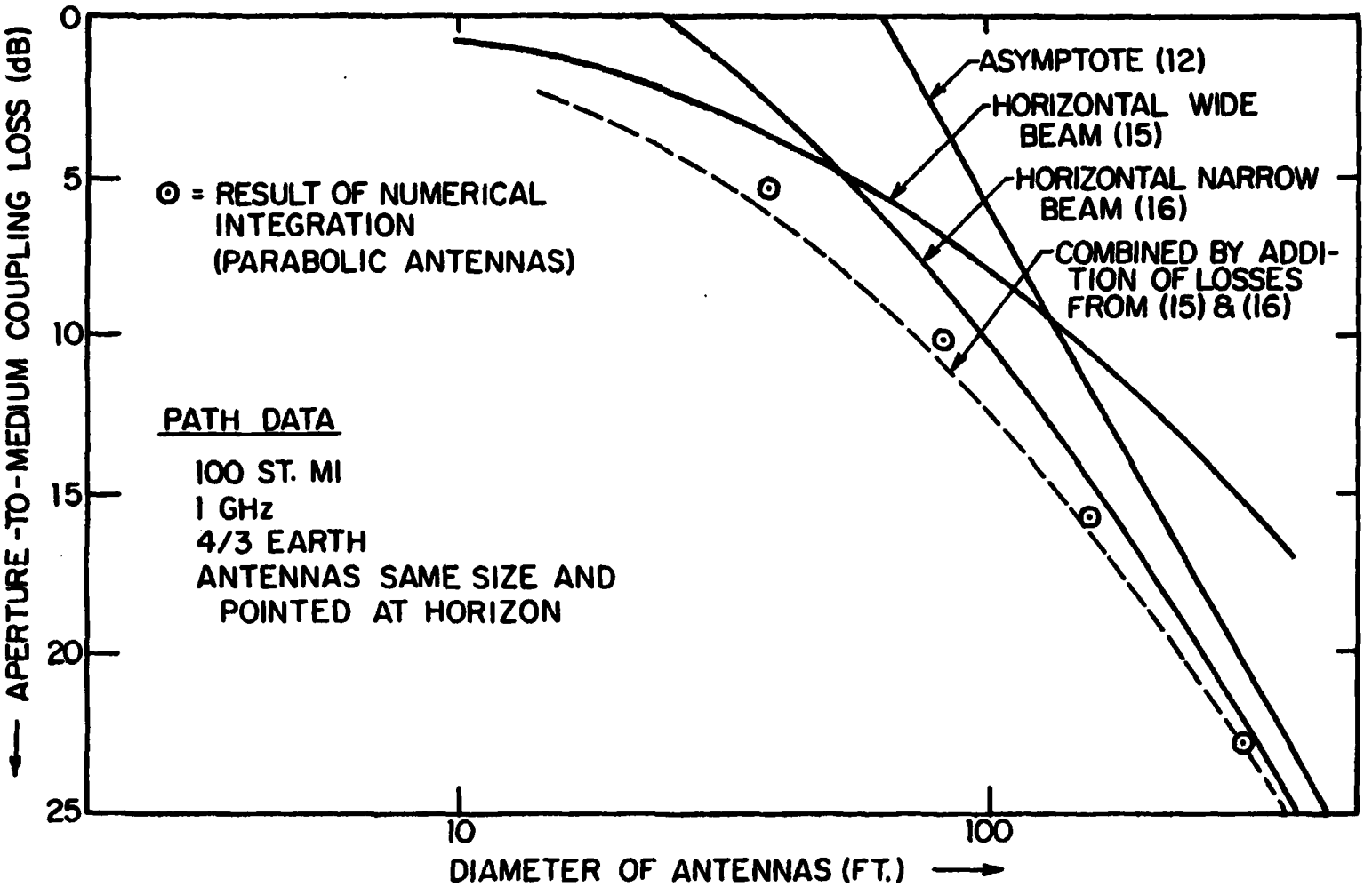

Fig. 3.4 Comparison of Derived Coupling Loss with Numerical Integration - Symmetric Path

ter assumption used here. At lower frequencies (< 1 GHz), a separate analysis of layer effects is required to complete a pathloss prediction program. The NBS method [Rice et al, 1965] accomplishes this by using empirical data. However, the turbulent scatter model is most useful at higher frequencies, and even at lower frequencies when concerned primarily with the weak-signal situation.

The asymptotic form of the coupling loss is sometimes used to approximate the actual loss [Gjessing and McCormick, 1974]. Our results indicate that the coupling loss is very slow in approaching the asymptote and that use of the asymptotic result is much too optimistic (see Figs. 3.3 and 3.4). The formulas derived in subsection 3.5 provide an alternative to using the asymptotic form without this deficiency.

f. Summary of Troposcatter Model

In this subsection we summarize the troposcatter model developed by SIGNATRON, and its relation to atmospheric and climatic factors. The dependence of path loss on key parameters is also developed.

(1) Path Geometry

A typical path is shown in Fig. 3.5 with some of the parameters involved. The parameters are

- Frequency f
- Distance d
- Heights h_T, h_R of transmitter and receiver antennas above mean Sea Level (MSL).
- Horizon elevations above horizontal (θ_{TG},θ_{RG}) at transmitter and receiver. These angles can depend on the atmospheric conditions.
- Antenna boresight elevations above horizontal (θ_T,θ_R) at transmitter and receiver.

  Note that $\theta_T-\theta_{TG}$ and $\theta_R-\theta_{RG}$ are then the elevation of the antennas above the

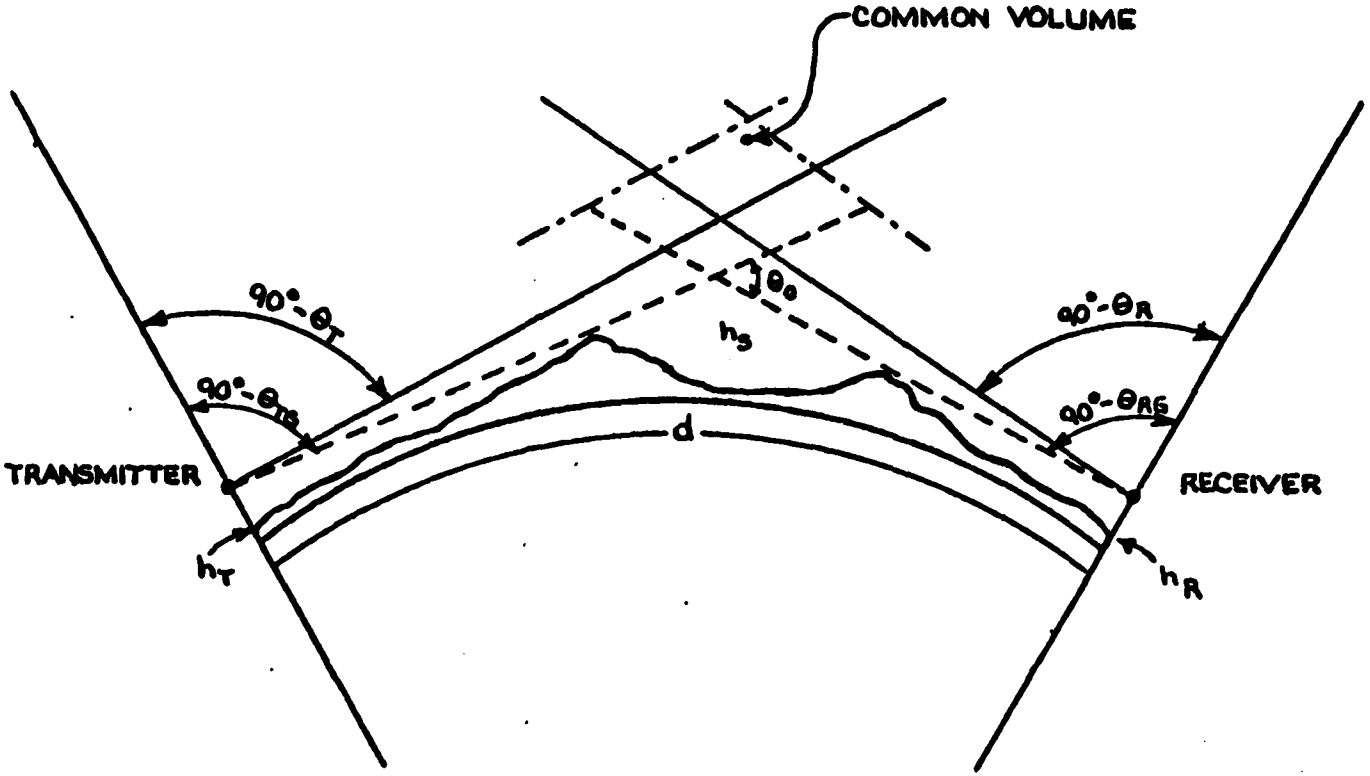

Fig. 3.5 Path Geometry

horizon. The definition of "boresight" need not be the direction of maximum gain, but may be defined from mechanical consideration (e.g., the normal to a phased array).

- Azimuth pointing angles ϕ_T, ϕ_R if horizontal diversity is employed, or beam swinging experiment performed.
- Gain patterns $G_T(\theta,\phi)$, $G_R(\theta,\phi)$ of transmitting and receiving antennas. Determination of the gain patterns requires a number of additional parameters - size and type of antennas, height above ground, ground profile and reflectivity. The patterns should be referenced with respect to the boresight direction. Both amplitude and phase of the voltage gain patterns are required when the cross correlation between two (diversity) paths is to be calculated.
- Polarization of transmitter and receiver.

(2) Turbulent Scatter Model

It is well known that the power received from a small scattering volume can be written

$$P_R = P_T \cdot \frac{G_T}{4\pi R_T^2} \cdot \frac{a_s}{4\pi R_R^2} \cdot \frac{\lambda^2 G_R}{4\pi} \cdot A_a^{-1}$$

where

P_T = Transmitter power

G_T = Power Gain of transmitting antenna

R_T = Distance from transmitter to scatterer

a_s = Scattering cross-section of the turbulent volume

R_R = Distance from scatterer to receiver

λ = Wavelength

G_R = Power gain of receiving antenna

A_a = Atmospheric attenuation

The above transmission equation also serves as a definition of the scattering cross-section (some authors define $a_s/4\pi$ as the scattering cross-section). Tatarski [1971] has derived the cross-section of turbulent scatter with a given wave number spectrum,

$$a_s = 8\pi^2 k^4 \Phi_n \left(2k \sin \frac{\theta}{2}\right) \sin^2 \chi \, dV, \quad \ell_o << \lambda << L_o.$$

In this equation,

$k = 2\pi/\lambda$	is the wave number,
$\Phi_n(k)$	is the locally homogeneous and isotropic wave spectrum
θ	is the scattering angle
$\sin^2\chi$	accounts for loss due to polarization mismatch (usually negligible)
χ	angle between incoming electric field and direction of propagation
dV	is the infinitesimal volume.

The equation is derived under the assumption

$$L_o << \sqrt{\lambda R_R}, \sqrt{\lambda R_T}.$$

If a spectrum of the von Karman type is assumed, it is found

$$a_s = \sigma_n^2 \, 8 \sqrt{\pi} k^{4-m} r_o^{3-m} \frac{\Gamma\left(\frac{m}{2}\right)}{\Gamma\left(\frac{m-3}{2}\right)} \left(2 \sin \frac{\theta}{2}\right)^{-m} dV,$$

r_o is approximately the correlation distance L_o of the turbulence. Polarization losses have been ignored in this equation. For $m = 11/3$ we get the cross-section prediction by

the Kolmogorov-Obukhov theory, while for m = 5 we get the formula on which the NBS method [Rice, et. al, 1967] is based. Measurements agree with the Kolmogorov-Obukhov theory at frequencies above 1 GHz.

Combining the general expression for a_s with the transmission equation, we get

$$P_R = P_T \; C \iiint_V \frac{G_T(\underline{r}) \; G_R(\underline{r})}{R_T^2(\underline{r}) \; R_R^2(\underline{r})} \quad 2 \sin\left[\frac{\theta(\underline{r})}{2}\right]^{-m} d^3\underline{r}, \qquad (3.18)$$

where

$$C = \sigma_n^2 \; r_o^{3-m} \; k^{2-m} \cdot \frac{\Gamma\left(\frac{m}{2}\right)}{2\sqrt{\pi}\,\Gamma\left(\frac{m-3}{2}\right)} \cdot A_a^{-1}$$

and V is the total scattering volume.

In the SIGNATRON computer prediction model, the path loss (3.18) is calculated using a numerical integration procedure. This procedure accurately includes the effects of the actual beam pattern, including sidelobes. The computer program does this simultaneously for several receiver beams so that diversity performance can be estimated accurately. The program also models long term variability adapted from the NBS method. Climatological effects must be taken into account when selecting the atmospheric parameters, σ_n^2 and L_o. The path loss computed by the numerical integration procedure contains contributions from both the basic path loss and the aperature-to-medium coupling loss. This result is used in all subsequent calculations for digital modem predictions. In addition, the closed form approximations previously described are computed as a means of verifying the utility of these expressions for applications where numerical integration is not possible or convenient. In this calculation the path loss is evaluated in two steps. First, the basic path loss with wide beams is evaluated. Then the increase in the path loss due to narrow beams is found. This loss is commonly called the aperture-to-medium coupling loss. The <u>basic path loss</u> is found to be

$$L_{BAS} = -10 \log \left[\sigma_r^2 \; r^{3-m} \; k^{2-m} \; \frac{m-3}{4(m-1)(m-2)} \; \frac{e^{2-m}}{d}\right]$$

where

σ_ℓ^2	=	variance of refractive index fluctuations (5.10^{-14} in dry air
r_o	=	correlation distance of refractive index (typically 70 m)
k	=	$2\pi/\lambda$ = wavenumber of incident wave
m	=	spectrum slope (m=11/3)
Θ	=	scattering angle
d	=	distance between terminals

This simple expression is valid for a wide range topographical condition. The aperture-to-medium coupling loss can be evaluated approximately by the formula

$$L_C \approx -10 \log F_{m-1}\left(\frac{\beta_{TV}}{\Theta}, \frac{\beta_{RV}}{\Theta}\right)$$

$$+10 \log \left(1 + \frac{4m}{(m+1)(m-2)} \frac{\Theta}{\beta_H}\right)$$

$$+10 \log \left(1 + \frac{1}{\Theta}\left|\frac{2(h_R - h_T)}{d} + \Theta_{RG} - \Theta_{RG}\right|\right)$$

where

β_{TV}, β_{RV}	=	vertical beam width of transmitter and receiver, respectively
β_H	=	horizontal beam width of transmitter and receiver

$$F_m(x,y) = 1-(1+x)^{1-m} - (1+y)^{1-m} + (1+x+y)^{1-m}$$

This result assumes terminal antennas with the same horizontal dimensions. Results for the nonsymmetric case have been previously presented.

(3) Path Loss Dependence on Key Parameters

The total path loss, L_T is

$$L_T = L_{BAS} + L_C - G$$

where G is the total antenna gain. For two terminals with antenna diameter D, we have

$$G \approx 15 \text{ dB} + 40 \log \frac{D}{1 \text{ ft}} + 40 \log \frac{f}{1 \text{ GHz}} .$$

If the frequency is doubled and the antenna diameters halved, then G and L_C are unchanged. From the expression for L_{BAS} we tnen have the simple rule of thumb

- The path loss increases 5 dB for each factor of two up in frequency if antenna dimensions are decreased proportionally.

Hence, existing 5 GHz links with 8' antennas would perform 5 dB worse at 10 GHz with 4' antennas and 10 dB worse at 20 GHz with 2' antennas. The attenuation due to water vapor absorption and rain increases these losses substantially at higher frequencies.

The dependence on distance is:

- The path loss increases 3 dB for each factor of two in distance as long as the scattering angle is constant.
- For zero elevation angles, the path loss increases 8 dB for each distance octave when the coupling loss is negligible.

The dependence on the scattering angle is:

- The basic path loss increases 5 dB for each factor of two in the scattering angle θ, assuming constant path length.
- The aperture-to-medium coupling increases up to an asymptotic limit of 9 dB for each factor of two in scattering angle.

BIBLIOGRAPHY

Booker,H.G., and W.E.Gordon (1950), A theory of radio scattering in the troposphere, Proc. IRE, 38, 401-402.

Brookner,E (1971), Improved model for structure constant variation with altitude, Appl. Optics, 10, 1960-1963.

Eklund,F. and S.Wickerts (1968), Wavelength dependence of microwave propagation far beyond the radio horizon, Radio Science, 3, 1066-1074.

Fried, D.L. (1967),Optical heterodyne detection of an atmospherically distorted wave front, Proc. IEEE, 55, 57-67.

Friis,H.T.,A.B.Crawford and D.C.Hogg (1957), A reflection theory for propagation beyond the horizon, Bell System Tech. J., 36, 627.

Gjessing,D.T.(1969), Atmospheric structure deduced from forward-scatter wave propagation experiments, Radio Science, 4, 1195-1210.

Gjessing,D.T. and K.S.McCormick (1974), On the prediction of the characteristic parameters of long distance tropospheric communication links, IEEE Trans.Comm., COM-22, 1325-1331.

Gossard,E.E. (1957), Refractive index variance and its height distribution in different air masses, Radio Sci., 12, 89-105.

Hardy, K.R. and I.Katz (1969), Probing the clear atmosphere with high power, high resolution radars, Proc. IEEE, 57, 468-480.

Hartman,W.J., and R.E.Wilkerson (1959), Path antenna gain in an exponential atmosphere, J.Res.N.B.S., 63D, 273-286.

Larsen,R.E. (1968), A comparison of some troposcatter prediction methods, IEE London Tropospheric Wave Propagation Conf.

Panter,P.F. (1972), Communication Systems Design: Line-of-Sight and Troposcatter System, 589 pp., McGraw Hill Book Co., New York.

Rice, P.L., A.G.Longley, K.A.Norton and A.P.Barsis (1965), Transmission loss prediction for troposcatter communications circuits, N.B.S.Tech. Note 101.

Sirkis,M.D. (1971), Contribution of water vapor to index of refraction structure parameter of microwave frequencies, IEEE Trans. Ant. Prop. AP-19, 572-574.

Tatarskii,V.I. (1971), The effects of the turbulent atmosphere on wave propagation, 472 pp., Israel Program for Scientific Translation, Jerusalem.

Waterman, A.T., Jr. (1958), Some generalized scattering relationships in transhorizon propagation, Proc. IRE, 46, 1842-1848.

Yeh,L.P. (1962), Experimental aperture-to-medium coupling loss, Proc. IRE, 50, 205.

SECTION 4

PERFORMANCE MODEL FOR DIGITAL TROPOSCATTER

Performance of a digital troposcatter system can be expressed in terms of average bit error rate and outage probability. Although the average BER can be a useful parameter and is frequently measured in experimental tests, it lacks a direct relation of digitized voice quality in a troposcatter application. The outage probability is a measure of the fraction of time a fixed BER threshold is exceeded, i.e. the fraction of time the system is "out". The outage probability represents one point on the cumulative BER distribution function. Defense Communication System (DCS) standards for digital links are expressed in terms of a 7.5×10^{-4} outage probability with a BER threshold criterion of 10^{-4}, since this level corresponds to the start of degraded digitized voice performance in a PCM system. In this section we develop an extensive performance model of a digital troposcatter system which provides the means for computation of bit error rate statistics.

a. Bit Error Rate Statistics

The bit error rate performance of a digital data system operating over an angle diversity troposcatter link is dependent on the received power at each feedhorn, the correlation between diversity channels, and the multipath characteristics of the composite diversity system. In this analysis, we develop the mathematical model to predict (1) the bit error rate statistics as a function of the hourly median received power for the main beam diversity channel and (2) the long term probability that the bit error rate is exceeded. Statistics for the first prediction are based on the short term (less than a minute) fading characteristics of the troposcatter channel. The long term calculation deals with the availability of the digital tropo-

scatter system as a result of hourly and daily variations in path parameters.

Computation of bit error rate statistics implies a choice of digital modulation format and receiver processing technique. We have selected QPSK for the modulation format and a generalized adaptive decision-feedback equalizer (DFE) for the processor. QPSK is the present choice of the two developed troposcatter modems, MD-918 and the DAR-4, because of its bandwidth efficiency, nearly constant envelope characteristic, and optimal detection capability. The DFE has been shown in extensive field testing of the MD-918 modem to provide excellent performance over an extremely wide range of channel conditions such as might be anticipated in an angle diversity application. The MD-918 DFE modem was also the modem used in the AAC field tests.

The general problem of computing the short term bit error rate (BER) distribution for a fading multipath channel is a difficult if not impossible task. One can determine the BER distribution for a flat fading channel with diversity order D in a straightforward manner [4.1] but the introduction of implicit diversity and intersymbol interference effects due to multipath precludes a closed form transformation of variables. The short term average BER for a space or frequency diversity system has been determined following the procedure developed in [4.2] with a resulting expression in the form of a determinant. The BER distribution can be computed from knowledge of the eigenvalue structure of the implicit diversity configuration that results from this procedure. Two important assumptions are introduced which make calculation of this eigenvalue structure possible. The calculated eigenvalues represent a decomposition of the troposcatter channel into independent implicit diversity channels with average received powers equal to the eigenvalue set. This transformation to an equivalent independent diversity system then allows the computation of the mean BER and the BER distribution. In the sequel, the analysis developed in

[4.2] is extended to include angle diversity configurations and calculation of the BER distribution.

(1) Communication System Definition

The communication system model under consideration is shown in Fig. 4.1. Complex notation is used to represent in-phase and quadrature components and explicit modulation/demodulation operations are not shown. The data to be transmitted (s_k) are selected from the set ($\pm 1 \pm j$) for a quaternary phase-shift-keying system. The transmitted waveform is

$$s(t) = \sum_{k=-\infty}^{\infty} s_k f(t-kT) \tag{4.1}$$

where T is the interval between successive symbol transmission, i.e., symbol interval. The data rate for this QPSK system is 2/T bits/second. The transmitter impulse response f(t) is defined as a unit energy real function.

The fading multipath channel can be represented by an ensemble of zero-mean random functions with complex Gaussian statistics. Individual diversity channels in an angle diversity system will exhibit correlation between each other which can be completely described by the second moment of the channel impulse response $h_i(t)$,

$$\overline{h_i(t)\, h_j^*(\tau)} = \delta(t-\tau)\, \bar{E}_b\, A_{ij} p_{ij}(t), \quad i, j = 1,2,\ldots D, \tag{4.2}$$

where $\delta(t)$ is the impulse function, $\bar{E}_b$ is the mean received energy per bit for the main beam diversity channel, A_{ij} represents a relative received power difference between the diversity channels, and $p_{ij}(t)$ is a unit area function equal to the mean squared envelope of the impulse response. It represents the average cross power response at each delay value to impulse function excitation and will be referred to as the cross multi-

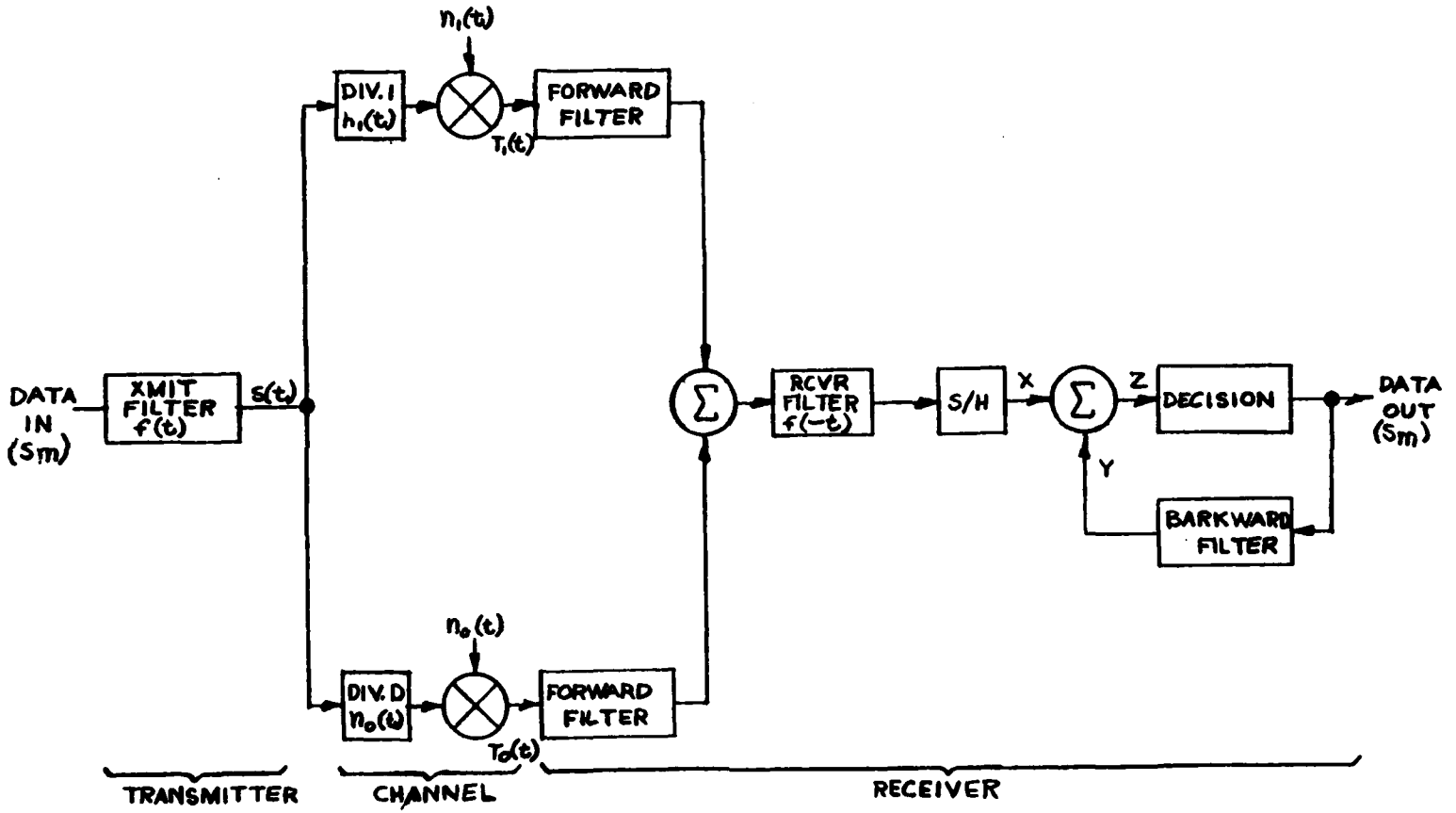

Fig. 4.1 Communication System Model

path profile. Twice the RMS width of the profile is the cross multipath spread, $2\sigma_{ij}$. For convenience the main beam diversity channel is designated as channel 1 which requires $A_{11} = 1$. In a typical angle diversity application utilizing dual vertical feedhorns on each antenna with odd numbers designating main beam diversities and even numbers designating elevated beam diversities, the characterization has the special form

$$A_{ii} = 1 \quad , \; p_{ii}(t) = p_1(t); \quad i \text{ odd} \tag{4.3.1}$$

$$p_{ii}(t) = p_2(t); \quad i \text{ even} \tag{4.3.2}$$

$$p_{i,i+1} = p_{12}(t); \quad i \text{ odd} \tag{4.3.3}$$

$$p_{ij}(t) = 0 \quad , \quad i \neq j \text{ and } i \text{ (odd)} \neq j-1 \tag{4.3.4}$$

Conditions (4.3.1) and (4.3.4) state that all main beam diversities have equal statistics and are independent of each other. Conditions (4.3.2) and (4.3.4) state that all elevated beams have equal statistics and are independent of each other. Finally, conditions (4.3.3) and (4.3.4) state that the cross multipath profile is the same for each feedhorn pair but that the correlation between feedhorn ports on different antennas is zero. The elevated beam powers $A_{ii,i}$ even, in a vertical angle diversity system generally have less received power because of the larger scattering angle, but nonhomogeneous conditions can cause A_{ii} to be greater than unity some fraction of the time.

The definition of $\bar{E}_b$ as the received energy per bit for the main beam diversity $A_{11} = 1$, follows from the fact that one received bit is represented by the pulse

$$\pm 1 \int_{-\infty}^{\infty} f(t-u)\, h_1(u)\, du$$

which has energy

$$\int_{-\infty}^{\infty} dt \left| \int_{-\infty}^{\infty} f(t-u) h_1(u) du \right|^2 = A_{11} \int_{-\infty}^{\infty} dt \int_{-\infty}^{\infty} f^2(t-u)\, \bar{E}_b p_1(u)\, du$$

$$= \bar{E}_b \int_{-\infty}^{\infty} p_1(u)\, du = \bar{E}_b$$

The ensemble representation is used here because the analysis to follow assumes a slowly varying multipath channel which the equalizer can track. Hence the BER statistical performance is determined by computing the channel ensemble statistics of the bit error probability for the Decision-Feedback Equalizer (DFE). An overbar is used to denote channel ensemble averages. Brackets <> will be used to denote average over noise or source statistics for a particular channel realization. For the white Gaussian noise channels the additive noise terms $n_i(t)$ are zero mean and have second moments

$$\langle n_i(t)\, n_j^*(\tau) \rangle = N_o\, \delta_{ij}\, \delta(t-\tau), \quad i, j = 1, 2, \ldots D,$$

where N_o is the noise spectral density in watts/Hz.

Each forward filter in a realizable DFE consists of a finite length tapped delay line filter with tap spacing of τ_s seconds. If there are K_2 "late" taps and K_1 "early taps", the tapped delay line filter impulse response is

$$w_i(t) = \sum_{k=-K_1}^{K_2} w_{ik}^*\, \delta(t-k\tau_s) \qquad (4.4)$$

where the tap gain value is chosen with a complex conjugate for notational convenience later. The receiver filter has impulse response f(-t) which matches the transmit pulse waveform. For this choice, in the absence of multipath, and after time synchronization, the optimum tap weights for the main beam diversity forward filter reduce to one tap on and the rest off. The output of the forward filter is sampled at the symbol rate 1/T to produce the sample x_m. The backward filter correction sample

is summed with the sampled receiver filter output x_m to produce the detection variable z_m at the mth symbol spoch. The backward filter weights previous decision $\hat{s}_{m-1}$, i>o, by the complex weight b_i to form the sample output

$$y_m = \sum_{i=1}^{B} b_i \hat{s}_{m-1} \tag{4.5}$$

at the decision time for the s_m symbol. The decision on s_m is denoted as $\hat{s}_m$. The decision process takes the form

$$z_m = x_m + y_m$$

$$\hat{s}_m = \text{sgn}\,(\text{Re}(z_m)) + j\,\text{sgn}\,(\text{Im}(z_m))$$

where sgn is the signum function.

The parameters of the DFE are the number of forward filter taps K, the forward filter tap spacing, τ_s and the number of backward filter taps, B. The optimum DFE requires K = ∞ = B and τ_s = 1/W where W is the two-sided bandwidth. A practical choice of parameters for troposcatter channels was determined from computer simulation of a fading channel equalizer application to be K = 3 = B and τ_s = T/2.

(2) DFE Performance Analysis

Previous methods of determining bit error rate (BER) performance of practical equalizer structures have been restricted to Monte Carlo simulations [4.3, 4.4] using an ensemble of multipath channels. An analytic approach for calculating the BER is complicated by the presence of an intersymbol interference term in the signal-to-noise ratio (SNR) expression for a particular channel realization. Because of this term, the calcula-

tion of the average over the channel ensemble is a formidable task. On the other hand, omission of the intersymbol interference term leads to a mean BER which for a fixed SNR monotonically decreases with increasing multipath spread. For any practical equalizer under a fixed SNR constraint the mean BER will initially decrease for increasing multipath spread but then increase as the multipath exceeds the equalizer's capability to mitigate the intersymbol interference. Elimination of the intersymbol term provides a convenient lower bound which both shows the intersymbol interference penalty and is an accurate performance estimate for small multipath spreads. However, the lower bound is too loose for performance calculation when the rms multipath spread is on the order of the forward filter width. The analytic procedure to be developed allows accurate calculation of the lower bound for no intersymbol interference and by an approximation of the intersymbol interference effect provides a performance estimate for the large multipath case.

Two key assumptions are introduced in the analysis of the performance of a DFE on a fading complex Gaussian channel. These assumptions have been used previously [4.2, 4.5] to derive predictions of average bit error rate (ABER) for conventional, i.e., 2S, 2F, and 2S/2F, diversity configurations. Test results both on a channel simulator and in field test measurements showed excellent agreement. These assumptions are again used and the analysis extended to include the prediction of ABER for angle diversity configurations and the prediction of the BER distribution for both conventional and angle diversity systems. The BER distribution predictions will be used subsequently to develop an outage probability prediction on a yearly basis.

We begin the analysis by considering a general Ith order diversity system. In the notation of the previous subsection, the received signal for the ith diversity path has the form

$$r_i(t) = \sum_{m=-\infty}^{\infty} s_m \int_{-\infty}^{\infty} h_i(x)\ f(t-mT-x)\ dx + n_i(t)$$

$$i = 1,2,\ldots I \qquad (4.6)$$

We define the combined transmitter and receiver response as

$$g(t) = \int_{-\infty}^{\infty} f(t+x)\ f(x)\ du$$

and its convolution with the channel as

$$\sqrt{\bar{E}_b} q_i(t) = \int_{-\infty}^{\infty} g(t-u)\ h_i(u)\ du. \qquad (4.7)$$

For a sampling time* t_i, $i = 1,2,\ldots I$, the detection variable z has the form

$$z = \sum_{i=1}^{I} \sum_{k=-K_1}^{K_2} \left[w_{ik}^* \sum_{m=-\infty}^{\infty} s_m \sqrt{\bar{E}_b} q_i(t_i - mT - k\tau_s) + v_i(t_i - k\tau_s) \right],$$

where the $K=K_1+K_2+1$ forward filter taps per diversity are apportioned between K_2 "past" taps and K_1 "future" taps and one center tap. The noise variate

$$v_i(t_i) = \int n_i(t_i-u)\ f(u)\ du$$

is zero-mean Gaussian with second moment

$$\langle v_i(t_i-k\tau)\ v_j^*\ (t_j-\ell\tau)\rangle = 0 \qquad i \neq j \qquad (4.8a)$$

$$\langle v_i(t_i-k\tau)\ v_j^*\ (t_j-\ell\tau)\rangle = N_0\ g(k\tau-\ell\tau). \quad i=j \qquad (4.8b)$$

*because the mean delay through individual angle diversity channels is different, different sampling times must be assumed for generality.

There exists an obvious representation in a $K=K_1+K_2+1$ dimensional column vector form, viz.,

$$z = \sum_{i=1}^{I} \underline{w}_i' \left(\sqrt{E_b} \sum_{m=-\infty}^{\infty} s_m \underline{g}_{mi} + \underline{v}_i \right) \tag{4.9}$$

where the accent mark refers to complex conjugate transpose. The vector $\underline{w}_i$ represents the forward filter complex tap gains for diversity i, $\underline{g}_{mi}$ represents the ith diversity sampled continuous filter response for the mth transmitted symbol, and $\underline{v}_i$ is a zero-mean Gaussian noise vector process with positive definite covariance matrix $N_0 G_0$ where

$$G_0(k,\ell) = g(k\tau - \ell\tau) \tag{4.10}$$

For QPSK, every other bit decision is made on the real part of z and there is quadrature symmetry and thus the real noise power affecting that decision is

$$\delta_0^2 = \langle \mathrm{Re}(\sum_{i=1}^{I} \underline{w}_i' \underline{v}_i)^2 \rangle = \frac{N_0}{2} \sum_{i=1}^{I} \underline{w}_i' G_0 \underline{w}_i \tag{4.11}$$

If one assumes $s_m = 0$, $m \neq 0$, there is no intersymbol interference and the analysis for the BER statistics leads to an SNR expression for a particular channel realization which is a quadratic form of the type $\underline{g}_0' G_0^{-1} \underline{g}_0$ where $\underline{g}_0$ is a complex Gaussian vector with statistics determined by the channel and G_0 is a positive definite matrix. After a diagonalization procedure the bit error rate statistics as a function of the SNR can be computed for differentially coherent detection. This calculation leads to lower bound expressions. When the intersymbol interference is present, an effective signal-to-noise ratio can be defined which leads to a quadratic form, but both the vector and the matrix have random components. A method of deriving sta-

tistics of this quadratic form is not apparent. One course which has proved effective is to approximate the intersymbol interference effect in a manner which will modify the matrix in the quadratic form in order to keep its deterministic nature. This can be accomplished if the following two approximations are made.

(1) Assume the interference symbols s_m, $m \neq 0$, are Gaussian distributed rather than complex binary.

(2) Approximate the power from the fading intersymbol interference by its mean.

This approach assumes that the intersymbol interference (ISI) after equalization in a fading multipath channel can be well approximated by an equivalent non-fading additive Gaussian noise term. Since after equalization, the ISI is generally small, most bit errors are a result of fades in the desired signal component. Thus, approximation of the interference characteristics does not significantly alter the BER statistical analysis.

In the absence of error propagation which can be neglected in the analysis, the backward filter cancels the interference contribution due to past symbols, i.e., symbols which arrive before the symbol currently being decided on. If we arbitrarily take the symbol selected for decision as s_0, the remaining interference is classified as future and the contribution for the ith diversity is given by

$$\sqrt{E_b} \sum_{m=1}^{M} s_m \underline{w}_i' \underline{q}_{mi} \equiv \underline{w}_i' \underline{u}_i. \tag{4.12}$$

where

$$\underline{u}_i = \sqrt{E_b} \sum_{m=1}^{M} s_m \underline{q}_{mi} \tag{4.13}$$

is defined as the ith diversity ISI vector.

The sum can be truncated after a few terms as the dot product will disappear for large m due to the finite duration of the pulse function $q_i(t)$. The first approximation is to take s_m as a zero mean complex Gaussian variate with mean magnitude squared value ν^2. This quantity should be less than two because the approximation of a unit magnitude binary variable by a unit variance Gaussian variable will certainly lead to pessimistic performance results due to the tails of the Gaussian distribution. For large multipath spreads, a choice of $\nu^2=1/2$ was found to provide good agreement between calculated and measured values in a average BER evaluation [4.2, 4.5] for conventional diversity systems.

Equation (4.9) can be rewritten as

$$z = \sum_{i=1}^{I} \underline{w}_i' \left(\underline{q}_{0i} \sqrt{E_b}\, s_0 + \underline{v}_i + \underline{u}_i \right) \tag{4.14}$$

where the desired signal component, the noise component, and the ISI component are shown explicitly. Note that the power in the signal component fades due to random variation in the vector $\underline{q}_{0i}$ and that the power in the ISI component also fades due to the dependence on the random vectors q_{mi}, m = 1,2,...M. The noise power component does not fade as has been shown in Eq. (4.11) where a fixed noise power independent of the transmission medium variations results. The second assumption leading to a tractable analysis is to assume that the power from the fading ISI components can be approximated by its mean. Let $\tilde{\delta}^2$ represent the actual detected power from the noise and ISI components. Since the additive noise contribution from $\underline{v}_i$ is independent of the source digit contribution from u_j, $\forall$ i,j, the effective noise power for the decision on the real part of z is

$$\tilde{\delta}^2 = \left\langle \left[\mathrm{Re}\left(\sum_{i=1}^{I} w_i'(v_i + u_i) \right) \right] \right\rangle$$

$$\tilde{\delta}^2 = \sum_{i=1}^{I} \left[\frac{N_0}{2} \underline{w}_i' G_0 \underline{w}_i + \frac{1}{2} \underline{w}_i' \sum_{j=1}^{I} \langle \underline{u}_i \underline{u}_j' \rangle \underline{w}_j \right] \tag{4.15}$$

Note that in forming the real part in (4.15) for complex representation of bandpass waveforms, terms of the form

$$\underline{w}_i'\underline{u}_i\underline{w}_j'\underline{u}_j$$

are double frequency terms and average to zero. The ISI covariance matrix in (4.15) after averaging over the source statistics is

$$\langle \underline{u}_i\underline{u}_j' \rangle = \bar{E}_b \sum_{m=1}^{M}\sum_{n=1}^{M} \underline{q}_{mi}\underline{q}_{nj}' \langle s_m s_n \rangle$$

$$= \bar{E}_b \sum_{m=1}^{M} \underline{q}_{mi}\underline{q}_{mj}' \qquad (4.16)$$

The second approximation used in the analysis is to consider the fading ISI power due to (4.16) to be equivalent to the fixed power

$$\frac{1}{2}\,\underline{w}_i'\,\overline{\langle \underline{u}_i\underline{u}_j \rangle}\,\underline{w}_j = \frac{1}{2}\,\bar{E}_b\,\underline{w}_i' \sum_{m=1}^{M} \overline{\underline{q}_{mi}\underline{q}_{mj}'}\underline{w}_j \qquad (4.17)$$

where the overbar is used to denote averages with respect to the channel variations. Replacing δ^2 by its approximation $\tilde{\delta}^2$ we have

$$\delta^2 = \sum_{i=1}^{I} \frac{N_0}{2}\,\underline{w}_i' G_0 \underline{w}_i + \frac{\bar{E}_b}{2}\,\underline{w}_i' \sum_{j=1}^{I}\sum_{m=1}^{M} \overline{\underline{q}_{mi}\underline{q}_{mj}'}\underline{w}_j \qquad (4.18)$$

We now find it notationally convenient to define the extended IK column vectors

$$\underline{w} = \begin{bmatrix} \underline{w}_1 \\ \underline{w}_2 \\ \vdots \\ \underline{w}_I \end{bmatrix} , \quad \underline{q}_m = \begin{bmatrix} q_{m1} \\ q_{m2} \\ \vdots \\ q_{mI} \end{bmatrix} , \tag{4.19a}$$

the K x K sub-matrices

$$S_{ij} = \frac{\bar{E}_b}{N_0} \sum_{m=1}^{M} \overline{\underline{q}_{mi}\underline{q}'_{mj}} , \tag{4.19b}$$

and the IK x IK extended matrix

$$G = \begin{bmatrix} G_0 + S_{11} & S_{12} & \cdots & S_{1I} \\ S_{21} & G_0 + S_{22} & S_{23} & \cdots & S_{2I} \\ & & \ddots & & \\ S_{I1} & \cdots & S_{I,I-1} & G_0 + S_{II} \end{bmatrix} \tag{4.19c}$$

The matrix G_0 has been previously defined in (4.10). The outer product $\overline{\underline{q}_{mi}\underline{q}'_{mj}}$ is related to the cross channel multipath profile channel moments

$$\overline{h_i(t)h_j^*(t)} = \delta(t - \tau)\bar{E}_b A_{ij} p_{ij}(t) , \quad i,j = 1,2,\ldots I \tag{4.20}$$

AD-A091 764 SIGNATRON INC LEXINGTON MA F/G 9/5
ADAPTIVE ANTENNA CONTROL (AAC) PROGRAM.(U)
AUG 80 P MONSEN, S PARL DAAB07-76-C-8085
UNCLASSIFIED A212 CSA-76-8085-F NL

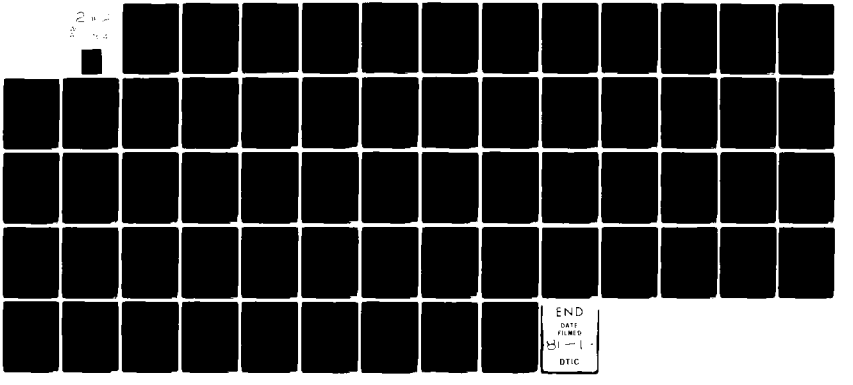

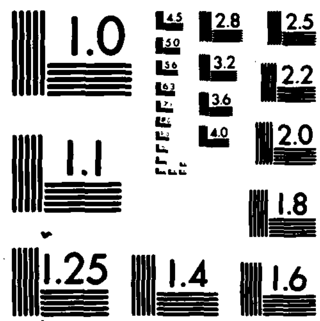

MICROCOPY RESOLUTION TEST CHART

NATIONAL BUREAU OF STANDARDS-1963-A

We can write the outer product contributions to (4.19b) as a K x K matrix with elemental values at the k,ℓ location equal to

$$a_{k\ell}^{ij}(m) = \overline{q_i(t_i - mT - k\tau_s)\, q_j^*(t_j - mT - \ell\tau_s)} \quad , \; i,j = 1,2,\ldots I \tag{4.21a}$$

Performing the indicated integration in Eq. (4.7) and using the second moment result of Eq. (4.20), we have

$$a_{k\ell}^{ij}(m) = A_{ij} \int g(t_i - mT - k\tau_s - x)\, g(t_j - mT - \ell\tau_s - x)\, p_{ij}(x)\, dx \tag{4.21b}$$

This set of integrals (Eq. 4.21b) completely describes the transmission medium effects on the DFE performance.

The noise and ISI power in the real channel symbol detector reduces from (4.18) to

$$\delta^2 = \frac{N_0}{2}\, \underline{w}' G \underline{w} \tag{4.22a}$$

and the signal power at the same decision device is

$$P_s = \bar{E}_b \left[\mathrm{Re}(\underline{w}' \underline{q}_0) \right]^2 \tag{4.22b}$$

We define signal-to-noise ratio (SNR) as $P_s/2\delta^2$ at the detector as this definition is consistent with the SNR definition which provides a BER of

$$\mathrm{BER}_{\mathrm{IDEAL}} = \frac{1}{2}\, \mathrm{erfc}\, (\sqrt{\mathrm{SNR}}) \tag{4.23}$$

for the ideal non-fading, Gaussian-noise, binary-symbol channel. The signal-to-noise ratio for this fading channel application is then

$$\rho \equiv \frac{\bar{E}_b}{N_0} \; \mathrm{Re}(\underline{w}' q_0)^2 / (\underline{w}' G \underline{w}) \tag{4.24}$$

which we seek to maximize as a function of the forward filter weight vector, $\underline{w}$. Consider the generalized dot product defined on the positive definite matrix G, i.e.,

$$(\underline{u}, \underline{v}) = \underline{u}' G \underline{v}. \tag{4.25}$$

Equation (4.24) can be written as

$$\rho \equiv \frac{\bar{E}_b}{N_0} \frac{[\mathrm{Re}(\underline{w}, G^{-1} q_0)]^2}{(\underline{w}, \underline{w})} \tag{4.26}$$

and by a generalization of the Schwartz Inequality we obtain

$$\rho \leq \frac{\bar{E}_b}{N_0} \frac{|(w, G^{-1} q_0)|^2}{(\underline{w}, \underline{w})} \leq \frac{\bar{E}_b}{N_0} (G^{-1} q_0, G^{-1} q_0) \tag{4.27}$$

with equality if and only if

$$\underline{w}_{opt} = G^{-1} q_0 \tag{4.28}$$

Note (4.28) results in a pure real term in (4.26) to satisfy the Re (·) requirement.

The maximum SNR is then

$$\rho_{max} = \frac{\bar{E}_b}{N_0} \; q_0' \; G^{-1} q_0 \tag{4.29}$$

As a check on the normalization, if $I = 1$, $\sigma_1 = 0$ and $t_1 = 0$ we have from Eq. (4.7)

$$q(-k\tau) = g(-k\tau) = G_{0k} \tag{4.30}$$

and then

$$\rho_{max} = \frac{\bar{E}_b}{N_0} g(0) = \frac{\bar{E}_b}{N_0} \tag{4.31}$$

as is expected in the absence of multipath and diversity. In this trivial example the ideal BER (4.23) is achieved for every fading channel realization.

We will now establish that the mean square error function

$$\langle \epsilon^2 \rangle = \frac{1}{2} \langle |z - ds_0|^2 \rangle \tag{4.32}$$

which is minimized by the decision-feedback equalizer leads to the same set of forward filter weights as maximization of the SNR in (4.26) for the appropriate choice of scale factor d. After squaring and averaging, equation (4.32) becomes

$$\begin{aligned} \langle \epsilon^2 \rangle &= \bar{E}_b \underline{w}' \underline{q}_0 \underline{q}_0' \underline{w} - 2\sqrt{\bar{E}_b}\, d\, \mathrm{Re}(\underline{w}' \underline{q}_0) + \frac{1}{2} N_0 \underline{w}' G \underline{w} + d^2 \\ &= |\sqrt{\bar{E}_b}\, \underline{w}' \underline{q}_0 - d|^2 + N_0 \underline{w}' G \underline{w}. \end{aligned} \tag{4.33}$$

Minimization of (4.33) is equivalent to the LaGrange multiplier problem

$$\min_{\underline{w}} \quad \underline{w}' G \underline{w} - 2\beta \underline{w}' \underline{q}_0 \tag{4.34}$$

which has solution

$$\underline{w} = \beta G^{-1} \underline{q}_0. \tag{4.35}$$

Since Eq. (4.28) and (4.35) are the same except for an unimportant scale factor, we have established that the maximum signal-to-noise ratio for a minimum mean-square error DFE and a particular channel realization is the quadratic form given by Eq. (4.29).

The maximum SNR result (Eq. 4.29) indicates the optimum DFE performance for a particular fading channel realization. Since $\underline{q}_0$ is a function of the transmission medium, the BER statistics must treat $\underline{q}_0$ as a random process. Note our two approximations have led to a deterministic form for the matrix G which makes an analytic treatment feasible. We now turn our attention to the evaluation of BER statistics; in particular, the average BER and the BER probability density function. We begin with the easier task.

(3) Average Bit Error Rate

The average bit error rate is computed by taking the average over the channel ensemble. The bit error probability for QPSK for any member of the channel ensemble is

$$p_c = \frac{1}{2} \, pr\{\xi > 1\} + \frac{1}{2} \, pr\{\xi < -1\} \tag{4.36}$$

where ξ is a zero-mean Gaussian random variable with standard deviation equal to $\sqrt{1/2\rho_{max}}$. The bit error probability is

$$P_c = (2\pi)^{-\frac{1}{2}} \int_{2\rho_{max}}^{\infty} \exp(-u^2/2)\,du = \frac{1}{2}\,\mathrm{erfc}\,\sqrt{\rho_{max}} \qquad (4.37)$$

The subscript c denotes that the detection process was coherent, i.e. the receiver knows the transmitted carrier phase. Differential detection of phase-shift-keyed signals yields a bit error probability [4.6]

$$P_d = \frac{1}{2}\,e^{-\rho_{max}} \qquad (4.38)$$

The tap gains of an adaptive MMSE equalizer remove the phase and frequency difference between the transmitter and receiver carrier clocks to an ambiguity of 180° for binary transmission and 90° for quaternary transmission. This ambiguity is eliminated by differentially encoding the transmitted data. The performance of coherently detected and differentially encoded data signals for a fixed ρ_{max} is approximately double the error rate given by (4.37). When practical degradations are included in the analysis the performance is closer to the differential detection expression (4.38). Thus the ensemble average of P_c is of interest as a fading channel performance bound and the ensemble average of P_d is of interest as an estimate of realizable modem performance.

Let y(x) be the probability density function for ρ_{max} and Y(S) its Laplace transform. We want to calculate the ensemble averages

$$\bar{P}_c = \int_0^{\infty} \frac{1}{2}\,\mathrm{erfc}\,\sqrt{x}\; y(x)\,dx \qquad (4.39)$$

$$\bar{P}_d = \int_0^{\infty} \frac{1}{2}\,e^{-x} y(x)\,dx = \frac{1}{2}\,Y(1) \qquad (4.40)$$

The Laplace transform Y(s) is easily obtained after a diagonalization of the quadratic form in Eq. (4.29)

$$x = \frac{\bar{E}_b}{N_0} g_0' G^{-1} g_0 = \frac{\bar{E}_b}{N_0} \underline{\alpha}' \underline{\alpha} \tag{4.41}$$

where $\underline{\alpha}$ is a zero-mean complex Gaussian vector with a diagonal covariance matrix $\Gamma ij = \lambda_i \delta_{ij}$, i=1,2,...Ik, where I is the number of explicit diversity channels and k is the number of forward filter weights. The diagonalization resulted from the transformation

$$\underline{\alpha} = MG^{-\frac{1}{2}} g_0 \tag{4.42}$$

and M is the normalized orthogonal matrix for the matrix

$$G^{-\frac{1}{2}} \overline{g_0 g_0'} G^{-\frac{1}{2}}, \text{ i.e.} \tag{4.43}$$

$$G^{-\frac{1}{2}} \overline{g_0 g_0'} G^{-\frac{1}{2}} M = M\Gamma \tag{4.44}$$

$$M'M = I. \tag{4.45}$$

Thus the eigenvalues λ_i are also the eigenvalues of the symmetric matrix $G^{-\frac{1}{2}} \overline{g_0 g_0'} G^{-\frac{1}{2}}$ and the unsymmetric matrix $G^{-1} \overline{g_0 g_0'}$. Since the components of $\underline{\alpha}$ are uncorrelated Gaussian, the probability density for ρ_{max} is the convolution of exponential densities which yields a Laplace transform in product form.

$$Y(s) = \prod_{k=1}^{IK} (1 + \frac{\bar{E}_b}{N_0} \lambda_k s)^{-1} \tag{4.46}$$

The mean BER for DPSK is

$$\bar{P}_d = \frac{1}{2} Y(1) = \frac{1}{2} \prod_{k=1}^{IK} (1 + \frac{\bar{E}_b}{N_0} \lambda_k)^{-1} . \tag{4.47}$$

For coherent detection it is necessary to find the coefficients A_{ik} in a partial fraction expansion of Y(s), i.e.,

$$Y(s) = \sum_{k=1}^{IK} A_k \left(1 + \frac{\bar{E}_b}{N_0} \lambda_k s\right)^{-1} .$$

A recursive method for finding the coefficients and the resulting error probability for coherent detection is detailed in [4.7] where the mean BER for the infinite length optimum single pulse receiver was determined. We will concentrate on the DPSK expression (4.47) because the DPSK bit error probability curve for the Gaussian noise non fading channel closely matches the BER for the MD-918 modem, i.e., the implementation loss and differential encoding loss in the CPSK detection system is approximately equal to the loss incurred in ideal DPSK relative to ideal CPSK. Figure 4.2 illustrates this result. Since in a fading channel application most of the bit errors will occur during periods of low SNR, good correspondence between ideal DPSK and the measured DFE modem at low SNR is desirable for a DPSK representation.

For a DPSK system or for the use of the DPSK expression to approximate the Gaussian noise non fading performance of a practical modem, calculation of the average bit error probability does not require the determination of the eigenvalues. Note that (4.47) has the determinant form

$$\bar{P}_d = \frac{1}{2} \left(\det\left|I + \frac{\bar{E}_b}{N_0} G^{-1} C\right|\right)^{-1} \qquad (4.48)$$

where the covariance matrix C is defined by

$$C = \overline{g_0 g_0^T} \qquad (4.49a)$$

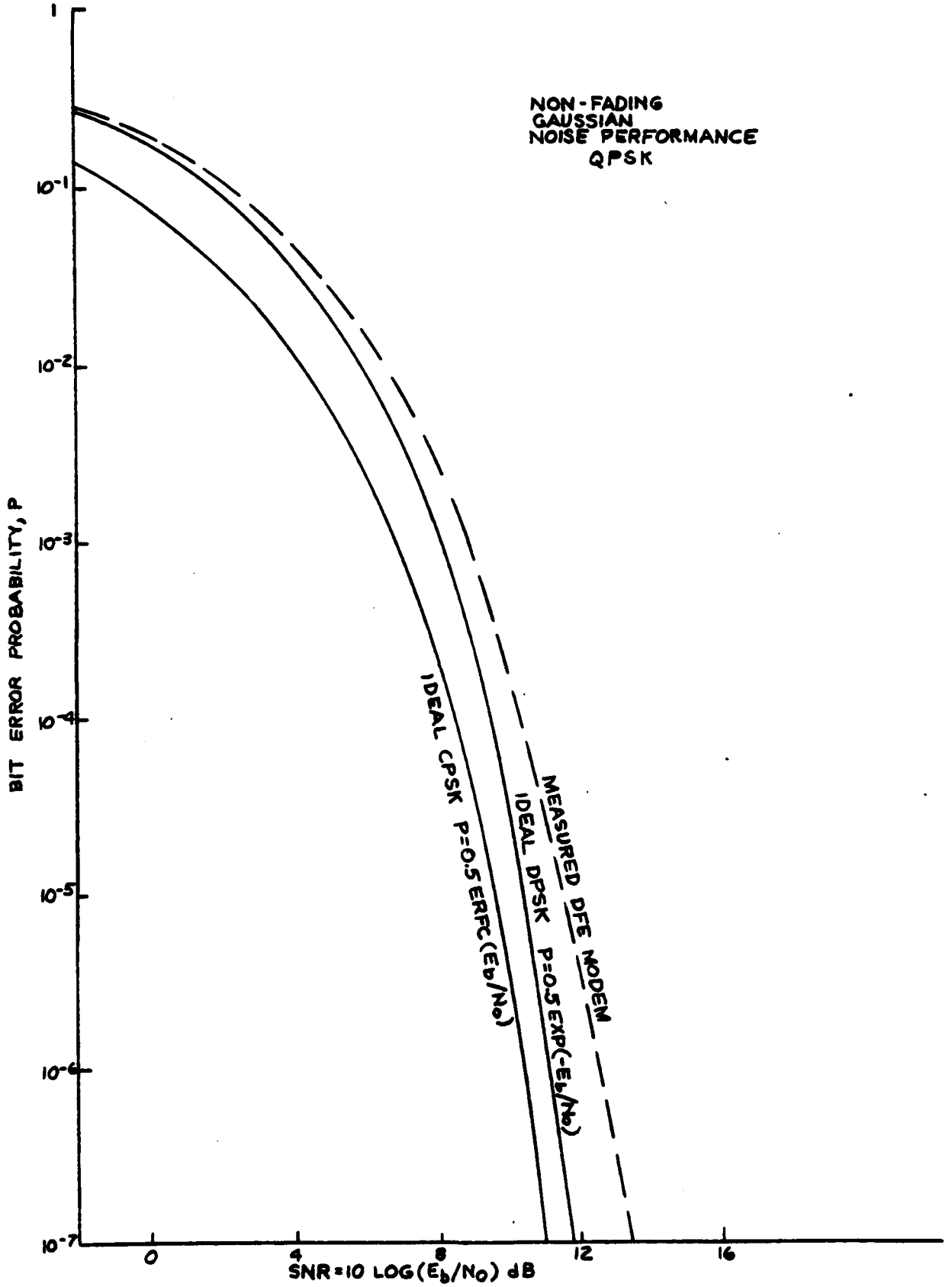

Fig. 4.2 Non Fading Performance

The matrix C is of rank IK and has a submatrix structure of the form

$$C = \begin{bmatrix} R_{11} & R_{12} & \cdots & R_{1I} \\ R_{21} & R_{22} & \cdots & R_{2I} \\ & & & \\ R_{I1} & R_{I-1,2} & \cdots & R_{II} \end{bmatrix} \qquad (4.49b)$$

where R_{ij} is a K x K matrix defined by

$$R_{ij} = \overline{q_{0i} q_{0j}^{\prime}} \qquad (4.49c)$$

and thus it has elemental values at the k,ℓ location equal to $a_{k\ell}^{ij}(0)$ which was defined in Eq. 4.21b.

The general result (Eq. 4.48) is valid for any Ith order diversity system. In subsection 4.1.2.3 we examine how these matrices simplify when specific diversity configurations are assumed. First we derive the formulas for the BER probability density function and describe how a yearly outage probability estimate can be obtained.

(4) Bit Error Rate PDF and Outage Probability

For a particular channel realization the signal-to-noise ratio has been expressed as the sum (c.f. Eq. 4.41),

$$\rho_{max} = \frac{E_b}{N_0} \sum_{i=1}^{IK} |\alpha_i|^2 \qquad (4.50)$$

The random fading causes the α_i to be independent zero-mean complex Gaussian values with variance

$$\overline{|\alpha_i|^2} = \lambda_i \qquad i = 1,2...IK \tag{4.51}$$

where the λ_i are eigenvalues of the non symmetric matrix $G^{-1}C$. The matrices G and C are defined by Eqs. (4.19) and (4.49), respectively. The bit-error-rate is itself a random process equal to

$$p_d = \frac{1}{2} e^{-\rho_{max}} \tag{4.52}$$

The probability density function (PDF) of p_d can be found by a transformation from tne PDF of ρ_{max}. The random variable $|\alpha_i|^2$ has an exponential PDF whose Laplace transform is

$$Y_i(s) = (1 + \lambda_i s)^{-1} \tag{4.53}$$

and since the $|\alpha_i|^2$ are independent, the Laplace transform of the PDF for ρ_{max} is

$$Y(s) = \int_0^\infty y(p) e^{-sp} d\rho = \prod_{i=1}^{IK} (1 + \frac{\bar{E}_b}{N_0} \lambda_i s)^{-1} \tag{4.54}$$

The λ_i values are the eigenvalue set from the matrix $G^{-1}C$.

Partial fraction expansion techniques discussed in the previous subsection can be used in a straightforward but somewhat tedious calculation to obtain the PDF $y(\rho)$. To calculate the BER PDF $x(p)$ we use (4.52) in the transformation

$$x(p) = y(\rho) \left|\frac{d\rho}{dp}\right| = \frac{1}{p} y(\ln(1/2p)) \tag{4.55}$$

$$\rho = \ln(1/2p)$$

The outage probability has been defined as the probability that the bit error rate exceeds a value p and is equal to the

cumulative distribution of the PDF. This distribution is a function of the mean bit energy to noise power ratio

$$\gamma = \bar{E}_b/N_0$$

or in dB units $\Gamma = 10\ \mathrm{Log}(\gamma)$ dB.

Thus, we have the conditional outage probability

$$B(p|\Gamma) = \mathrm{prob}\{BER \geq p | \bar{E}_b/N_0 = \gamma\} = \int_p^{1/2} x(p)dp \qquad (4.56)$$

The integration in (3.56) is more easily accomplished before the transformation, i.e.

$$B(p|\Gamma) = \mathrm{prob}\{\rho_{max} < \ell n(1/2p) | \bar{E}_b/N_0 = \gamma\}$$

$$= \int_0^{\ell n(1/2p)} y(\rho)d\rho. \qquad (4.57)$$

The unconditional outage probability averages over the long term variations in $\bar{E}_b/N_0$ which occur on any fading channel. In troposcatter propagation these variations over a year are well described by the Gaussian PDF

$$f(\Gamma) = \frac{1}{\sigma\sqrt{2\pi}}\ e^{-(\Gamma-m)^2/2\sigma^2} \qquad -\infty < \Gamma < \infty \qquad (4.58)$$

where m and σ are the mean and standard deviation of the long term $\bar{E}_b/N_0$ variations expressed in dB units. The unconditional outage probability for troposcatter is then*

$$B(p) = \int_p^{1/2} \int_{-\infty}^{\infty} x(q|\Gamma) f(\Gamma) d\Gamma\, dq$$

*This calculation assumes that the multipath distribution can be approximated by its mean value. This assumption is suggested by conditional outage probability results presented later.

where the dependence of the BER PDF on Γ has been shown explicitly. The unconditional outage probability can be expressed as an average of the conditional form in (4.56) by

$$B(p) = \int_{-\infty}^{\infty} f(\Gamma)B(p|\Gamma)d\Gamma \qquad (4.59)$$

In practice the calculation of the above integral is difficult because each value of Γ requires a different partial fraction expansion solution to obtain $x(p|\Gamma)$. Fortunately, $B(p|\Gamma)$ is a very steep function of Γ relative to the PDF $f(\Gamma)$ so a relatively simple numerical integration routine should approximate $B(p)$ for a few fixed values of p quite well. Of particular interest in this analysis are the values $p = 10^{-2}$, 10^{-4}, and 10^{-6}. A numerical procedure to estimate $B(p)$ might proceed as follows. First find the value of SNR from the analysis of the previous subsection which gives a mean BER of p. Call this value Γ_0. When $\Gamma = \Gamma_0$ the instantaneous BER is most of the time much smaller than the average BER. Hence, non negligible values of $x(p|\Gamma)$ must be for a Γ value smaller than Γ_0. Let the SNR decrease in Δ dB steps, i.e.

$$\Gamma_{i+1} = \Gamma_i - \Delta \qquad i = 0,1,2,... \qquad (4.60)$$

and find the corresponding values $B(p|\Gamma_i)$ by inverting the relationship given in (4.56). This involves for each Γ_i performing the partial fraction expansion to obtain $B(p|\Gamma)$ and then in a look-up operation determining $B(p|\Gamma)$ for a specific p. The values of $B(p|\Gamma_i)$ should start small and increase toward unity. After $B(p|\Gamma_i)$ exceeds a threshold the procedure can be terminated and $B(p)$ approximated by

$$B(p) \doteq \sum_{i=0}^{N} f(\Gamma_i)B(p|\Gamma_i) \Big/ \sum_{i=0}^{N} f(\Gamma_i) \qquad (4.61)$$

In this manner the outage probability distribution for the year can be determined.

b. Special Diversity Configurations

In this subsection we consider specific diversity configurations of practical interest and we examine what simplifications in the previous analysis are possible. The two special cases of interest are identical/independent diversity systems and angle diversity systems. The former includes conventional 2S/2F diversity and the latter includes the angle diversity configurations such as 2S/2F/2A, 2S/2A, and 2F/2A.

(1) Identical/Independent Diversity

For this example if the number of identical/independent diversity paths is D then the eigenvalues are repeated D times. This result follows from the identical and independent statistical nature of each diversity path, i.e. the fading channel impulse response is characterized by

$$\overline{h_i(t)h_j^*(\tau)} = \delta(t-\tau)E_b\delta_{ij}p(t),\ i,j=1,2,\ldots D$$

The set of integrals (Eq. 4.21b) which describe the effects of the transmission medium on the DFE performance reduce to

$$\sigma_{k\ell}^{ii}(m)\int_{-\infty}^{\infty} g(t_i-mT-k\tau_s-x)g(t_i-mT-\ell\tau_s-x)p(x)dx$$

$$\sigma_{k\ell}^{ij}(m) = 0 \quad i\neq j$$

For statistically identical diversities the mean path delay through each of the diversity paths is the same. The sampling times t_i are all chosen equal and hence $\sigma_{k\ell}^{ii}(m)$ does not depend on i. The extension to form the matrices G and C; (4.19c) and

(4.49b), respectively, thus requires the submatrix G_0+S_{11} in G and R_{11} in C to be repeated on the diagonal D times. Since the eigenvalues are determined from the matrix $G^{-1}C$, the K distinct implicit diversity eigenvalues are computed from the matrix

$$(G_0+S_{11})^{-1}R_{11}.$$

For this special case we can summarize the procedure for evaluating performance as follows. First let

$$R = R_{11},\ R(k,\ell) = \int_{-\infty}^{\infty} g(t_1-k\tau_s-x)g(t_1-\ell\tau_s-x)p(x)dx$$

$$S = S_{11},\ S(k,\ell) = \frac{\bar{E}_b}{N_0}\sum_{m=1}^{m} R\left(k+\frac{mT}{\tau_s},\ \ell+\frac{mT}{\tau_s}\right)$$

$$G_0(k,\ell) = g(k\tau_s-\ell\tau_s).$$

where k and ℓ represent the K integer values indicating the equalizer tap locations. The integer M is the number of significant future symbol interferers. The average BER is equal to

$$\bar{P}_d = \frac{1}{2}\left(\det\left|I + \frac{\bar{E}_b}{N_0}(G_0+S)^{-1}R\right|\right)^{-D}$$

To find the BER PDF and the outage probability the procedure outlined in the previous subsection is to be followed using the positive definite eigenvalue set $\lambda_1,\lambda_2,\ldots\lambda_K$ repeated D times. The eigenvalue set is determined from the non symmetric matrix $(G_0 + S)^{-1}R$.

(2) Angle Diversity

Consider a diversity configuration with I angle diversity paths and D independent frequency or space diversity paths. The effect of the D independent diversities is to repeat the IK eigenvalues of the correlated diversity system. Since the extension of the result for D>1 is clear, we restrict ourselves here to examining the pure angle diversity system, i.e. D=1.

We now wish to establish that under certain conditions, the correlation between an angle diversity pair does not significantly effect performance and it can be neglected. Under this condition angle diversity reduces to an independent diversity example but with different diversity branch strengths and multipath profiles.

Consider dual vertical angle diversity (I=2) with a K tap forward filter in the DFE. The taps are equally spaced with a width of T/2. The transmission medium is completely characterized by

$$\overline{h_1(t)h_1^*(\tau)} = \delta(t-\tau)A_{11}P_{11}(t)$$

$$\overline{h_2(t)h_2^*(\tau)} = \delta(t-\tau)A_{22}P_{22}(t)$$

$$\overline{h_1(t)h_2^*(\tau)} = \delta(t-\tau)A_{12}P_{12}(t)$$

The multipath profiles $p_{ii}(t)$ have rms multipath spreads of σ_i where

$$\sigma_i^2 = \int_0^\infty t^2 p_{ii}(t)dt - \left(\int_0^\infty t\, p_{ii}(t)\, dt\right)^2, \quad i=1,2.$$

For vertical angle diversity σ_2 is normally a little larger than σ_1. The correlation between angle diversity channels for CW transmission is

$$\xi_{CW} = \frac{1}{\sqrt{A_{11}A_{22}}} \overline{\int h_1(t)dt \int h_2^*(s)ds} = \frac{A_{12}}{\sqrt{A_{11}A_{22}}}$$

where we have used the unit area definition of the multipath profiles. We assume that ξ_{CW} is not negligible, in fact for dual vertical angle diversity it is on the order of 0.6. Correlation effects a digital transmission system through the second moment

$$a_{k\ell}^{ij}(m) = A_{ij} \int_{-\infty}^{\infty} g(t_i - mT - k\tau_s - x) g(t_j - mT - \ell\tau_s - x) p_{ij}(x)dx$$

If this moment is negligible when $i \neq j$, correlation will not effect the digital system. Note that the autocorrelation function $g(\tau)$ has width on the order of T seconds. Now because the mean path delay is longer for the elevated beam, we have to choose a later sampling time for the elevated beam diversity, i.e.,

$$t_2 = t_1 + \Delta$$

where Δ is the estimate of additional transmission delay through the elevated beam. The value of Δ is on the order of $2\sigma_1$. For high data rate systems when T is on the order of Δ, the integral $a_{k\ell}^{12}(m)$ is small compared to $\sqrt{|a_{k\ell}^{11}(m)||a_{k\ell}^{22}(m)|}$

---

* In practice, this effect is achieved by adding a fixed delay to the lower beam diversity.

except when

$$t_1 + \Delta - \ell\tau_s \approx t_1 - k\tau_s,$$

as then the autocorrelation functions approximately line up.

For a two tap forward filter (k=0,1) with τ_s=T/2, the above condition can not be satisfied and performance is approximately the same if A_{12} was taken to be zero. When an additional tap is added to the equalizer, the implicit diversity of the system increases and performance improves. The improvement from two to three taps is not particularly large, however. With three taps (k=-1,0,1) there will be some off axis correlation contributions to the submatrices when k=1, ℓ=-1 and when k=-1, ℓ=1. Since the performance improvement between two and three taps is not large and since the two tap system is not affected by nonzero correlation $A_{12} > 0$, it follows that these off-axis submatrix terms can be neglected for a three tap DFE evaluation. Also note that even for a CW system, the neglect of a correlation equal to 0.6 leads to only about a 1dB error.

The omission of the off-axis submatrix terms eases the eigenvalue determination problem because with independent angle diversity pairs, the three tap DFE requires the calculation of the roots of two cubic equations rather than calculation of eigenvalues from a matrix of rank 6.

In principle these considerations suggest that the correlation effect is reduced for high speed data systems when the data symbol interval becomes sufficiently short to be on the order of the mean delay between angle diversity branches.

For the special case of dual vertical angle diversity with neglected correlation between the angle diversity beams, the performance is calculated as in the previous subsection except two sets of K eigenvalues must be found corresponding to the two multipath profiles $p_1(t)$ and $p_2(t)$. These eigenvalues are weighted by the angle diversity power factors A_{11} and A_{22}. The 2K eigenvalues are then repeated D times for a D identical/independent configuration. The analysis then proceeds as for the identical/independent configuration examined in the previous subsection.

SECTION 4

REFERENCES

[4.1] J.L. Osterholz and D.R. Smith, "The Effects of Digital Tropo Error Statistics on Asymchronous Digital System Design," NTC Conf. Rec., Vol.2, New Orleans, Dec. 1975, pp. 28-25 to 28-31.

[4.2] P. Monsen, "Theoretical and Measured Performance of a DFE Modem on a Fading Multipath Channel," IEEE Trans. on Communications, Vol. COM-25, No. 10, Oct. 1977, pp. 1144-1153.

[4.3] P. Monsen, "Feedback Equalization for Fading Dispersive Channels," IEEE Trans. on Information Theory, Vol. IT-17, No. 1, Jan. 1971, pp. 56-64.

[4.4] P. Monsen, "Adaptive Equalization of the Slow Fading Channel," IEEE Trans. on Communications, Vol. COM-22, No. 8., Aug. 1974.

[4.5] D.R. Kern and P. Monsen, Megabit Digital Troposcatter Subsystem, Final Report, ECOM-74-0040-F, Apr. 1977.

[4.6] J.G. Lawton, "Theoretical Error Rates of Differentially Coherent Binary and Kineplex Data Transmissions," Proc. IRE, Vol. 47, pp. 334-344, Feb. 1959.

[4.7] P. Monsen, "Digital Transmission Performance on Fading Dispersive Diversity Channels," IEEE Trans. on Communications, Vol. COM-21, No. 1, Jan. 1973, pp. 33-39.

[4.8] P. Monsen and S. Parl, Adaptive Antenna Control, 2nd Interim Technical Report, AD A055-820, Contract No. DAAB07-76-C-8085 to Signatron, Inc., Feb. 1978.

SECTION 5

PERFORMANCE STANDARDS AND EXAMPLE COMPUTATION

The communication channel model, path propagation prediction method, and modem performance calculation technique have been combined for prediction of digital troposcatter link performance. Proposed standards for U.S. military communication networks containing troposcatter links have been developed by the Defense Communications Engineering Center (DCEC). In this section we review these standards and discuss the method of application. The RADC troposcatter test link is then used as an example for comparison of performance prediction against the DCEC standard.

a. Performance Standards

Performance standards for evaluation of U.S. DCS digital troposcatter systems are based on the communication requirement established in DCEC Technical Report 12-76 dated November 1976. This report identifies five ranges of outages and performance requirements for each outage range. The five outage ranges are defined as follows:

Range I. Outages under 200 milliseconds duration which are significantly separated in time from any other outage. Such outages will normally occur on a troposcatter link operating with adequate margin. The allowable probability of occurrence of these outages need not be specified since their effect on the user is trivial.

Range II. Outages with durations in the range from 200 milliseconds to five seconds which are significantly separated in time from any other outage. Such outages may occur on either a line-of-sight or a troposcatter link operating with adequate margin (or less than adequate margin if the frequency of occurrence is high). The

allowable probability of occurrence of such an outage should be specified with a value based on its annoyance to the user.

Range III. Outages with durations greater than 5 seconds but less than 2 minutes. Such outages will normally occur on a line-of-sight link. The allowable probability of occurrences of such outages should be specified with a requirement more stringent than that for Range II since such an outage is considered to be a disruption to the user which would cause call termination.

Range IV. A recurrent set of outages of average duration under 200 milliseconds which occurs at an average rate of from 2 to 5 per minute. This condition will normally occur on a troposcatter channel operating with barely adequate margin. The allowable probability of existence of such a condition should be specified with a value based on its annoyance to the user.

Range V. Outages with duration greater than 2 minutes or recurrent outages of any duration which occur more frequently than 5 per minute. The duration of any such outages or period of recurrent outages should be included in the total unavailability specification since the channel is considered essentially unusable. The outages described by this range will normally occur on a troposcatter channel with long-term fading in excess of the fade margin, or on a line-of-sight channel experiencing anomalous index of refraction conditions.

The troposcatter channel is most accurately viewed as having a compound fading characteristic with short term (e.g., hourly) Rayleigh fading impressed on a longer diurnal and annual fading distribution. Historically, the performance of troposcatter links was related to the percentage of time that a particular short term average Signal-to-Noise Ratio (SNR) could be maintained out of the longer term fading ensemble (i.e., time availability). The essence of this convention is used in DCEC TR12-76 and is continued here.

The short term average $\overline{SNR}$ is defined as the ratio of the average received bit energy divided by the noise power in a 1 Hz RF bandwidth. This ratio is frequently denoted $\bar{E}_b/N_0$ where the overbar denotes an average over the fading. In the comparison of diversity configurations, $\bar{E}_b/N_0$ is the value associated with a receiver in a conventional space/frequency diversity system. For PSK systems $\bar{E}_b$ is equal to the average received power per bit times the symbol duration, i.e.

$$\bar{E}_b = \bar{P}_R T/LOG_2(M)$$

where $\bar{P}_R$ = average received power

T = symbol length

M = number of bits per symbol.

The data rate in bits/second is

$$R_b = LOG_2(M)/T \qquad \text{bits/second}$$

and thus $\bar{E}_b/N_0$ can be expressed as the ratio of average received power to noise power in the bit rate bandwidth, i.e.,

$$\bar{E}_b/N_0 = \bar{P}_R/N_0 R_b.$$

Consistent with the notation in TR12-76, this parameter, short

term $\overline{SNR}$, will be denoted throughout this discussion by the symbol, γ_0. The γ_0 necessary to obtain a specified short term performance (here described on the basis of acceptable outage rates and duration) will then be described in unavailability fashion (i.e., to be maintained for all but a certain percentage of time) and converted into required system gains for various DCS digital troposcatter configurations. The performance criteria selected in TR12-76 to be used in these determinations are indicated in Table 5.1.

Table 5.1

DCS PCM VOICE PERFORMANCE CHARACTERISTICS

A OUTAGE RANGE	B CRITERIA	C OUTAGE PROBABILITY
II	.2 sec $\leq$ outage < 5 sec.	$7.5 \cdot 10^{-4}$
III	5 sec < outage < 1 min.	$7.5 \cdot 10^{-5}$
IV	2 < outages/min. < 5 outage < .2 sec.	$2.5 \cdot 10^{-3}$
V	5 < outages/min. or outage > 2 min.	$1 \cdot 10^{-4}$

An analysis in TR12-76 relates these performance criterion to a value of γ_0 exceeded all but a certain fraction of time. Because of the analytic complexity of the problem, key assumptions are used in deriving γ_0 criteria. These assumptions are:

(1) implicit diversity doubles the effective order of diversity and

(2) the outage probability as a function of $\overline{SNR}$ is taken

as either unity or zero in the computation of yearly outage probability.

The analysis developed here extends the work in TR12-76 by calculating the exact contribution of the implicit diversity and the exact form of the outage probability vs. $\overline{SNR}$ for integration over the yearly $\overline{SNR}$ distribution. Significantly, these new results show that implicit diversity does not double the effective diversity order and that the piece-wise linear approximation of the outage probability is poor when comparing diversity configurations.

Qualitatively the analysis in TR12-76 revealed that the L-band (755-985MHz) systems were most susceptible to outage range condition II with respect to the performance criteria in Table 5.1. This suggests an L-band yearly outage probability requirement of 7.5×10^{-4}, i.e., the probability that the BER exceeds 10^{-4} for 0.2 sec. $\leq$ outage < 5 sec. over a year is less than 7.5×10^{-4}. The higher frequency C-band systems were analyzed in TR12-76 using a 5Hz rms Doppler spread in the evaluation. As a result, the outage range II requirement was not the most demanding criterion for C-band systems. However, measured rms Doppler spread does not indicate that 5Hz spreads will be achieved very often on C-band systems. As an example, Figure 5.1 compares the measured 2σ rms Doppler spread for a 168 mile path using both C band and L band transmissions. The small difference between these distributions suggests that the outage range II criterion should be applied to all troposcatter systems regardless of frequency.

This result can be further established by considering the outage range II criterion in light of the measured results of Fig. 5.1

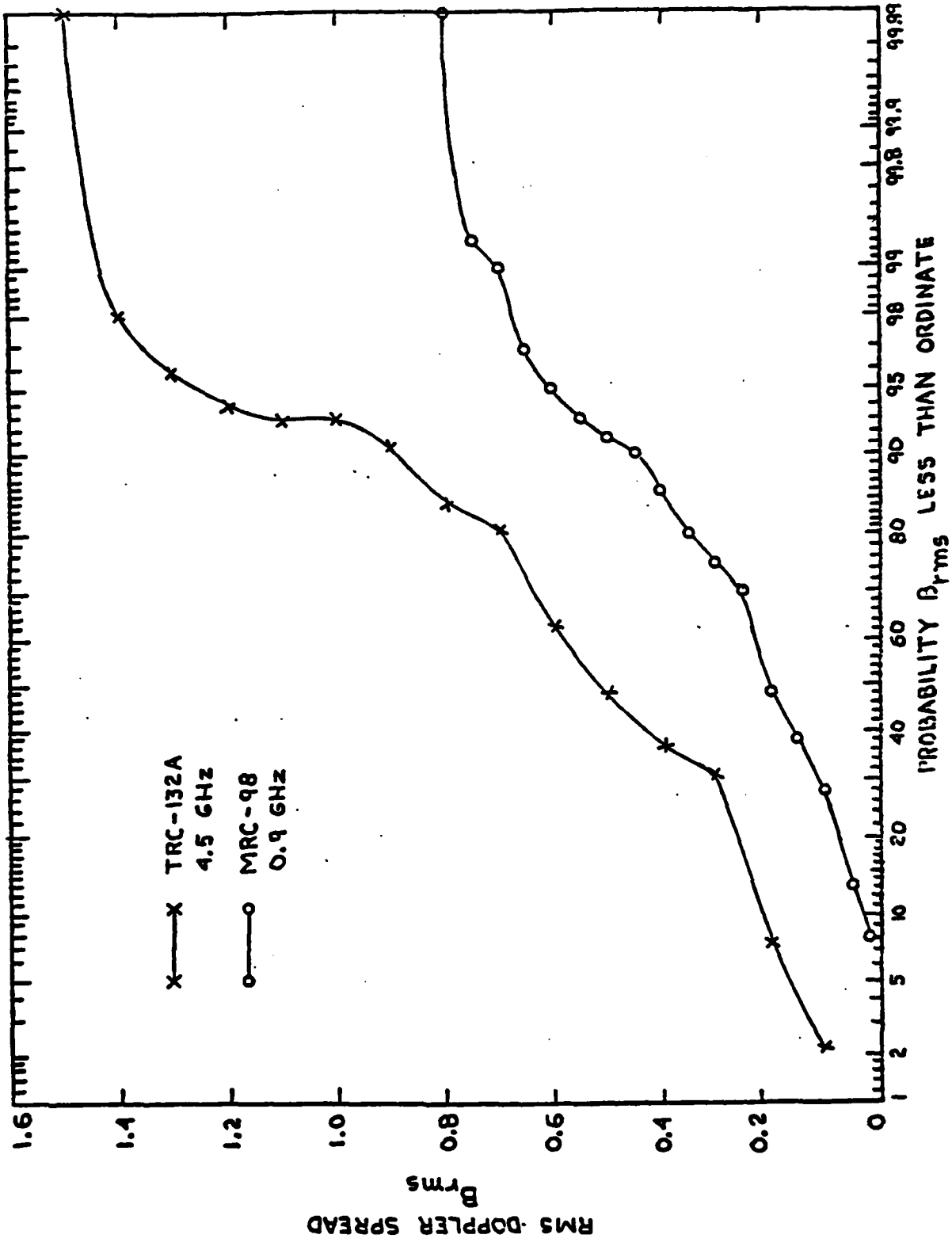

Fig. 5.1 RMS Doppler Spread Distribution; L AND C BAND

and the theoretical results of TR12-76. The troposcatter link outage duration and the distribution of link outage duration derived in TR12-76 are presented here as Figs. 5.2 and 5.3, respectively. If the outage range II criterion is to be met, the averaging process to find the yearly outage probability results in values close to hourly outage probabilities for a γ_0 of 10dB. At 10dB when the rms Doppler spread (N) is 5 Hz, the mean outage duration is less than 0.1 seconds. Since the outage duration must exceed 0.2 seconds to count in range II, the results of Fig. 5.3 show that less than 10% of the outages count toward an outage. Thus it is not surprising that outage range II was not found most critical when 5 Hz was used as the C-band rms Doppler spread. However, the median value of measured rms Doppler spread for the C-band systems of Fig. 5.1 was only 0.5Hz. A crude interpolation of the mean outage duration in Fig. 5.2 indicates that the mean would be significantly greater than 0.2 seconds and hence from Fig. 5.3 we can expect almost all outages to be in outage range II.

In addition to these factors, the limited amount of rms Doppler spread data makes computation of outage range criteria based on duration statistics subject to significant error. For these reasons, we have elected a conservative approach which uses the outage range II criterion for all DCS troposcatter frequency ranges and assumes that all outages exceed 0.2 seconds in duration. This selection is only slightly conservative for C-band systems because few outages are less than 0.2 seconds according to the data presented here. Additionally, frequent recurring outages of the type in ranges IV and V are not consistent with the slow fading measured in the C-band system at RADC.

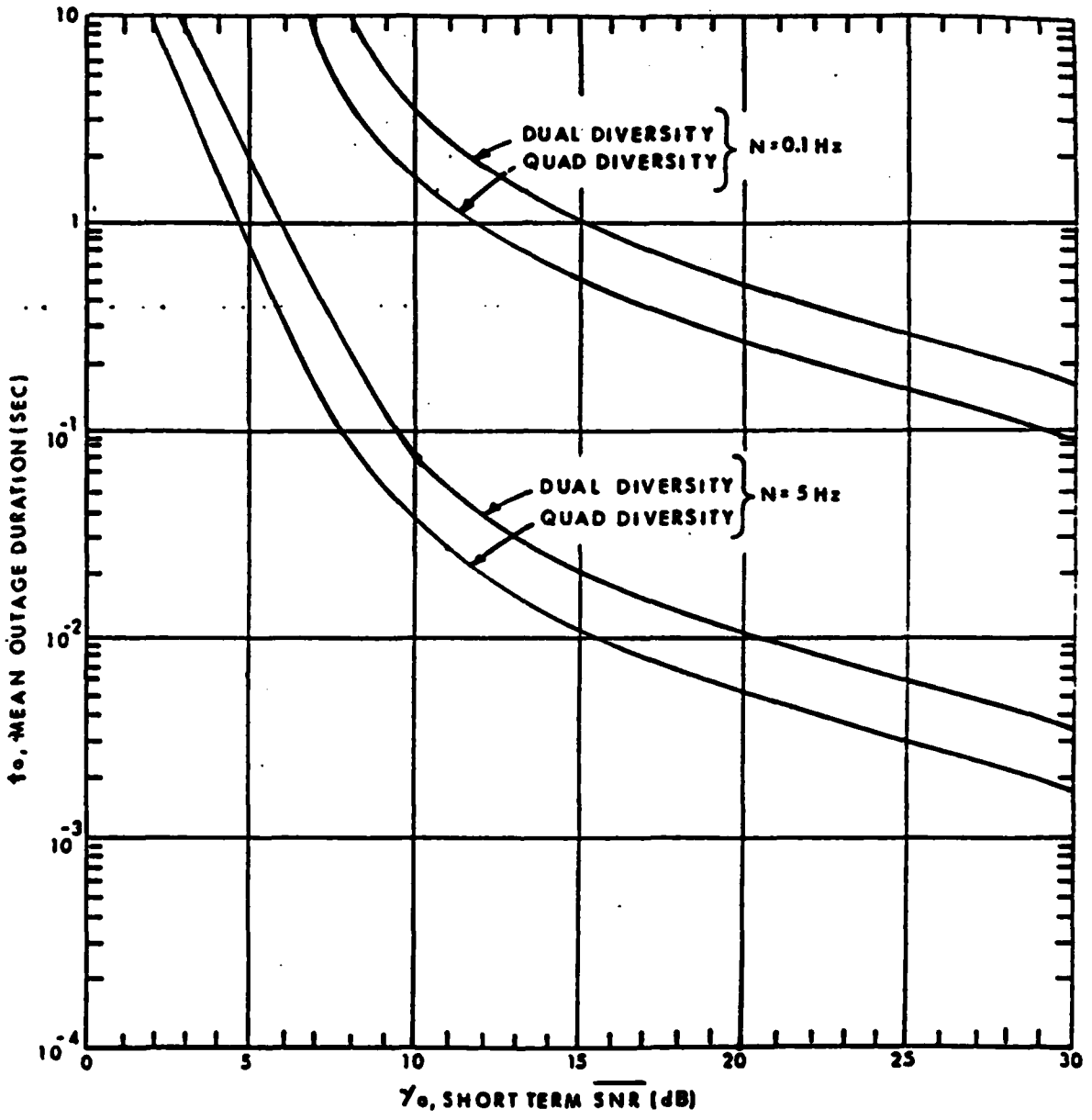

Fig. 5.2 Troposcatter Link Outage Duration

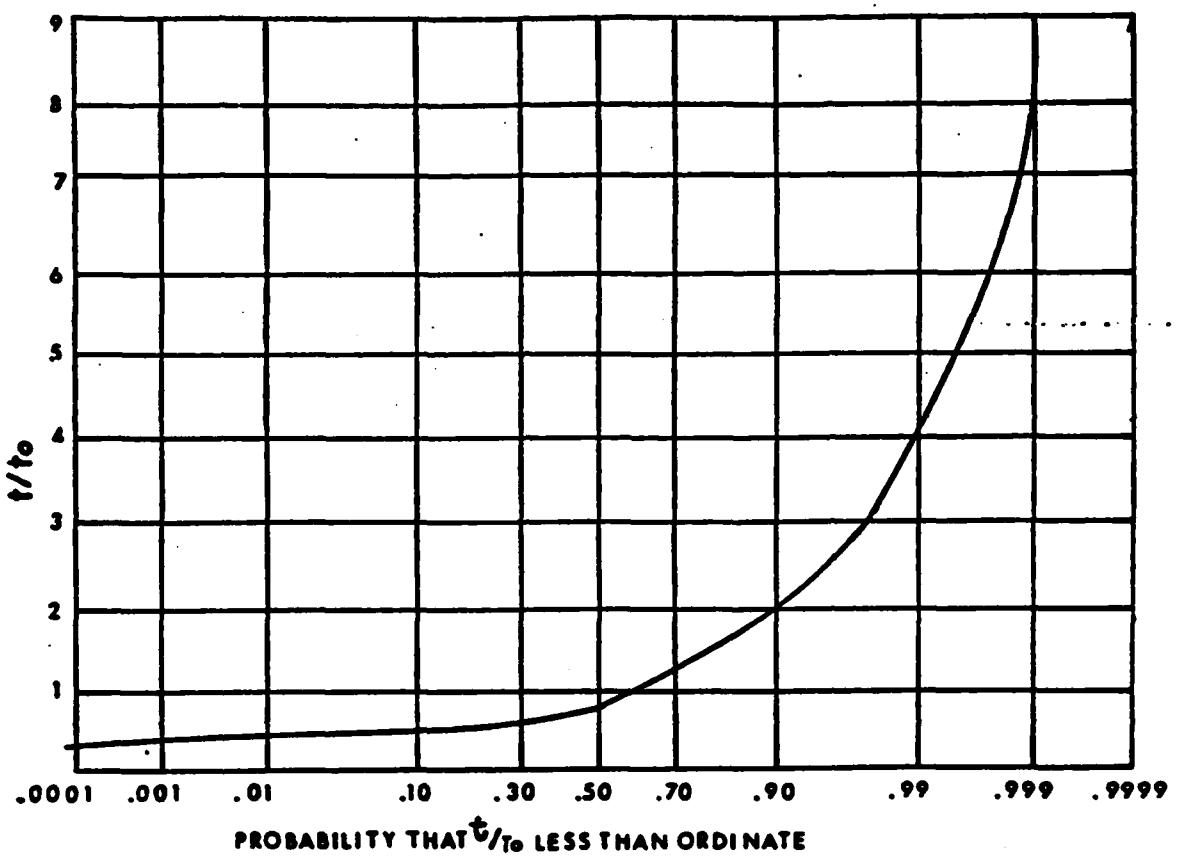

t_0 = mean outage duration (SEC)

Fig. 5.3 Distribution of Troposcatter Link Outage Duration

Using this criterion, the procedure to find the system gain surplus (deficit) is as follows. The yearly outage probability for a BER of 10^{-4} is computed for diversity configurations 2S/2F, 2S/2A, and 2S/2F/2A. In the long term averaging, this calculation uses the mean multipath spread for the quadruple diversity systems and an assumption of zero multipath spread for an 8th order diversity system. We present evidence in the next subsection which shows that the averaging process will be insensitive to the 2σ multipath spread and hence little error is introduced by using the mean value for the quad diversity systems. The implicit diversity improvement is small for the eighth order diversity system, and hence the use of zero multipath spread is slightly conservative. When the yearly outage probability is plotted on the short term BER distribution as a function of γ_0, the dB shift relative to the yearly objective of 7.5×10^{-4} is the approximate system gain surplus or deficit. The result of this procedure is presented in the next subsection for the RADC test link.

b. Computer Program Results

The method of computing the bit error rate (BER) statistics and path loss distributions for a troposcatter equalizer has been applied to a troposcatter system example. The path parameters for this system are given in Table 5.2. The troposcatter equalizer chosen for the analysis is the MD-918 modem developed by Sylvania/SIGNATRON for U.S. Army ECOm under the Megabit Digital Troposcatter Subsystem [5.1]. The modem uses differentially encoded 4PSK modulation with a four channel adaptive decision-feedback equalizer [5.2] for reception.

TABLE 5.2

PATH PARAMETERS

Name	RADC Test Link
Path Distance(mi.)	168.3
Transmitter Height(ft.)	340.
Receiver Height(ft.)	460.
Transmitter Antenna(ft.)	28.
Receiver Antenna(ft.)	28.
Transmitter Boresight/Horizontal ∢ (°)	1.27
Transmitter Boresight/Horizon ∢ (°)	0.27
Receiver Boresight/Horizontal ∢ (°)	0.77
Receiver Boresight/Horizon ∢ (°)	0.27
Squint Angle (°)	0.54
Frequency (GHz)	4.5

Transmitter power - kw
N.F.

TABLE 5.3

2σ MULTIPATH SPREAD

System	Boresight/ Horizon Angle	Squint Loss	Main Beam	Elev. Beam
	Beamwidth	dB	nsec	nsec
RADC (4.4-5.0GHz)	1/2	1.9	141.	174.

There are three taps per forward filter diversity channel with tap spacing equal to one-half a 4PSK symbol interval. The backward filter uses three taps in its transversal filter realization with tap spacing equal to the symbol interval.

Before presenting the BER statistics for our example link, the short term BER characteristics of the DFE modem are summarized. The predicted average BER performance of the MD-918 modem as a function of multipath dispersion is shown in Fig. 5.4. The quantity $2\sigma/T$ represents the ratio of twice the rms multipath spread to the 4PSK symbol interval. Note how performance improves with increasing $2\sigma/T$ due to implicit diversity utilization by the equalizer but then performance falls off again as the intersymbol interference penalty exceeds the implicit diversity gain. The amount of implicit diversity improvement and reduction of intersymbol interference penalty is a function of the number and spacing of forward filter taps in the DFE. The MD-918 uses 3 taps with a spacing of T/2.

The BER distribution can be derived in closed form [5.3] when the rms multipath spread is zero, i.e. when the fading channel is non frequency selective (flat fading). The results of this computation for 4PSK transmission and a Gaussian noise detection characteristic comparable to DPSK detection are shown in Figs. 5.5 and 5.6 for the flat fading channel. $\bar{E}_b/N_0$ is a signal-to-noise ratio measure defined as the hourly average received energy per bit divided by the noise power in a 1 Hz RF bandwidth. In Section 4, we derived for the first time an approach for the calculation of the short-term BER distribution when the channel is frequency selective fading.

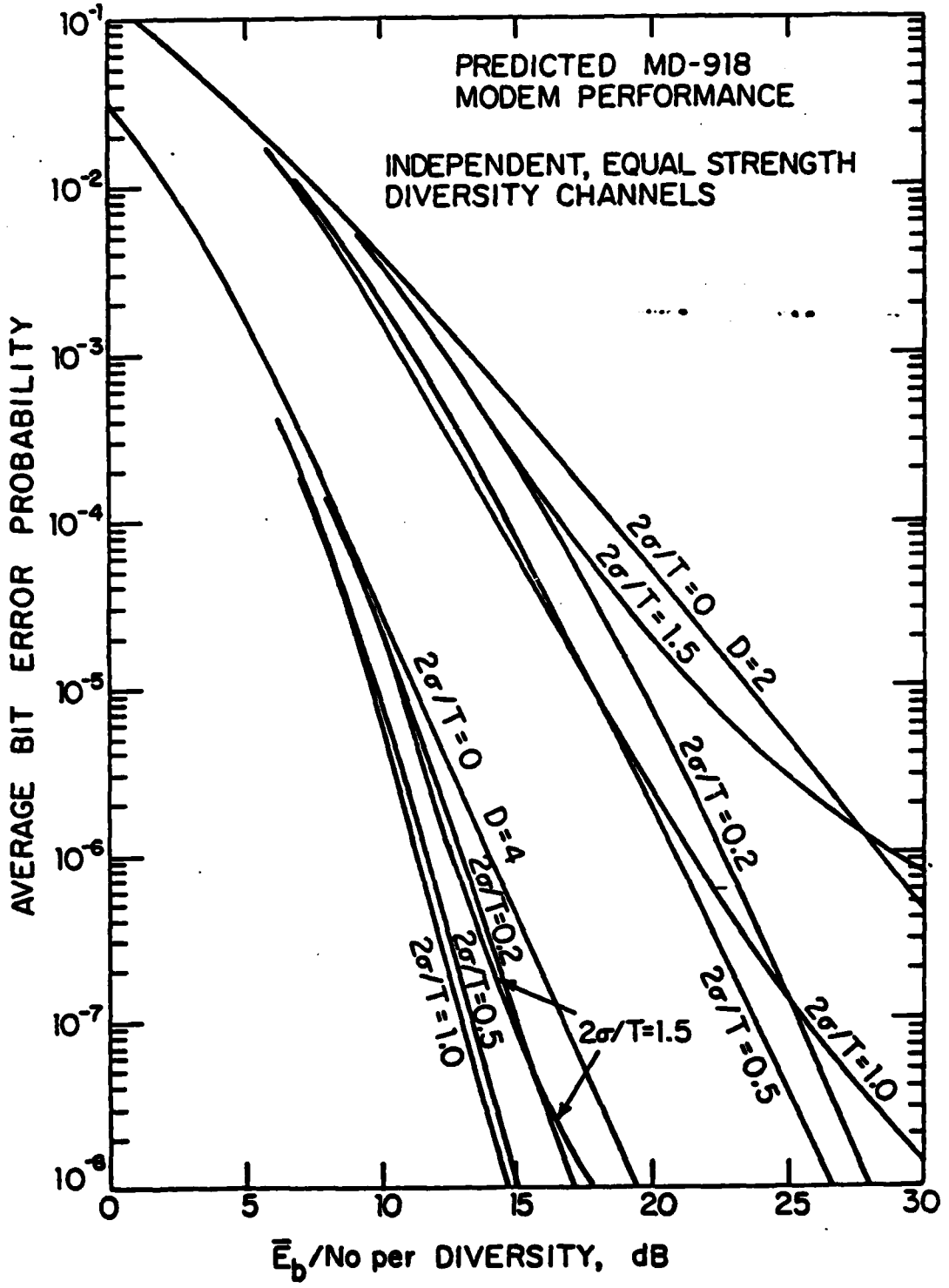

Fig. 5.4 Short-Term Average BER

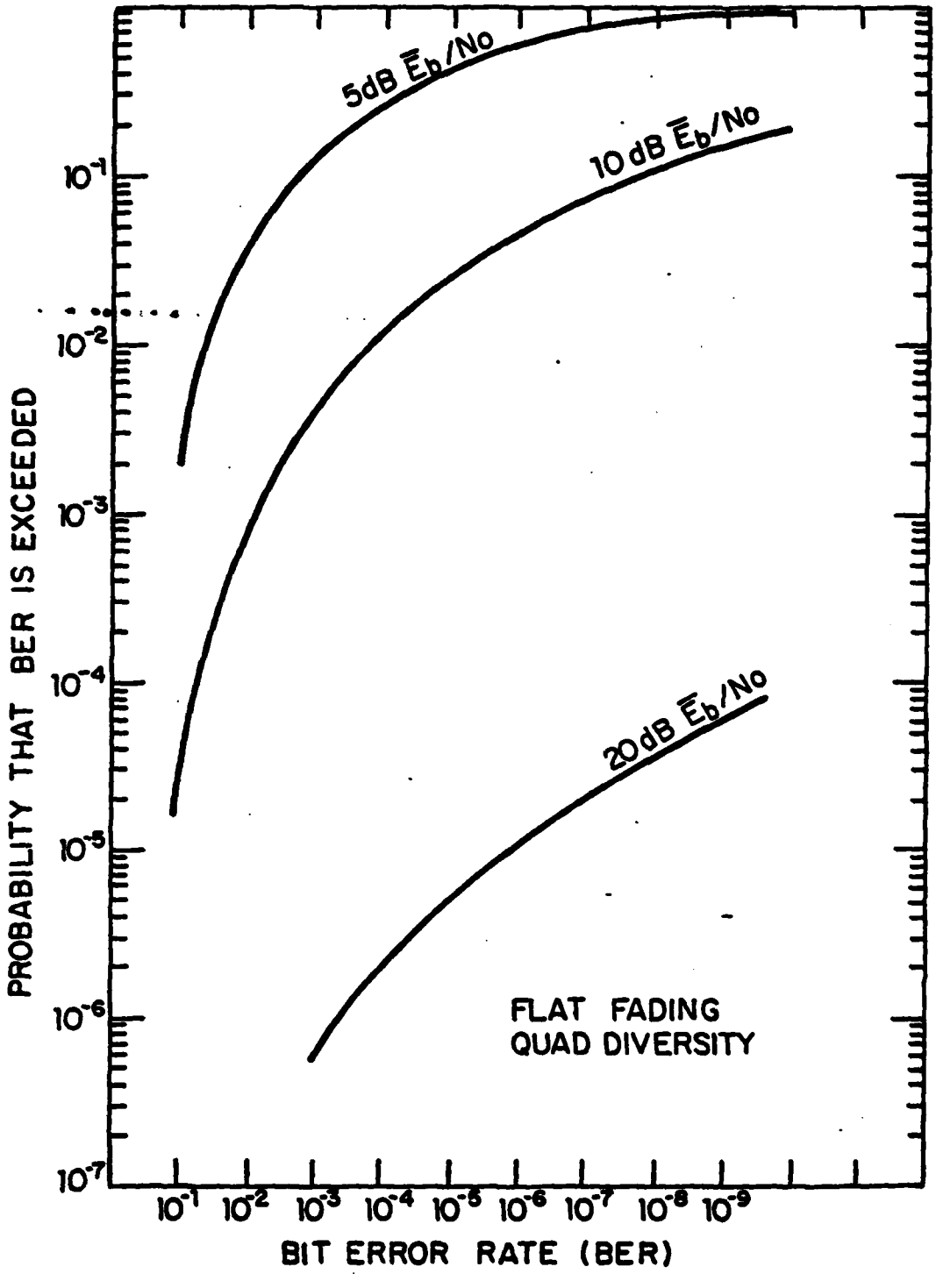

Fig. 5.5 Short-term BER Distribution
Flat Fading

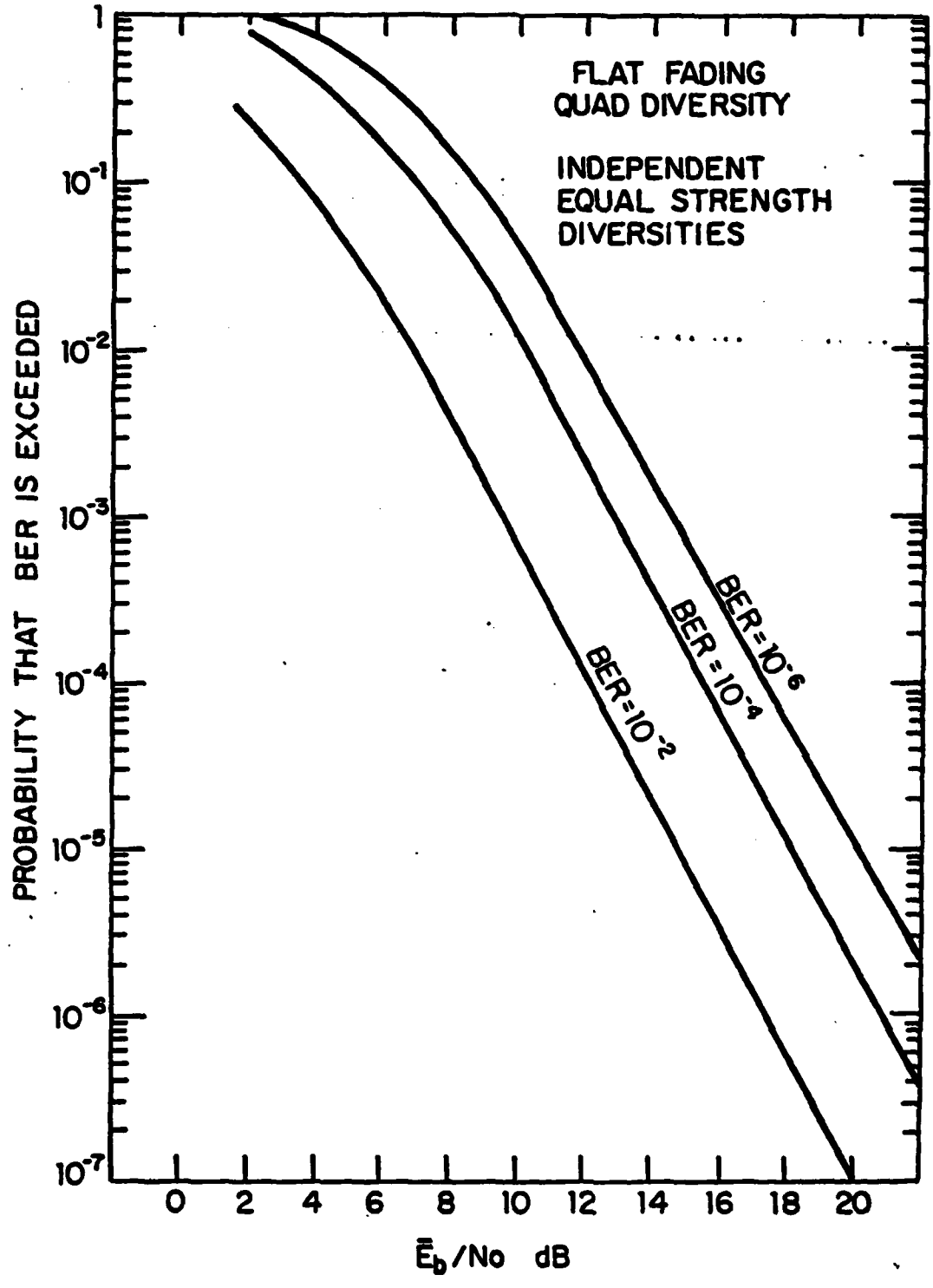

Fig. 5.6 Short Term BER Distribution as a Function of $\bar{E}_b/N_0$

The results from that analysis for independent equal strength diversity channels are shown in Fig. 5.7. Note that in the critical probability range of 10^{-1} to 10^{-4} the DFE modem characteristic is not very sensitive to variations in the rms multipath spread. This result allows us to estimate the yearly outage probability accurately without knowing the form of the long term multipath distribution.

Before tne bit error rate statistics for the example link can be computed, squint loss is calculated and the 2σ multipath spread is determined for the main beam and elevated beam, multipath profiles. These values are given in Table 5.3.

The data rate chosen for the calculation was 6.3 Mb/s as it corresponds to typical user requirements for strategic digital troposcatter. With a 4PSK modulation format, the bit symbol interval T is then 317 nanoseconds. The $2\sigma_0/T$ value for the main beam diversity is 0.42 for the RADC path.

The results of the bit error rate computation have been calculated as a function of the mean value $\bar{E}_b/N_0$ for a 2S/2F diversity receiver. To accomplish this comparison we first determine the distribution of the median path loss using the common volume integration model of Section 3 and the NBS time availability analysis discussed in Section 6. The common volume integration model includes the effect of aperture to medium coupling loss and provides a path loss parameter normalized to unit gain antennas. To convert median path loss into $\bar{E}_b/N_0$ in dB, the relationship is

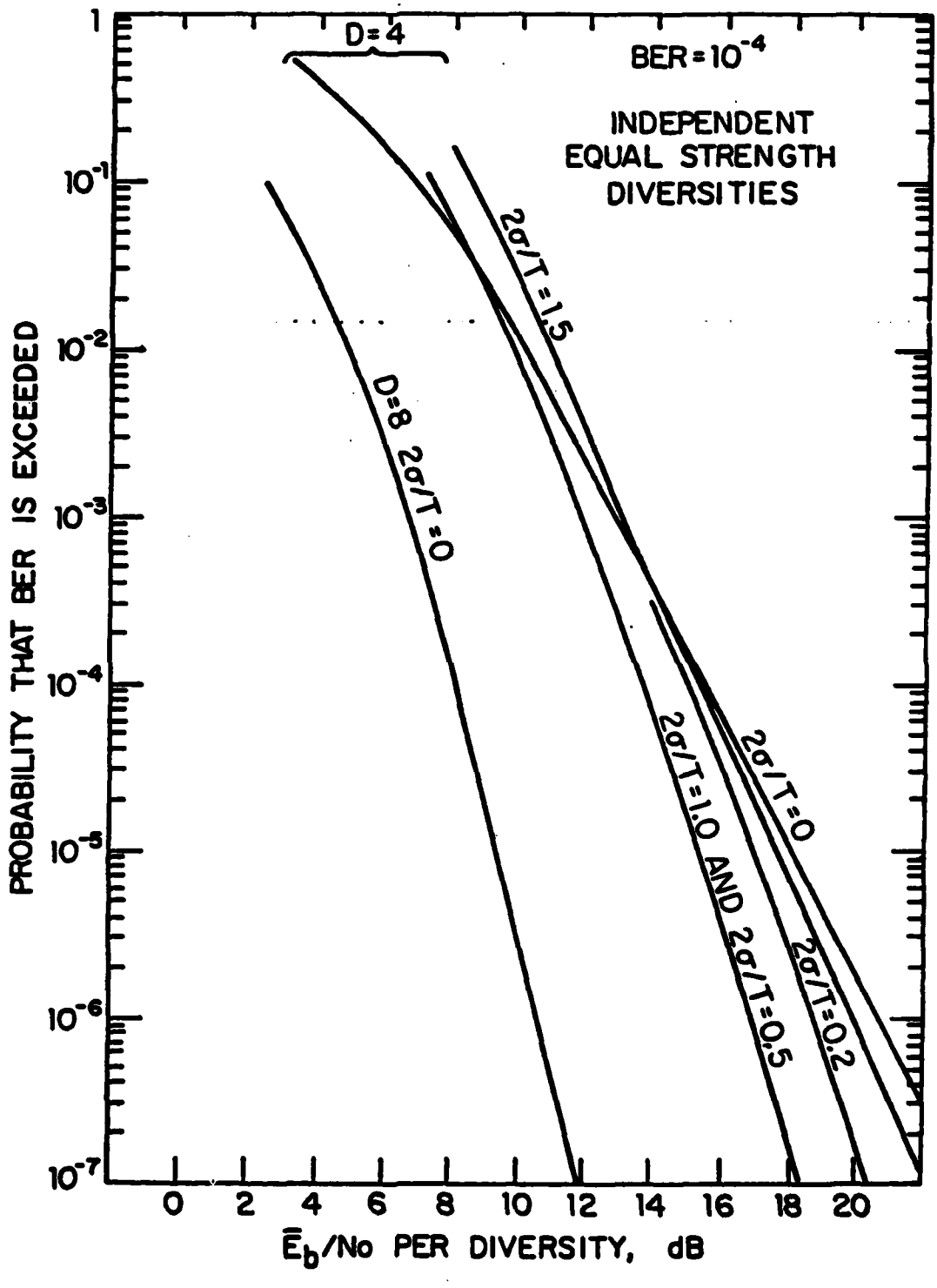

Fig. 5.7 Short Term BER Distribution for Frequency Selective Fading

$$E_b/N_o = P_T+G_T+G_R-L-NF-10 \log (R_b)+174+1.6$$

where

P_T = transmit power in dBm

$G_{T/R}$ = antenna gain of transmitter receiver in dB

L = total path loss including coupling loss effects

NF = noise figure

R_b = data rate in b/s

174 = noise power in 1 Hz bandwidth in dBm

1.6 = dB amount that the mean exceeds the median for a Rayleigh fading channel.

The antenna gain formula for troposcatter reflectors of diameter D is

$$G = 10 \log \left(\pi^2 D^2 \epsilon/\lambda^2 \right)$$

where $0 < \epsilon < 1$ is the antenna efficiency with typical value on the order of 0.57.

In the calculation of median path loss the refractive index variance dependence is based on Fried's [5.3] results at optical wavelengths. Also a service probability of 0.95 has been selected as a conservative measure. We have not collected sufficient empirical data to establish the absolute accuracy of the prediction model. For the RADC test link where empirical data is available, the winter median path losses for the two space diversity antenna receivers were measured [5.5] to be 258 and 260 dB. Our angle diversity test program from October to May 1979 measured an average of the four receivers of 256 dB. Our predicted value for this link for all year conditions is 254 dB which is good agreement.

For an angle diversity application, the squint loss and the availability of a redundant power amplifier has been considered in the system comparison with conventional systems. Since the 2S/2F configuration requires two power amplifiers, any comparison with angle diversity should be on the same basis. It also follows that a 2S/2A system would require a second power amplifier for failure and maintenance redundancy reasons. For these practical considerations the 2S/2A system utilizes two power amplifiers tuned to the same frequency.* Thus, in effect, the transmit power per diversity of a 2S/2A system is 3 dB more than in an analogous 2S/2F system. The 3 dB advantage of the 2S/2A system over the 2S/2F system is included in the comparison of bit error rate statistics.

The link performance is summarized in a graph of the short term BER distribution for three diversity configurations at 6.3 Mb/s: dual space/dual frequency (2S/2F), dual space/dual angle (2S/2A), and dual space/dual frequency/dual angle (2S/2F/2A). On this graph the yearly objective for the outage probability, the yearly median $\overline{E}_b/N_0$, and the yearly outage probability for each diversity configuration are noted. The dB shift to the right (left) of the yearly outage probability relative to the yearly objective is the system gain surplus (deficit). Fig. 5.8 shows these results for the RADC test link. Note that all three diversity configurations fail to meet the TR12-76 objective. For a 2S/2A configuration the system gain deficit is approximately 3 dB. Use of the eighth order system reduces this deficit to about 2 dB. Measured

*Each power amplifier drives one of the two transmit antennas producing a composite antenna pattern with nulls spaced at intervals equal to the antenna spacing. Since the null width is small compared to the common volume dimension defined by the beamwidth, the nulls can be neglected. Experimental tests have verified the usefulness of this configuration.

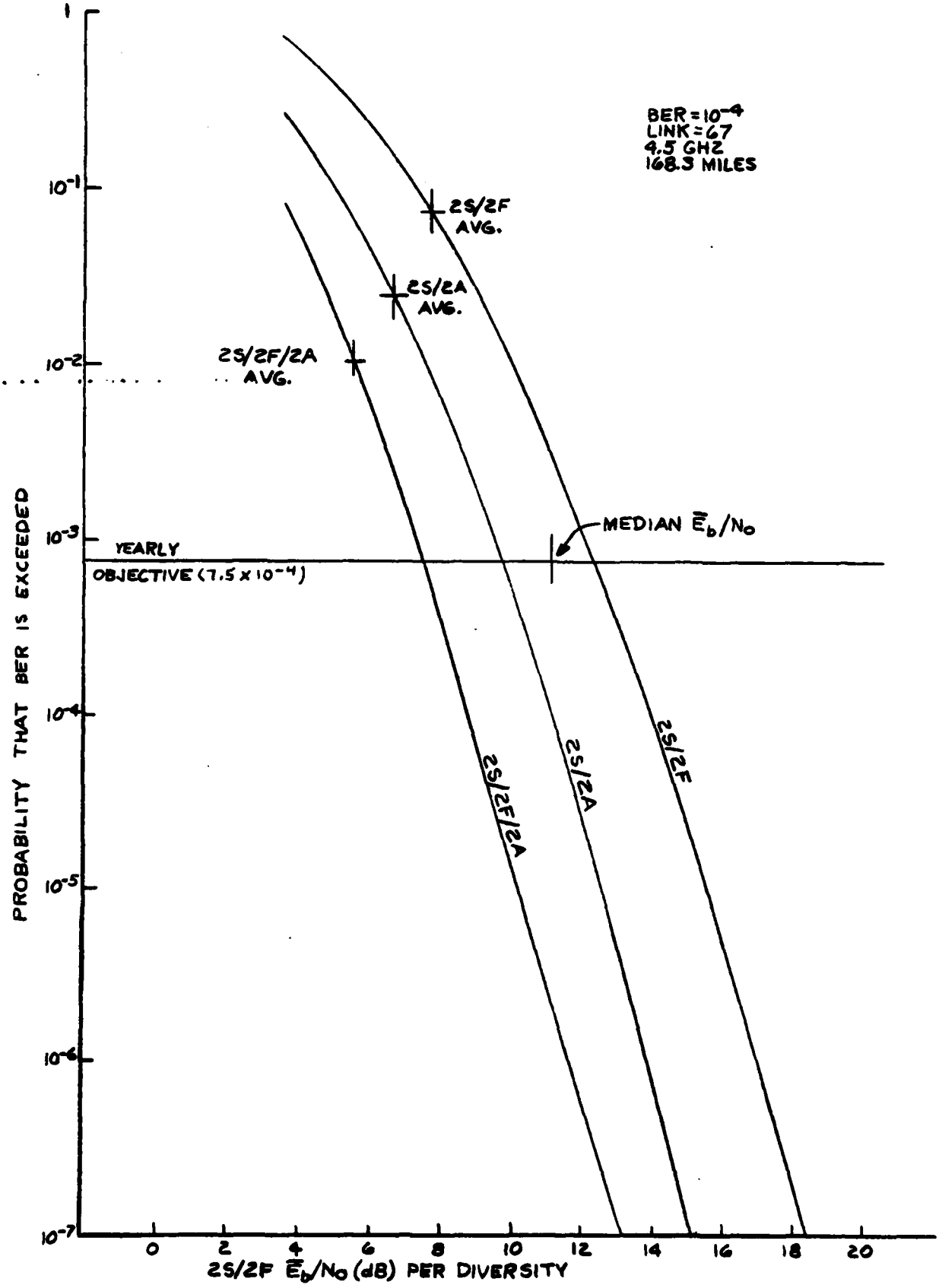

Fig. 5.8 RADC Test Link Predicted Performance

BER statistics summarized in the next section illustrate the negative performance margin of this test link relative to the DCS troposcatter link standards.

SECTION 5

REFERENCES

[5.1] C. J. Grzenda, D. R. Kern, and P. Monsen, "Megabit Digital Troposcatter Subsystem," NTC Conference Record, New Orleans, Dec. 1975, pp. 28-15 to 28-19.

[5.2] P. Monsen, High Speed Digital Communication Receiver, U.S. Patent No. 3,879,664, April 22, 1975.

[5.3] D.J. Kennedy, "Digital Error Statistics for a Fading Channel," Conference Record, ICC, Vol. 1, June 1973.

[5.4] D. L. Fried, "Optical Heterodyne Detection of an Atmosphereically Distorted Wavefront", Proc. IEEE Vol. 55, No. 1, 1967, pp. 57-67.

[5.5] A. Sherwood, and L. Suyemoto, Multipath Measurements Over Troposcatter Paths, Mitre Corporation, Report MTP-170, April 1976.

SECTION 6

LONG TERM VARIABILITY

Tropospheric scatter systems are subject to two fading phenomena - short term multipath fading and long term power fading. The short term fading of the instantaneous received power within periods of time ranging from less than a second to many minutes results from random fluctuations in the relative phasing between component waves arriving at the receiver over slightly different propagation paths. The long term power fading results from slow changes in average atmospheric refraction, in the intensity of refractive index turbulence, and in the degree of atmospheric stratification. The power fading is characterized by hourly or diurnal variations. The evaluation of troposcatter system performance is accomplished in part by determining the hourly median path loss where the median is computed to include the short term multipath fading and in turn considering the median path loss as a random variable subject to a power fading distribution. The median path loss calculation utilizes fixed values of the mean and variance of the refractive index and an assumption on the degree of atmospheric stratification. In the earlier portion of this report we have presented a prediction method for the computation of median path loss. This method has the following important characteristics:

- **The average atmospheric refraction is fixed by utilizing an effective earth's radius of K times the actual radius to account for the mean refractive index.**

- **The intensity of refractive index turbulence is fixed by the refractive index variance which is chosen to correspond to dry winter afternoons.* This period of time generally experiences the poorest propagation conditions.**

*This time period is referred to as Time Block 2 (TB2) in the NBS prediction method.

- The atmospheric structure is derived from turbulent scattering theory which leads to a refractive index spectrum slope of m=11/3. This structure is more applicable for higher frequency (> 1 GHz) troposcatter systems than the stratified layer assumption used in the NBS prediction method (m=5).

- The aperture-to-medium coupling loss is included as an integral part of the path loss calculations.

For this method the power fading of the median path loss is determined by variations in the effective earth radius factor K, variations in the refractive index variance σ_n^2, and changes in the atmospheric structure leading to other values of the refractive index spectrum slope m. Given probability density functions on the parameters K, σ_n^2, and m, the computation of the median path loss long term distribution would be straightforward. Unfortunately there is little empirical data available to derive such densities. Some experimental evidence and analysis [Gossard, 1977] indicate that the refractive index variance σ_n^2 is the dominating factor in producing significant variations in the median path loss. Development of experimental data on σ_n^2 over long periods of time for different geographical areas would provide a basis for predicting long term variability of troposcatter systems. At the present time the only method of predicting this variability is to use path loss data taken from existing systems and integrated into the NBS variability model [Rice, 1967]. Much of the empirical path loss data has been taken from systems with operating carrier frequencies below 1 GHz. The performance prediction for new troposcatter systems operating in the 4 to 5 GHz frequency region may be subject to large errors as a result. However, in the absence of empirical data on either σ_n^2 or median path loss at these new frequencies, an extrapolation of the NBS variability model is the only realistic

engineering choice. In the first subsection we briefly review the NBS model and describe the specific parameters integrated into the SIGNATRON prediction computer program for computation of long term variability. In the subsequent subsection the special issues which must be addressed in the evaluation of the long term variability of an angle diversity system are considered.

a. NBS Long Term Variability Model

Considerable experimental evidence suggests that the long term distribution of the hourly median path loss is normally distributed in dB. If we denote L(p) as the hourly median path loss in dB, which is not exceeded p% of the time, the normal distribution is defined as follows:

$$\frac{p}{100} = \text{prob}\left\{\text{median path loss} \leq L(p)\right\}$$

$$\frac{}{\sigma_L\sqrt{2\pi}} \int_{-\infty}^{L(p)} \exp\left[\left(\xi - L(50)\right)^2 / 2\sigma_L^{\,2}\right] d\xi \,. \qquad (6.1)$$

where L(50) is the median path loss computed using the numerical integration of (3.2)3.2 is received power and σ_L is the long term standard deviation. The NBS Long Term Variability Model [Rice, 1967] uses empirical data to determine L(10) and L(90) from which normal probability graph paper can be used to plot L(p) at other values of p. This calculation includes the effect of prediction uncertainty through a parameter called service probability. The service probability is the probability that a new system will meet the long term performance predictions.

A parameter called effective distance, d_e, has been found to be superior to other parameters such as path length, angular distance, and distance between actual or theoretical horizons, in predicting the long term variability. The effective distance is defined in terms of d_{s_1} which is the distance for equal diffraction and scatter path loss and d_{s_o} which is the smooth earth distance between radio horizons. These parameters are computed from the following relations

$$d_{s_1} = 65(100/f)^{1/3} \text{ km} \tag{6.2}$$

$$d_{s_o} = d - 3\sqrt{2\,h_{t_e}} - 3\sqrt{2\,h_{r_e}} \tag{6.3}$$

where the effective antenna heights h_{t_e} and h_{r_e} are expressed in meters, the path length d is in kilometers, and the radio frequency f is in MHz. The effective distance is defined in the NBS model as

$$d_e = \begin{cases} 130/\,[1+(d_{s_1} - d_{s_o})/d] \text{ km}, & d_{s_o} \le d_{s_1} \\ 130 + d_{s_o} - d_{s_1} \text{ km}, & d_{s_o} \ge d_{s_1} \end{cases} \tag{6.4}$$

A variability function Y(p) which depends on the effective distance and can be corrected for frequency and climate effects is used to determine L(10) and L(90) from the relation

$$L(p) = L(50) - Y(p). \tag{6.5}$$

The variability function is defined by

$$Y(p) = Y_o(p, d_e)\, g(p, f)$$

where $g(p, f)$ represents an average of many effects that are frequency sensitive. The NBS variability model provides empirical curves and an analytic function representation for $Y_o(p,d_e)$. In addition, the model uses a parameter $V(50,d_e)$ to adjust the long term reference median path loss computed by the NBS method to the median loss L(50) in (6.5). For dry winter afternoons this adjustment is 0 dB.

The analytic function representation for $Y_o(p,d_e)$ is given for dry winter afternoons (Time Block 2) as

$$\left.\begin{matrix} Y_o(10, d_e) \\ -Y_o(90, d_e) \end{matrix}\right\} = \left[c_1 d_e^{n_1} - f_2(d_e)\right] \exp\left(-c_3 d_e^{n_3}\right) + f_2(d_e) \tag{6.6}$$

where

$$f_2(d_e) = f_\infty \left[1 - (1-f_m/f_\infty) \exp(-c_2 d_e^{n_2})\right] \tag{6.7}$$

and the constants have values (d_e in kilometers)*

*The values for f_m and f_∞ given in Annex III, Tech Note 101 do not agree with the continental temperate climate variability curve given in Section 10.5 of Tech Note 101. The quantities f_m and f_∞ in the table have been adjusted to provide good agreement.

	$Y_o(10, d_e)$	$-Y_o(90, d_e)$
c_1	1.04×10^{-5}	1.05×10^{-5}
c_2	4.28×10^{-8}	7.00×10^{-13}
c_3	3.51×10^{-8}	7.64×10^{-8}
n_1	2.71	2.59
n_2	2.91	4.80
n_3	3.41	3.68
f_m	10.5	8.5
f_o	3.0	2.3

For frequencies greater than 400 MHz, the curves for g(p,f), winter afternoons, provided in the NBS model can be well approximated by

$$g(10, f) = g(90, f) = \begin{cases} 1-0.6 \text{ LOG } (.0005 f) & 400 < f < 2000 \\ 1.0 & 2000 < f. \end{cases} \quad (6.8)$$

For a normal distribution, other points on the loss distribution are calculated from

Y(0.01)	= 3.33Y(10)	Y(99.99)	= 2.90Y(90)
Y(0.1)	= 2.73Y(10)	Y(99.9)	= 2.41Y(90)
Y(1.0)	= 2.00Y(10)	Y(99)	= 1.82Y(90).

These calculations and the loss distribution resulting from (6.5) provide the long term variability of the median path loss

for a continental temperate climate during winter afternoons. The NBS variability model provides numerous curves and other variability functions to accommodate other portions of the season and other climatic areas.

The path loss distribution (6.5) corresponds to a service probability of 50%, i.e., 50% of the systems built would exceed the performance predictions. Conservative engineering practice would recommend the selection of a service probability of 95%. For this choice the loss distribution must be adjusted by the prediction error according to the NBS formula

$$L_{0.95}(p) = L(p) + 1.65\sqrt{12.73 + 0.12Y^2(p)}. \qquad (6.9)$$

The variability predictions used in this study utilize the NBS long term variability model with a service probability of 95%. The median path loss L(50) is computed from the previously described numerical integration procedure which corresponds to the loss for turbulent scattering conditions during dry winter afternoons in a temperate continental climate. The formulas (6.1) thru (6.9) are then used to derive the loss distribution. The mean E_b/N_o distribution for evaluation long term variations in digital system performance is determined from the path loss distribution by the formula

$$\frac{\bar{E}_b}{N_o}(p) = P_T + G_T + G_R - L_{.95}(p) - \left[10 \text{ LOG } (R_b) + NF - 174\right] + 1.6 \qquad (6.10)$$

where

P_T = transmit power in dBm

G_T = transmit antenna gain in dB

G_R = receiver antenna gain in dB

$L_{.95}(p)$ = path loss not exceeding p% of the time for unit gain antennas* and a service probability of 0.95

R_b = data rate in b/s

NF = receiver noise figure in dB

-174dBm = received noise power in 1 Hz bandwidth

1.6 dB = factor relating median to mean for a complex Gaussian scatter channel.

b. Long Term Variability in an Angle Diversity System

In space and frequency diversity systems, the common scattering volume is virtually the same for each diversity and hence the long term median path loss varies the same for each diversity. In angle diversity system, however, the common volumes are separated and the long term variability is not identical for the angle diversity beams. The effect of this decorrelation of the diversity power fading may improve the system availability because a power fade in the main beam diversity is not always accompanied by a power fade in the squinted diversity beam. Physically one can imagine this situation in a vertical angle diversity system where the inhomogeneous structure of the atmosphere results in say a larger refractive index variance or superior atmospheric stratification at heights corresponding to the elevated beam than at heights defined by the main-beam common volume. Since the common volumes in a vertical angle diversity system are separated by approximately one beamwidth Ω at a distance d/2 from the link terminals, this decorrelation results from atmospheric variations over distances on the order of $\Omega d/2$. For typical troposcatter applications this distance is on the order of one or more miles at a height above the

* Aperture to medium coupling loss of the actual diameter antennas is included in this parameter.

earth's surface also on the order of a few miles. Experimental evidence verifying the long term power fading decorrelation in angle diversity systems has been reported on by [Monsen, 1972] and [Troitskiy, 1972]. Data from these angle diversity experiments and data from the AAC field tests will be used to establish the availability improvement from power fading decorrelation.

The long term medial path loss or received signal level (RSL) can be described by a multi-variated normal distribution when each path loss or RSL is given in dB. Path loss and RSL are related by a sign change and an additive constant. We use RSL in the subsequent analysis because emperical data is more often expressed in this quantity. We consider a dual vertical angle diversity system with or without additional frequency or space diversity. Let x_i represent the medial RSL in dB for diversity I and we number the diversities such that the main beam diversities are odd and the elevated beam diversities are even, e.g., for a 2S/2F/2A system we have

x_1, x_3 mainbeam space diversity channels

x_5, x_7 mainbeam frequency diversity channels

x_2, x_4 elevated beam space diversity channels

x_6, x_8 elevated beam frequency diversity channels.

Because of the power fading correlation in space and frequency diversity, one has

$$x_1 = x_3 = x_5 = x_7$$

$$x_2 = x_4 = x_6 = x_8$$

and x_1 and x_2 are described by the joint normal density function

$$f(x_1, x_2) = \frac{1}{2\pi\sigma |R|^{\frac{1}{2}}} e^{-\underline{x}' R \underline{x} / 2\sigma^2} \qquad (6.11)$$

where

$$\underline{x} = \begin{bmatrix} x_1 - m_1 \\ x_2 - m_2 \end{bmatrix}$$

$$R = \begin{bmatrix} 1 & a\rho \\ a\rho & a^2 \end{bmatrix}.$$

m_1 = mean value of median RSL for diversity 1 (main beam)

m_2 = mean value of median RSL for diversity 2 (elevated beam)

σ = mainbeam RSL standard deviation

$a\sigma$ = elevated beam RSL standard deviation

ρ = power fading correlation coefficient.

The NBS variability model discussed in the last subsection provides a method for determining the path loss (RSL) standard deviation σ. Since $\rho=0$ and $a=1$ for space and frequency diversity systems, determination of σ completely specifies the long term variability for these systems. In angle diversity systems the parameters ρ and a will also influence the long term variability of the effective received signal power.

In order to assess the effect of decorrelated power fading and an increase in the elevated beam standard deviation, we use the mean diversity RSL in dB as a system measure of performance. This measure corresponds to the geometric mean of the diversity signal-to-noise ratios which asymptotically for large signal-to-noise ratio governs the short term performance of both analog and digital systems. Thus we define the mean diversity RSL

$$x = \frac{1}{2}(x_1 + x_2) \tag{6.12}$$

and a system availability function as $x(p)$, where $x(p)$ is the mean diversity RSL which is exceeded 100% of the time, viz.,

P = prob {mean diversity RSL $\geq$ x(p)}.

Since the sum of two normal random variables is also normal, we have

$$P = \frac{1}{\sigma_x \sqrt{2\pi}} \int_{x(p)}^{\infty} \exp[\xi - \bar{x})^2 / 2\sigma^2] d\xi \qquad (6.13)$$

where the long term mean and variance are equal to

$$\bar{x} = \frac{1}{2} (\bar{x}_1 + \bar{x}_2)$$

$$\sigma_x^2 = (x - \bar{x})^2 = \frac{1}{4} \overline{[(x_1 - m_1) + (x_2 - m_2)]^2}$$

$$= \frac{\sigma^2}{4} (1 + 2\rho a + a^2) \quad .$$

For convenience we define the function

$$f_{a,\rho} = \left[\frac{1 + 2\rho a + a^2}{4} \right]^{1/2} \qquad (6.14)$$

which reduces to unity for frequency diversity systems, a=1, ρ=1.

The availability for the angle diversity system is

$$p = 1 - Q\left[\frac{x(p) - (m_1+m_2)/2}{\frac{1}{2}\sigma \sqrt{1+2\rho a+a^2}}\right] = 1 - Q\left(\frac{x(p) - \frac{m_1+m_2}{2}}{\sigma f_{a,\rho}}\right) \qquad (6.15)$$

where Q(.) is the normal distribution function

$$Q(u) = \frac{1}{\sqrt{2\pi}} \int_{-\infty}^{u} e^{-v^2/2} \, dv \quad .$$

Equation (6.15) for angle diversity should be contrasted with the result for frequency diversity when ρ=1, a=1.

and $m_1=m_2$ but both are reduced by 3 dB. The availability for frequency diversity is

$$p = 1 - Q\,\frac{x(p) - m_1 + 3}{\sigma} \qquad (6.16)$$

The reduction of the mean RSL in a frequency diversity system relative to an angle diversity system results from the necessity to return one of the two power amplifiers in an angle diversity system to adjacent frequency for a frequency diversity application. This action reduces the received power for diversity by 3 dB.

Let's compare the frequency (2S/2F) and angle (2S/2A) diversity systems as a function of availability level. An availability of p is realized in the two systems when the argument of Q in (6.15) and (6.16) is equal to $-q_p$ where

$$p = 1 - Q(-q_p). \qquad (6.17)$$

For equal availabilities, the availability levels for RSL for the two systems are then

$$X_A(p) = \frac{m_1+m_2}{2} - q_p\sigma f_{a,\rho} \quad ; \quad \text{Angle Diversity}$$

$$X_F(p) = m_1 - 3 - q_p\sigma \quad ; \quad \text{Frequency Diversity}$$

The availability improvement in dB for the angle diversity system is

$$I_{A/F} = X_A(p) - X_F(p)$$

$$I_{A/F} = 3 - \frac{m_1-m_2}{2} + q_p\sigma\,(1 - f_{a,\rho}),\ \text{dB} \qquad (6.18)$$

The first term is the power amplifier differential, the second is the squint loss, and the third term represents the combined effects of increased standard deviation in the elevated beam ($a>1$) and long term decorrelation of the main and elevated beam common volumes ($\rho < 1$) .

In (6.14) one can see that the effect of the power fading correlation coefficient is to improve system availability with decreasing values of the coefficient but, on the other hand, an increase ($a > 1$) in the elevated beam path loss standard deviation decreases the system availability. In order to evaluate the result of these competing effects, we examine some previous angle diversity experimental data.

Long term variability data was taken on the Bell Laboratories experimental angle diversity link reported on by [Monsen, 1972] The important characteristics of this link were

- triple vertical angle diversity
- 2.17 GHz operating frequency
- 179 statute mile path
- 28' transmit antenna, 50' steerable receive antenna
- 1 Kw transmit power
- 1.6 beamwidth separation between beams.

Measurements of hourly median signals once or twice a week over a period from September 1970 through February 1971 provided

a set of 43 independent hourly median samples. The long term received power means, standard deviations, and correlation coefficient for the lowest two vertical beams have been computed and are given in the following table as a function of antenna pointing angle relative to the horizon. The last addition in the table is the computed angle diversity improvement at an availability of 99.9%. ($q_p = 3.1$).

For large take-off angles when the squint loss ($\bar{X}_1 - X_2$) is large, the angle diversity system is seen to be inferior to a frequency diversity system. As the take-off angle is reduced, a point is reached wehre the angle diversity is superior. In this experimental system at a take-off angle of 0.5°, the angle diversity system is 1/2 dB poorer at 99.9% availability. By reducing the take-off angle to 0.16°, thus reducing the mean received power by

$$(89.3 - 86.7) + (91.3 - 93.0) = 0.9 \text{ dB}$$

one realizes a 3.2 dB improvement in the angle diversity system for a net gain of 2.3 dB. Thus an angle diversity system with a take-off angle of 0.16 is 2.3 dB better than a frequency diversity system with a take-off angle of 0.50. In this experiment system, no attempt was made to minimize the squint angle. A feedhorn with a squint angle of approximately 1.6 beamwidths which produced a squint loss of 6.3 dB at the take-off angle of 0.5. Using the feedhorn design developed under this program, a reduction in the squint loss to 2 or 3 dB is judged reasonable. In an optimized design the angle diversity improvement relative to frequency diversity is judged on the basis of this data to be about 3 dB.

Table 6.1

Long Term Variability Data, BTL Link

Antenna Angle to Horizon Beamwidths	$\bar{x}_1$ dBm	$\bar{x}_2$ dBm	MAIN σ dB	ELEV $a\sigma$ dB	ρ	Computed Angle Diversity Improvement
1.50	-89.1	-98.8	6.8	7.2	0.875	- 1.8 dB
1.16	-87.4	-97.4	6.5	7.5	0.846	- 2.7
0.83	-86.4	-95.4	6-3	7.4	0.828	- 2.3
0.50	-86.7	-93.0	6.1	7.2	0.743	- 0.5
0.16	-89.3	-91.3	6.7	7.3	0.711	+ 2.7
-0.16	-93.8	-89.7	6.8	6.8	0.735	*
-0.50	-99.9	-87.8	6.2	6.9	0.907	*
-0.83	-105.0	-87.2	5.8	7.0	0.922	*

* main beam excessively blocked

When the squint loss is equal to 6 dB there is exact cancellation of the 3 dB power amplifier gain with the mean diversity loss associated with a squinted dual angle diversity system. For operational systems the net gain due to these two factors will normally be positive since the antenna beams can be placed closer together than the 1.6 beamwidth separation in the BTL experimental system. The new gain due to the power fading correlation coefficient and elevated beam standard deviation is more difficult to assess because of the rather limited empirical data. [Troitskiy, 1972] has presented data on three links which show a smaller power fading correlation coefficient than found from the BTL data. Table 6.2 summarizes Troitskiy's experimental results. The power fading correlation coefficient was measured between envelope powers in watts rather than dBm and is designated $\tilde{\rho}$. In the 2nd Interim report [Monsen, Parl, 1978] we determined that ρ is overbounded by ρ but the bound is tight and to a good approximation $\tilde{\rho} = \rho$

It is surprising that the results in Table 6.2 show a smaller power fading correlation coefficient when these links have the beams closer together in the sky than the beams were in the BTL experimental link. Also it is unfortunate that Troitskiy did not report on data from which the elevated beam standard deviation can be calculated.

Table 6.2

Experimental Results, Ref. [Troitskiy, 1972]

Path Length Miles	Freq. GHz	Beam-width mr	Angle Between Beams mr	Scatter Angle mr	Hours of Data	$\tilde{\rho}$
188	1.0	12.5	11.6	35	500	0.50
174	4.35	12.5	8.7	33	240	0.56
267	4.35	5.8	6.9	50	100-150	0.679

However, the smaller value of long term correlation suggests larger values of angle diversity improvement than calculated from the BTL data.

The final set of experimental data examined as part of an angle diversity availability evaluation is the field test data taken during the AAC program. The RADC link for the AAC tests had the following characteristics:

- vertical angle diversity in a 2S/2F/2A configuration
- 4.5 and 4.69 GHz receive frequencies
- 168 statute mile path
- 28' antennas
- 2 to 4 Kw transmit power
- 1.3 beamwidth separation between beams.

The measurement of medial received powers covered a period from September 1977 to October 1979. The statistical results from that test period are given in Table 6.3.

Note that the RADC link also has less correlation between beams that measured in the Bell Laboratories experiment and the beams are closer together. Outside of statistical and measurement error effects, this result suggests a more homogeneous tropospheric structure in the S-band BTL tests than in the C-band RADC tests. Also the elevated beam RSL has less variation than the main beam in the RADC experiments whereas it had more variation in the BTL experiments.

To compute the angle diversity availability improvement from (6.18) we reduce the data in Table 6.3 to

Mean Mainbeam RSL = -94.1 dBm = m_1

Mean Elevated RSL = -97.4 dBm = m_2

Mainbeam Std. Dev. = 7.5 dB = σ

Elevated Beam St. Dev. = 6.3 dB = $a\sigma$, $a = 0.84$

Avg. Correlation Coeff. = 0.71 = ρ

The availability improvement for angle diversity at a 99.9% availability is

Table 6.3
AAC Field Test Data

RCVR A/S/F (RADC)	$\bar{x}_1$ MEAN RSL dBm	σ STD. dB	$\bar{x}_2-\bar{x}_1$ MEAN SQUINT dB	$\alpha\sigma$ STD. SQUINT dB	ρ CORR. COEFF.
000	-93.4	8.5	3.3	5.5	0.77
001	-96.7	7.2	1.7	5.4	0.70
010	-90.8	7.6	5.8	5.0	0.75
011	-95.6	6.5	2.5	5.7	0.61
100	-96.8	6.4	-	-	-
101	-98.3	6.5	-	-	-
110	-96.6	5.9	-	-	-
111	-98.1	6.4	-	-	-

$$I_{AF} = 3 - \frac{3.3}{2} + (3.1)(7.5)(0.1487)$$

$$= 4.8 \text{ dB.}$$

The improvement of the angle diversity system over frequency diversity is also supported by a direct computation of the availability from the actual RSL data taken in the RADC experiment. In the RADC experiment, data was taken on pairs of frequencies, antennas, and feedhorns. From this data base, three hypothetical systems can be examined. These are

1. Conventional 2S/2F using 4.50 and 4.69 GHz
2. Angle diversity: 2S/2A using 4.50 GHz
3. Angle diversity: 2S/2A using 4.69 GHz

The composite RSL for each of these systems is an accurate measure of the short term performance. For the 8 receivers defined in Table 6.3 (A = angle, S = space, F = frequency), the composite RSL is defined as

$$X = \begin{cases} \frac{1}{4}(X_1+X_2+X_3+X_4) & 2S/2F \\ \frac{1}{4}(X_0+X_2+X_4+X_6) + 3 & 2S/2A \quad 4.50 \text{ GHz} \\ \frac{1}{4}(X_1+X_3+X_5+X_7) + 3 & 2S/2A \quad 4.69 \text{ GHz} \end{cases}$$

where 3dB has been added to the angle diversity systems to accurately reflect the two power amplifier configuration of a traffic bearing system. The long term variation of the composite RSL (x) for the three hypothetical systems is shown in Fig. 6.1. At low RSL values both angle diversity systems show a significant improvement. For example at 95% availability, the angle diversity systems improve on the conventional system by about $1^{1}/2$ and 4dB. Note that the weaker angle diversity system has a poorer

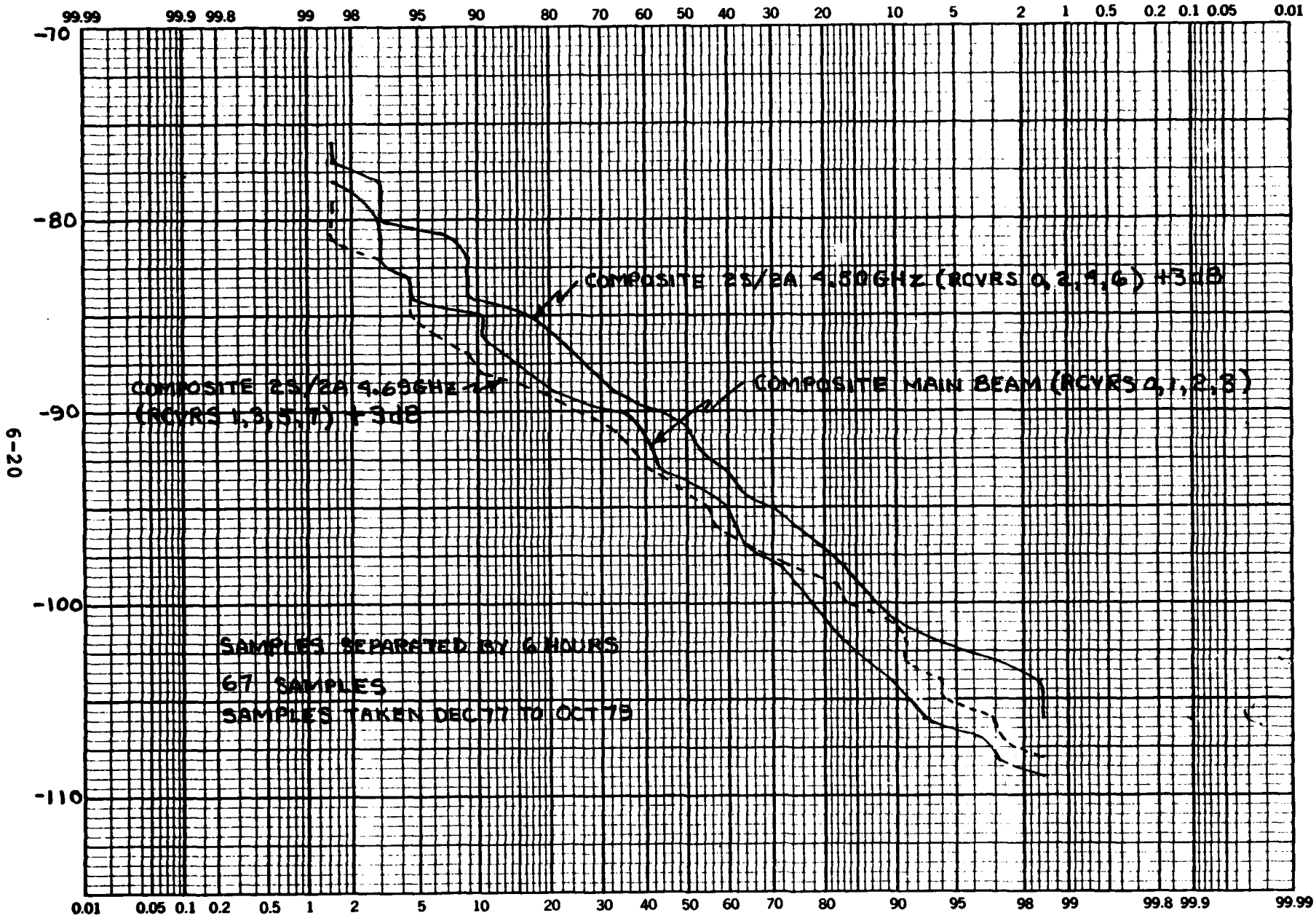

Fig. 6.1 Probability RSL Exceeds Ordinate

median composite RSL, but, due to the long term decorrelation effect, the angle diversity system has a larger RSL at high availability values.

The empirical results presented in this subsection clearly indicate the system gain superiority of angle diversity systems over frequency diversity systems. This system gain advantage is complemented by the 2 to 1 bandwidth advantage of the angle diversity systems.

SECTION 6

BIBLIOGRAPHY

Monsen, P. (1972), "Performance of an Experimental Angle Diversity Troposcatter System", IEEE Trans. on Comm., Vol. COM-20, No. 2, April 1972, pp. 242-247.

Monsen, P. and S. Parl (1978), Adaptive Antenna Control, 2nd Interim Technical Report, SIGNATRON, Inc., Lexington, MA, Feb. 1978.

Rice, P. L., A. G. Longley, K. A. Norton and A. P. Barsis (1965, Rev. 1967), "Transmission Loss Predictions for Troposcatter Communications Circuits", N.B.S. Techn., Note. 101.

Troitskiy, V. N. (1972), "Efficiency of Angle-Diversity Reception in Long-Distance Tropospheric Propagation," Telecommun. & Radio Eng., 1972, 27, pp. 17-23.

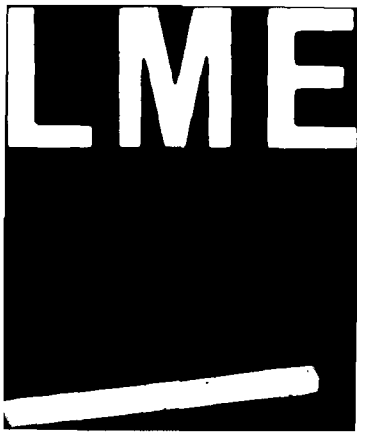
LME